

Dissertation
submitted to the
Combined Faculties for the Natural Sciences and for
Mathematics
of the Ruperto-Carola University of Heidelberg, Germany
for the degree of
Doctor of Natural Sciences

put forward by

Dipl.-Phys. Tobias Hartwich

born in Stuttgart

Oral Examination: 31. January 2013

Development and Characterization of Single-Molecule Switching Nanoscopy Approaches for Deeper and Faster Imaging

Referees:

Prof. Dr. Joachim Spatz

Prof. Dr. Jörg Bewersdorf

Abstract:

Novel single-molecule switching super-resolution microscopy overcomes the diffraction limit of far-field fluorescence microscopy by precisely localizing individual fluorescent molecules from thousands of images of stochastic, sparse blinking-molecule distributions. However, this technique has so far mostly been limited to thin, fixed samples: usually, fluorescent molecules are activated throughout the whole depths of the sample and not just in the 1 - 2 μm thick optical section where they can be localized. In thick samples, this incurs excessive background and unwanted bleaching of probe molecules out of focus. Using two-photon absorption allows to limit activation of photo-activatable fluorescent proteins to the optical section where they can be localized. However, no spectroscopic information about the two-photon activation of the most commonly used molecules has been available so far. Live-cell imaging is additionally hampered by the typically used EM-CCD cameras which can only record up to 60 full frames/second. Novel sCMOS cameras feature much higher readout speeds and have the potential for fast live-cell imaging, but artifact-free performance at high speed has not been demonstrated yet. In this thesis, I have realized a new super-resolution microscope capable of two-photon activation of photo-activatable probes. I have characterized PAmCherry1, PA-GFP and PAmKate, three of the most popular photo-activatable fluorescent proteins, spectroscopically for two-photon activation. My results suggest a modified model of photo-activation of PAmCherry1. Super-resolution images of ring canals in thick *Drosophila* egg chambers have been recorded in three dimensions using this new microscope. Furthermore, I present the first artifact-free super-resolution microscopy using a sCMOS camera. Microtubules could be imaged at 32 nm spatial resolution in only 33 ms.

Kurzbeschreibung:

Die neuartige einzelmolekülschaltende, hochauflösende Mikroskopie umgeht das Beugungslimit in der Fernfeld-Fluoreszenzmikroskopie, indem sie die Positionen einzelner fluoreszenter Moleküle aus tausenden von stochastisch verteilten, spärlichen Ansammlungen blinkender Moleküle präzise bestimmt. Allerdings wurde diese Technik bislang hauptsächlich für dünne, fixierte Proben eingesetzt, da fluoreszente Moleküle üblicherweise über die gesamte Dicke der Probe hinweg aktiviert werden anstatt nur in der 1 – 2 µm dicken Schicht, in der sie lokalisiert werden können. In dicken Proben führt dies zu einem exzessivem Anstieg des Hintergrundsignals sowie dem ungewollten Bleichen von Markermolekülen außerhalb des Fokus. Durch die Benutzung von Zweiphotonenabsorption kann die Aktivierung photoaktivierbarer Fluoreszenzmoleküle auf die optische Schicht beschränkt werden, in der sie lokalisiert werden können. Es stehen bislang jedoch keine spektroskopischen Daten für die am häufigsten verwendeten Moleküle zur Verfügung. Zusätzlich ist das Aufnehmen von lebenden Proben dadurch eingeschränkt, dass die üblicherweise eingesetzten EM-CCD Kameras nur bis zu 60 ganze Bilder pro Sekunde auslesen können. Die neuartigen sCMOS Kameras haben zwar wesentlich schnellere Auslesegeschwindigkeiten und haben das Potential für schnelle Aufnahmen lebender Zellen eingesetzt zu werden, allerdings konnte bislang noch kein artefaktfreier Betrieb bei hohen Auslesegeschwindigkeiten vorgeführt werden. In dieser Arbeit habe ich ein neues hochauflösendes Mikroskop entwickelt, das photoaktivierbare Moleküle mittels Zweiphotonenaktivierung schalten kann. Ich habe drei der beliebtesten Fluoreszenzproteine, PamCherry1, PA-GFP und PAmKate, spektroskopisch bezüglich der Zweiphotonenaktivierung untersucht und dreidimensionale, hochaufgelöste Bilder von Ringkanälen in dicken *Drosophila* Eizellen mit diesem neuen Mikroskop aufgenommen. Desweiteren führe ich die erste artefaktfreie, hochauflösende Mikroskopie mittels einer sCMOS Kamera vor und konnte Mikrotubulie mit 32 nm räumlicher Auflösung in nur 33 ms aufnehmen.

Contents

1	Abstract:	5
2	Kurzbeschreibung:.....	7
	Abbreviations.....	11
1	Introduction	13
2	Background	16
2.1	Fluorescence	16
2.2	Two-photon excitation	17
2.3	Diffraction limit	18
2.4	Super-resolution microscopy.....	18
2.4.1	Stimulated Emission Depletion Microscopy	18
2.4.2	Stochastic single-molecule switching.....	19
2.4.2.1	Imaging isolated fluorophores	20
2.4.2.2	Localization-based nanoscopy setups.....	22
2.4.2.3	Cameras	25
3	Instrumentation	28
3.1	Two-photon activation Setup.....	28
3.2	sCMOS setup	33
4	Two-photon activation of photo-activatable fluorescent proteins	36
4.1	Biological background.....	36
4.1.1	Cloning	36
4.1.2	Sample preparation	36
4.2	Recording protocol.....	36
4.3	Data analysis	37
4.3.1	Curve preprocessing	37
4.3.2	Fitting	38
4.4	Activation rates for various photo-activatable fluorescent proteins.....	39
5	Ring Canal imaging.....	44
5.1	Biological background.....	44

5.2	Comparison of embedding media related influences on the camera background.....	45
5.3	Recording procedure.....	46
5.4	Results.....	47
6	sCMOS video-rate imaging	49
6.1	Sample preparation	49
6.1.1	Cell Culture	49
6.1.2	Imaging buffer preparation.	50
6.2	Imaging experiments.....	50
6.2.1	System performance	50
6.2.2	Reconstructed video-rate imaging of fixed microtubules	52
7	Summary and Outlook.....	54
	Bibliography	57
8	Appendix	62
8.1	Cloning protocol.....	62
8.2	Plasmid sequence	66
	Acknowledgements	83

Abbreviations

FOV:	field of view
2PA:	two-photon activation
FWHM:	full width at half maximum
QE:	quantum efficiency
3D:	three dimensional
sCMOS:	scientific complementary metal-oxide-semiconductor
EM-CCD:	electron multiplying charge coupled device
fps:	frames per second
AOTF:	Acousto-Optic Tunable Filter
ROI:	region of interest
STED:	Stimulated Emission Depletion Microscopy

1 Introduction

One of the most important tools in life sciences is fluorescence light microscopy. Fluorescent probes make it possible to label a target structure or protein of interest with very high specificity and thus study its organization or function in a cell or even a whole organism. Using fluorescent proteins, it is even possible to have cells express a fluorescent probe directly attached to the target protein, without requiring further labeling steps, which dramatically simplifies live-cell experiments. However, the achievable resolution is limited by diffraction. This resolution is usually described by the full width at half maximum (FWHM) of the point spread function (PSF), the image of a point-like light source, and is typically about 200 – 250 nm laterally (perpendicular to the optical axis) and about 500 – 700 nm axially (parallel to the optical axis). Structures smaller than this limit cannot be observed in the blurred image.

In recent years a range of super-resolution techniques have been developed that take advantage of the photophysical properties of the fluorescent labels to circumvent this limitation. Among these is fluorescence photo-activation localization microscopy (FPALM), a technique where photo-activatable fluorescent proteins (PAFPs) are used. The photo-activatable fluorophores can undergo a change in their excitation and emission characteristics which is triggered by the absorption of light of typically 405 nm wavelength. By using a sufficiently low intensity of the 405 nm light, sparse subsets of molecules can be activated, where each activated molecule is on average separated by more than the diffraction limit from the others. The position of these individual molecules can then be determined (localized) with a precision S_{loc} , which is proportional to

$$S_{loc} = \frac{S_{FWHM}}{\sqrt{N}} \quad (1)$$

where S_{FWHM} is the FWHM of the PSF of the imaged molecule and N is the number of photons collected before the molecule bleaches. For $N \geq 1,000$, the localization precision is thus much smaller than the diffraction limit. By repeatedly activating, imaging and bleaching these subsets over tens of thousands of frames a map of probe molecule positions can be generated that represents a super-resolution image of the sample. This approach can be expanded to three dimensions by imaging two axially shifted planes simultaneously (Biplane-FPALM) (Juetten et al., 2008), which makes it possible to localize molecules in a 1 – 2 μm thick optical section around the focal plane, with a typical resolution of about 25 nm laterally and 75 nm axially.

This improved resolution comes, however, at the disadvantage of a much slower image acquisition because tens of thousands of frames have to be recorded. The typically used electron multiplying charge coupled device (EM-CCD) cameras can only record up to 60 full frames per second (fps) which hampers the use of these techniques for live-cell imaging.

Additionally, the 405 nm laser used for photo-activation penetrates the whole depth of the sample, activating molecules not only in the focal region where they can be detected, but also outside the focal plane. This leads to an increased background of the image thus lowering the signal to noise ratio and negatively affecting the localization precision when recording thick samples. Since the molecules which got activated outside of the imaging plane cannot be localized, this also reduces the effective labeling density of the sample because only a small fraction of the activated molecules can be properly detected.

One way to overcome the limitation to thin samples is to use a two-photon absorption process for the activation of the sample. This has been shown to confine activation to an optical section of about 1.2 μm thickness, which reduced the background and simultaneously increased the number of localized molecules by more than twofold in cell culture (York, Ghitani, Vaziri, Davidson, & Shroff, 2011). However, no spectroscopic information about the two-photon activation (2PA) is available for the most commonly used PAFPs like PAmCherry1 (F V Subach et al., 2009), PAmKate (Gunewardene et al., 2011) and mEos2 (McKinney, Murphy, Hazelwood, Davidson, & Looger, 2009).

For this thesis, I have developed a new Biplane-FPALM microscope that uses a two-photon absorption process for the activation of photo-activatable fluorophores. As described in chapter 3, the Ti:Sapphire laser used for the 2PA is focused into the sample and scanned over the field of view (FOV) to confine the activation to an optical section $<1 \mu\text{m}$ thick. Chapter 4 summarizes spectroscopic studies with this new microscope that investigate the ability to use 2PA for the popular PAFPs PAmCherry1, PAmKate, PA-GFP (Patterson & Lippincott-Schwartz, 2002), mEos2 and Dendra2 (Gurskaya et al., 2006). Additionally, I present in chapter 5 super-resolution images in thick tissue samples with this new microscope by imaging ring canals in *Drosophila* egg chambers.

In order to speed up the acquisition for super-resolution imaging, it has been shown that novel scientific complementary metal-oxide-semiconductor (sCMOS) cameras can be used which feature much faster readout speeds (Z.-L. Huang et al.,

2011; Saurabh, Maji, & Bruchez, 2012). This makes super-resolution microscopy more compatible to live-cell imaging.

In chapter 6, I describe another super-resolution microscope that I have built which uses a sCMOS camera and new localization algorithms developed in our lab. The first artifact-free super-resolution images with these cameras at unprecedented video-rate are demonstrated.

2 Background

2.1 Fluorescence

In fluorescence microscopy a sample is illuminated with light of a certain wavelength that is able to excite the sample. The probe molecule will absorb a photon that carries the correct energy to lift one electron of the sample molecule from the electronic ground state into an electronic state of higher energy. Since the electronic states are further split into vibrational states of differing energy, the energy needed for the excitation transition varies depending on the final vibrational state. The excitation spectrum describes the wavelength dependency of the excitation process. After excitation the molecule will first relax into the vibrational ground state of the excited electronic state before typically falling back into one of the higher vibrational states of the electronic ground state by emitting a fluorescence photon with the energy corresponding to the energy difference of the transition. This leads to an emission spectrum that is usually red shifted due to the dissipated energy during the relaxation into the respective vibrational ground state. This shift towards longer wavelengths is called the Stokes shift.

Alternatively, there is a small chance for the excited electron to cross into a spin triplet state. Since the transition from this spin triplet state into the spin singlet electronic ground state through the emission of one photon is spin-prohibited these states are metastable and have a lifetime of microseconds or longer. Figure 1 summarizes these transitions in a Jablonski Diagram.

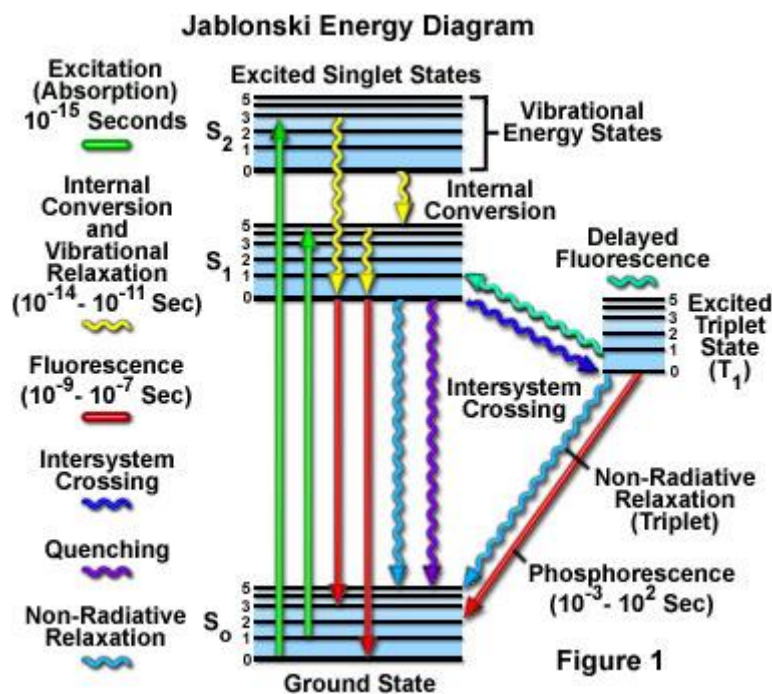


Figure 1. Jablonski diagram of a typical fluorescent probe molecule showing excitation and fluorescence emission as well as radiationless internal conversion and system crossing transitions and their respective time constants. (taken from <http://www.olympusmicro.com/primer/java/jablonski/jabintro/jablonskijavafigure1.jpg>)

2.2 Two-photon excitation

The energy necessary for the excitation can also be obtained from simultaneously absorbing two (typically near infrared (NIR)) photons of half the required energy each. This process, called two-photon excitation, has very low cross sections of the order of $10^{-50} \text{cm}^4 \text{s}$ (Denk, Strickler, & Webb, 1990; Hermann & Ducuing, 1972; Zipfel, Williams, & Webb, 2003). Because two photons have to be absorbed at the same time it is dependent on the square of the illumination intensity (Nakamura, 1999). Due to the low cross sections pulsed lasers with high peak powers are typically used.

The quadratic dependence on the laser intensity can be exploited to achieve so called optical sectioning. By focusing the laser into the sample, the illuminated area is proportional to z^2 outside of the focal plane, where z is the axial coordinate with $z = 0$ in the focal plane. The laterally integrated total number of absorption processes $N_{\text{lat}, 2\text{P}}$ ($\sim \text{area} * \text{intensity}^2$) is thus roughly proportional to $1/z^2$ and centered around the focal plane. In the one-photon absorption case, $N_{\text{lat}, 1\text{P}}$ ($\sim \text{area} * \text{intensity}$) is roughly independent of the axial position. This $1/z^2$ dependence in the two-photon case confines absorption processes to a volume centered around the focal plane when scanning the focus laterally thus creating the optical sectioning effect.

2.3 Diffraction limit

Resolution in a conventional light microscope is fundamentally limited by diffraction and can be represented by the image of a point-like light source, the point spread function (PSF). A typical definition for the resolution of a microscope is the full width at half maximum (FWHM) of the PSF. It can be approximated by:

$$\Delta r \approx \frac{\lambda}{2 NA} \quad (2)$$

$$\Delta z \approx \frac{n \lambda}{NA^2} \quad (3)$$

where Δr and Δz are the FWHMs of the PSF in lateral and axial direction, respectively, λ is the wavelength of the light, n is the refractive index of the medium and NA is the numerical aperture of the lens with $NA = n \sin \alpha$, where α is the semi-aperture angle of the objective (Abbe, 1873).

The image of any object can be interpreted as a superposition of PSFs for every light-emitting point comprising the sample. The diffraction-limited size of the PSF therefore limits what can be resolved since neighboring objects appear merged when closer than the size of the PSF. The diffraction limit greatly hinders biological studies on molecular length scales.

2.4 Super-resolution microscopy

Recently, several different techniques have been developed that can circumvent this limitation to achieve theoretically unlimited resolution, the most prominent being Stimulated Emission Depletion microscopy (STED) (S W Hell & Wichmann, 1994) and localization-based nanoscopy techniques (Gould, Hess, & Bewersdorf, 2012; Toomre & Bewersdorf, 2010) (see Figure 2).

2.4.1 Stimulated Emission Depletion Microscopy

STED is a point scanning technique similar to a conventional confocal microscope. It circumvents the diffraction limit by first exciting the fluorescent molecules in a diffraction-limited spot and then uses a second red-shifted, donut-shaped laser to force excited molecules back into the electronic ground state by stimulated emission before the molecules had a chance to spontaneously emit fluorescence. By using high laser powers to saturate this quenching process, only the excited molecules in the donut hole can still emit fluorescence. At the center of this hole is an intensity zero, so by saturating the stimulated emission process fluorescence emission is confined to the very center of the donut. Resolutions of typically tens

of nanometers can be achieved using high enough depletion laser intensities (Stefan W Hell, 2009) (see Figure 2b).

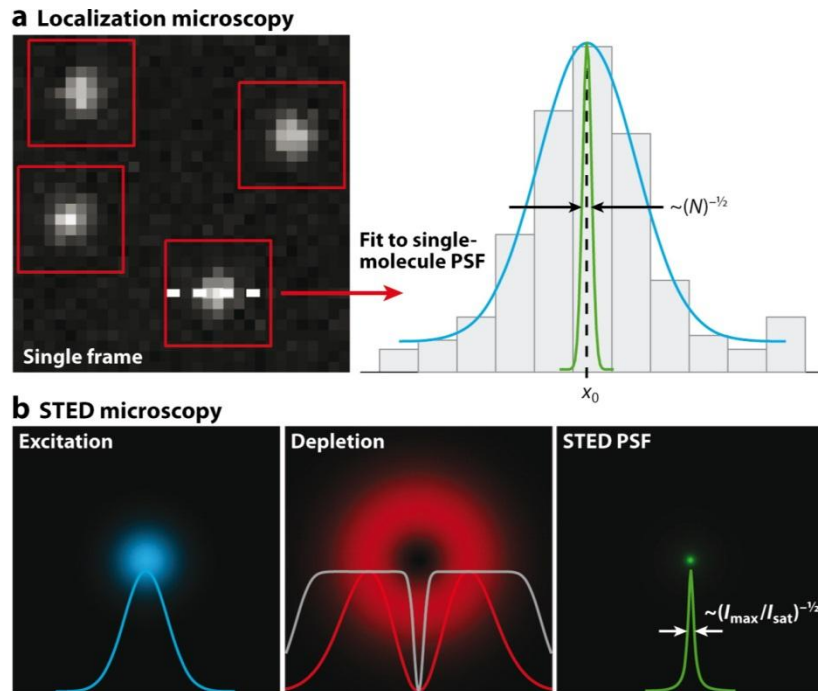


Figure 2. Concepts of diffraction-unlimited microscopy. (a) Concept of localization-based microscopy. Sparse subsets of single molecules are identified in a raw frame (red boxes). Each molecule is fitted (cyan curve) to determine its position (x_0) with a precision that is inversely proportional to the square root of the number of detected photons (N), as indicated by the green curve. A final image is generated from the coordinates of molecules localized from many frames. (b) Concept of stimulated emission depletion (STED) microscopy. The conventional excitation focus of a laser-scanning microscope (cyan) is coaligned to the donut-shaped depletion focus, which features an intensity zero at its center (red). Saturating the depletion efficiency quenches fluorescence emission except at the center of the depletion focus (gray curve). An effective STED point-spread function (PSF) (green) is generated with a size that is inversely proportional to the square root of the ratio of maximum depletion intensity to characteristic saturation intensity of the probe molecule (I_{\max}/I_{sat}). (modified from Gould TJ, et al. 2012. *Annu. Rev. Biomed. Eng.* 14:231-54)

2.4.2 Stochastic single-molecule switching

This thesis revolves around an alternative approach, localization-based nanoscopy techniques. In these techniques, individual fluorophores in a sample are imaged a few at a time. As point-like emitters the resulting images are akin to PSFs and the position of the emitters can be determined with a far higher precision than the resolution limit by determining the centers of the PSF images. This is typically called localization and the precision with which the center of a PSF can be determined can be approximated (for negligible background and pixel size) by

$$FWHM_{loc} = \frac{FWHM}{\sqrt{N}} \quad (4)$$

where FWHM is given by the dimensions of the PSF and N is the number of detected photons from the single emitter that comprise a the image of a single fluorophore (Ram, Ward, & Ober, 2006; Thompson, Larson, & Webb, 2002).

For a super-resolution image tens of thousands of camera frames are recorded in order to image a large fraction of molecules in the sample. After localizing all recorded emitter positions, the final image is generated as a map of all of the determined particle positions.

2.4.2.1 Imaging isolated fluorophores

In order to be able to image individual fluorophores either special fluorescent probes or special imaging conditions are necessary. In the original realizations of these techniques, named FPALM (Hess, Girirajan, & Mason, 2006), photoactivated localization microscopy (PALM) (Betzig et al., 2006) and stochastic optical reconstruction microscopy (STORM) (Rust, Bates, & Zhuang, 2006), this was achieved by using photo-switchable fluorescent probes that can change their emission characteristics upon absorption of typically a photon of 405 nm wavelength. By regulating the intensity of this activation light and using high excitation laser powers to immediately image and bleach activated molecules, the number of molecules that are in the fluorescent state at any given time can be controlled so that emitting molecules are isolated and can be properly localized.

These probes can be photo-activatable/switchable fluorescent proteins (PAFPs), like PA-GFP, PAmCherry1 or mEos2 to list some of the most popular ones, pairs of cyanine dyes that exhibit photo-switching when in close proximity to each other, such as a combination of Cy3 and Cy5 (Bates, Blosser, & Zhuang, 2005; Heilemann, Margeat, Kasper, Sauer, & Tinnefeld, 2005), or photo-switchable organic dyes, such as photo-switchable rhodamines (Belov, Bossi, Fölling, Boyarskiy, & Hell, 2009; Fölling, Polyakova, et al., 2008). The individual probes have different strengths and weaknesses. The PAFPs, for example, offer very high specificity because after transfection of the cell with the correct DNA they get directly expressed by the cell. This means no further labeling steps are required. Organic dyes first need to be conjugated to typically an antibody and have to be introduced into the cell before they can label the target protein. On the other hand, organic dyes can offer much higher brightness (photons per molecule) directly benefitting the precision of the localization.

PAFPs are typically separated into three different classes (Stepanenko et al., 2011; Wiedenmann, Oswald, & Nienhaus, 2009): irreversibly photo-activatable ones

(Figure 3 a,b) that activate from a dark state to a fluorescent state, such as PAmCherry1, PA-GFP and PAmKate. These molecules typically release CO₂ (decarboxylation) during photo-activation. The second type consists of irreversibly photo-convertible fluorescent proteins (Figure 3 c,d) that switch their emission spectrum, such as mEos2 and Dendra2, and the mechanism is typically accompanied by a backbone cleavage event. The third type consist of reversibly photo-switchable fluorescent proteins (Figure 3 e,f).

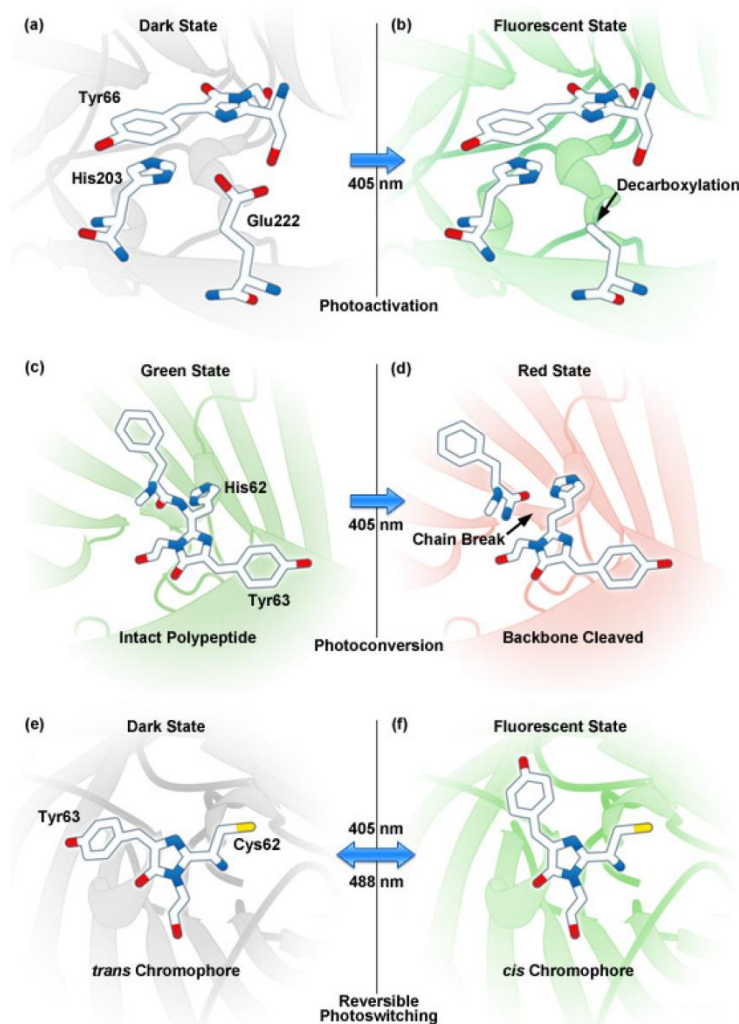


Figure 3. Classes of PAFPs. Based on the reversibility of the switching as well as if the non-activated state is fluorescent or not, PAFPs are typically classified as photo-activatable (a,b) if they irreversibly switch from a dark to a fluorescent state, photo-convertible (c,d) if they irreversibly switch their spectral emission characteristics or reversibly photo-switching if they can switch back and forth between the two states. [adapted from <http://zeiss-campus.magnet.fsu.edu/articles/probes/highlighterfps.html>]

As an example, we can take a closer look at the photo-activation mechanism of PAmCherry1 (see Figure 4). In its OFF form PAmCherry1 absorbs a violet photon and converts into an excited state and oxidizes the nearby group of anionic, carboxylic Glu-215. This leads to the formation of a radical at the Glu-215 residue which rapidly decarboxylates forming a [Glu-215-CH₂*] carbon radical. This

radical reacts with an oxygen molecule forming the [Glu-215-CH₂-O-O*] radical which then possibly abstracts a hydrogen from Tyr-67 C^β. This newly formed carbanion 2 is further oxidized by another O₂ molecule to form the ON state (adapted from (Fedor V Subach et al., 2009)).

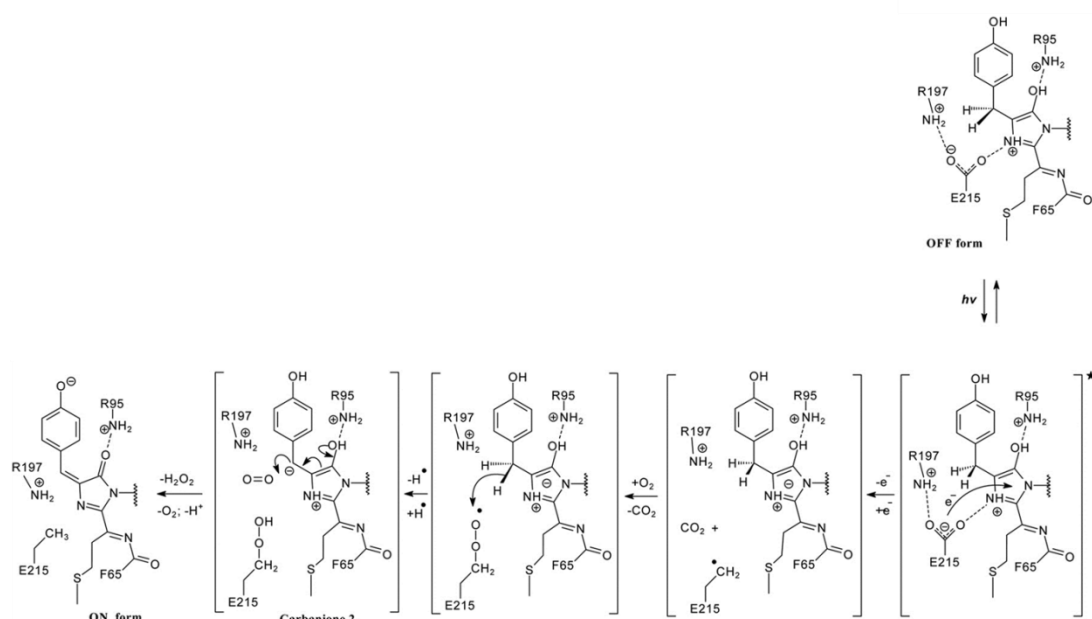


Figure 4. Suggested Photo-activation mechanism for PAmCherry1. Suggested mechanisms for the light induced conversion from the PAmCherry1 dark chromophore (OFF state) into the fluorescent state (ON state). Hydrogen bonds are shown with dashed lines. Intermediate compounds are shown in parentheses. The chromophore in the excited state is denoted with asterisk. $h\nu$, indicates the illumination with violet light. Migration of the electron density is shown with curved arrows. (adapted from (Fedor V Subach et al., 2009))

Imaging of individual fluorophores has also been achieved with conventional fluorescent probes by optically pumping all of the molecules into long-lived dark states and observing their spontaneous transitions back into the fluorescent state. This typically requires special embedding buffers to preserve the molecules in the dark states (Baddeley, Jayasinghe, Cremer, Cannell, & Soeller, 2009; Fölling, Bossi, et al., 2008; Vogelsang, Cordes, Forthmann, Steinhauer, & Tinnefeld, 2009).

2.4.2.2 Localization-based nanoscopy setups

Since the absorption of the near UV photons and thus the activation of the molecules is a stochastic process, these techniques are typically implemented using a widefield type illumination geometry for both the excitation and the activation laser. This requires the use of cameras with a high sensitivity to properly observe the single molecule events. Electron multiplying charge-coupled device (EMCCD) cameras have been the camera of choice due to their high sensitivity which makes them ideal for single-molecule experiments.

One of the advantages of light microscopy is that samples can be imaged in 3D. For nanoscopy techniques, this is typically achieved by forcing the PSF to change its shape depending on the axial position through, for example, the introduction of astigmatism in the detection beam path (B. Huang, Wang, Bates, & Zhuang, 2008), or by imaging multiple planes at a time as in the Biplane scheme (Juetten et al., 2008) that has been implemented for this work. As is shown in Figure 5a, in a Biplane setup, the emitted fluorescence light is split into two separate beam paths of different optical lengths using a 50/50 beam splitter cube and then imaged onto different regions of the camera chip. The camera is positioned so that one beam path is focusing in front of the chip while the other beam has a virtual focus behind the chip. This is equivalent to imaging two axially shifted planes, one slightly above the focal plane of the objective and the other one below, onto the two regions on the camera. With this geometry, the position of an emitter can be determined based on ratio of fluorescence in the two regions. Figure 5b shows a montage of images of an emitter at different axial positions. For better localization precision, the image of an emitter can be fit with prerecorded calibration data consisting of images of a typically 100 nm diameter fluorescent bead at different axial positions. In that case, emitters can be localized over a depth of about 1 – 2 μm around the focal plane (Mlodzianoski, Juetten, Beane, & Bewersdorf, 2009).

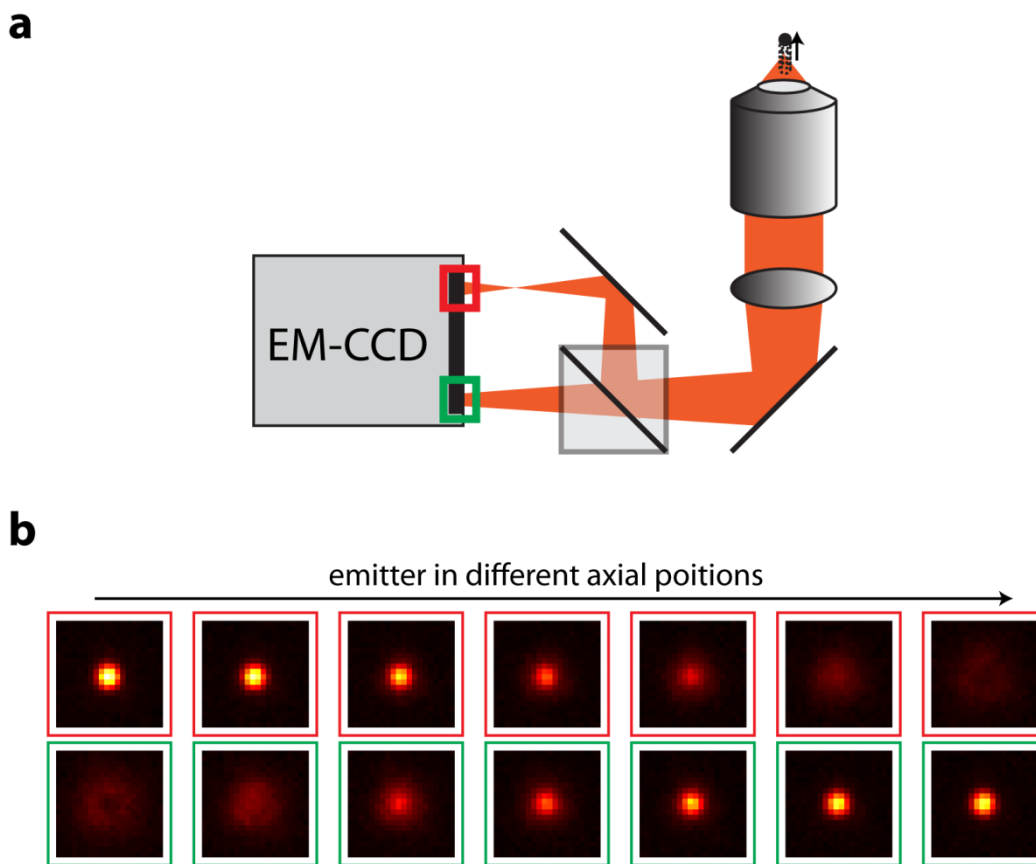


Figure 5. Biplane Scheme. (a) The collected fluorescence is split onto two beam paths of different optical length and imaged onto different regions of the camera. This is equivalent to the camera imaging two axially shifted regions at the same time. (b) Montage of images of an emitter in different axial positions.

The 3D nature of samples, however, can also be detrimental. Because of the widefield type geometry for the excitation and activation lasers, molecules will be activated and then excited throughout the whole depth of the sample. Because only molecules close to the focal plane can be properly localized, all of the out of focus molecules will be prematurely depleted from the pool of available labeling molecules while at the same time increasing the recorded background. This can significantly affect localization precision.

There are several ways to combat this effect. For experiments where one is only interested in events that happen very close to the coverslip total internal reflection geometries have been implemented that limit illumination of the sample to a depth of about 100 nm from the coverslip (Betzig et al., 2006). Or one can have the excitation and activation laser not parallel to the detection but instead at a highly inclined angle or even completely perpendicular using light sheets to illuminate the whole field of view (FOV) (Santi, 2011; Tokunaga, Imamoto, & Sakata-sogawa, 2008). In the case of perpendicular orientation this requires, however, more complex sample mounting geometries.

Another very promising alternative is to use a Ti:Sapphire laser for the activation. Due to the inherent optical sectioning of the two-photon process this confines activation events to the focal plane, preserving out of focus molecules for later imaging. This has already been demonstrated in cell culture (Diaspro et al., 2006; Schneider, Barozzi, Testa, Faretta, & Diaspro, 2005; Testa, Garre, et al., 2008; Testa, Parazzoli, et al., 2008; Vaziri, Tang, Shroff, & Shank, 2008; York et al., 2011) but spectral information about the efficiency of 2PA for the most commonly used PAFPs was not available. Chapter 4 summarizes spectroscopic studies that investigate the ability to use 2PA for the popular PAFPs PAmCherry1, PAmKate, PA-GFP, mEos2 and Dendra2.

2.4.2.3 Cameras

For localization-based nanoscopy techniques, one of the main factors that limit the imaging speed is the readout speed of the camera because tens of thousands of camera frames need to be recorded. Until recently, EM-CCD cameras were de facto the camera of choice because of their high sensitivity. This high sensitivity is caused mostly by two factors: the very high quantum efficiency (QE) of >90% of the back-thinned, back-illuminated camera chips and the very low readout noise. The low readout noise is due to the electron multiplication which gave these cameras their name. Figure 6 shows the typical structure of an EM-CCD camera. Similar to regular CCD cameras, the accumulated signal is shifted downwards towards the Horizontal serial register from where it is read out line by line and since the charge of each pixel passes through the same readout structure, the readout noise characteristic is the same for each pixel. In an EM-CCD camera, before being read out, each pixel charge first passes through an additional gain register, here called multiplying register, which consists of hundreds of stages. In each stage the signal has a chance to be amplified via impact ionization, similar to an avalanche diode. The probability for amplification at each stage is fairly small but due to the high number of stages the overall gain can be very high. Since the charge of each pixel is increased so dramatically before being read out, the typically few electrons introduced as readout noise by the readout process are negligible in comparison.

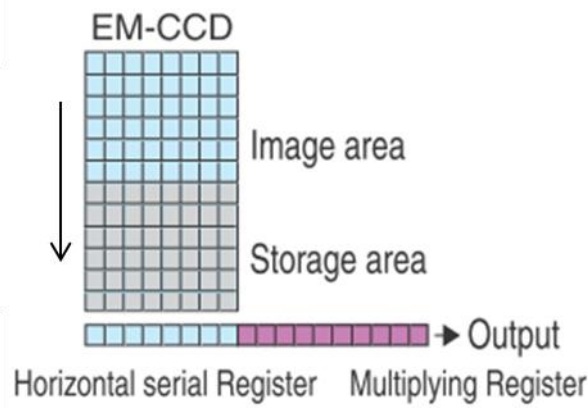


Figure 6. Readout structure for an EM-CCD camera. Accumulated signal is shifted downwards into the Horizontal serial Register and is converted to voltage and then digital units after passing through the Multiplying Register. Compared to the high overall gain of the Multiplying Register the few electrons readout noise are negligible.[adapted from http://sales.hamamatsu.com/assets/pdf/hpspdf/e_imagemtec.pdf?src=micro-camera]

However, the amplification process itself introduces a new source of noise that results in a decrease of the signal to noise ratio by a factor of $\sqrt{2}$ (Robbins, Member, & Hadwen, 2003). For localization experiments, this extra noise is equivalent to a factor of 2 worse QE. To account for this fact an effective QE is introduced as effective QE = QE / 2 \approx 47%. Additionally, the readout speeds of EM-CCD cameras are relatively slow due to this serial readout scheme.

The recently introduced sCMOS cameras, which offer a QE of up to 73% differ from the EM-CCD cameras in that each pixel has its own readout structure for converting the accumulated charge into voltage which is then converted into digital units on a column basis. This parallelization yields much higher readout speeds, up to 400 fps for a 512x512 camera pixel region of interest, but additionally, it means that every pixel on the camera chip has its own unique readout noise characteristic. This can be seen in Figure 7. It shows maps for the variation from pixel to pixel for the variance, the offset and the gain (a,c,e) and histograms for the variance, offset and gain (b,d,f). Huge differences can be seen between different pixels which would lead to the introduction of artifacts if they would not be accounted for.

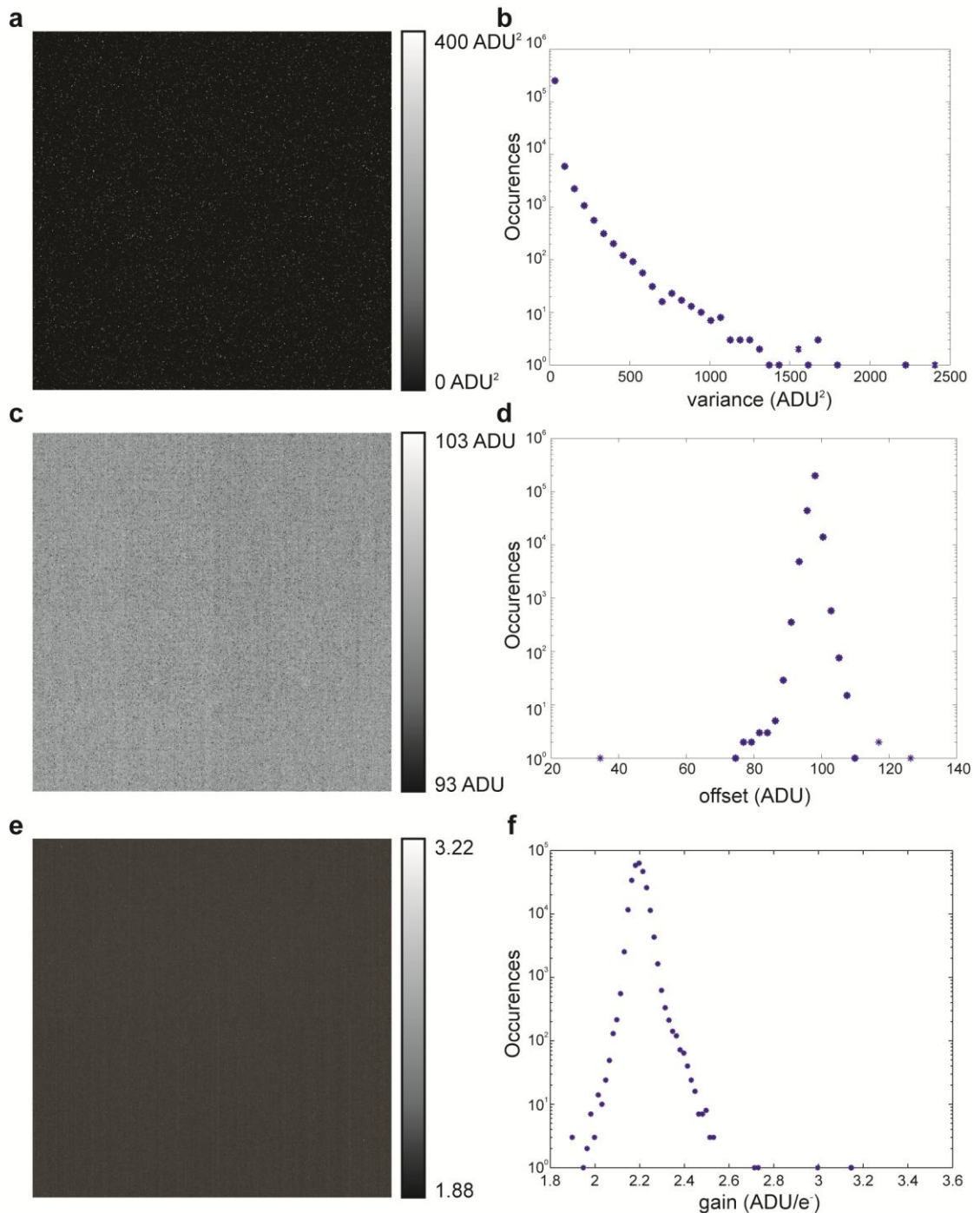


Figure 7. Maps and histograms of the pixel-dependent noise characteristics (pixel variance, offset and gain) in a 512x512 pixels sub-region centered on the sCMOS chip of a Hamamatsu ORCS Flash 4.0 camera. (a,c,e) Maps of values for noise variance (a), offset (c) and gain (e). (b,d,f) Histograms of the variance, offset and gain values, respectively. [adapted from submitted manuscript]

We have developed new sCMOS-specific localization algorithms for image segmentation, particle localization, particle rejection and uncertainty estimation in our lab that use calibration data recorded prior to an experiment to account for the pixel dependent variance.

3 Instrumentation

For this dissertation I constructed two setups which shared the same battery of lasers: one for 3D imaging with either 405 nm activation or 2PA and the other one for video-rate 2D imaging using a sCMOS camera.

A manuscript detailing the results for the 2PA setup is in preparation. A manuscript including the sCMOS setup has been submitted for publication.

3.1 Two-photon activation Setup

The 2PA setup consists of a wide field type system built around a commercial upright microscope stand (IX71, Olympus). To increase its versatility, five different lasers were used to supply activation and excitation wavelengths over the whole visible spectrum (see Table 1).

Table 1: Available Laser Lines

Laser Line [nm]	Maximum Laser Power [mW]	Product specification
405	20	compact solid state laser, CrystaLaser
488	1500	Innova 70, Coherent Inc.
556	250	compact solid state laser, Laserglow
568	700	Innova 300, Coherent Inc.
647	900	
700 - 1000	3500 (average power)	Mai Tai, Spectra-Physics

As shown in Figure 8, the lasers, except for the Ti:Sapphire laser, were arranged on a separate table and coupled into the system using a multimode fiber.

The 405 nm laser beam size was first expanded to match that of the other lasers by sending it through a pair of lenses (AC254-040-A and AC254-060-A, Thorlabs) in a 1.5x-telescope arrangement. The individual laser beams were then combined into a single beam using dichroic mirrors (FF593-Di02, Semrock; FF506-Di02, Semrock; z410rdc, Chroma) before being split into two beam for the 2PA setup and the sCMOS setup, respectively, using a polarizing beam splitter cube (PBS201, Thorlabs). By using half wave plates for the linearly polarized 488 nm, 556 nm and 568/647 nm lasers and a quarter wave plate for the circularly polarized 405 nm laser the orientation of polarization and thus the ratio of laser power being delivered to the two setups can be controlled for each laser individually.

In each of the beam paths after the polarizing beam splitter cube, an acousto-optic tunable filter (AOTF_nC-400.650, AA Opto-Electronic) is used for wavelength selection and power regulation before the laser beam is focused onto a rotating diffusor (NT47-989, Edmund Optics) using an achromatic lens (AC254-100-A, Thorlabs) and coupled into a multimode fiber using another lens (AC254-030-A, Thorlabs). The rotation for the diffusor is generated by a computer fan motor and produces a homogeneous intensity distribution at the fiber output when averaged over short time periods.

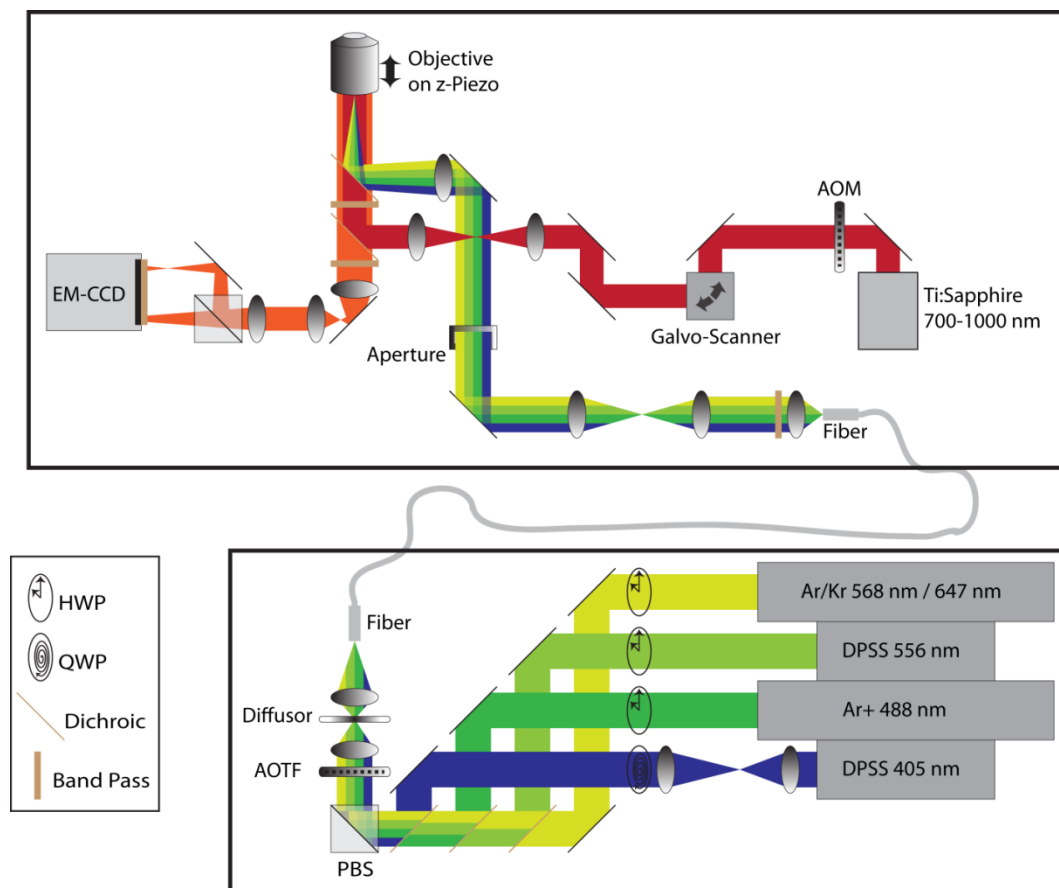


Figure 8. 2PA setup. The laser beams from 4 different lasers are combined using dichroic mirrors and then coupled into a multimode fiber after passing through an AOTF for wavelength selection and power control and through a rotating diffusor. The combined laser beams are coupled out of the fiber and then focused into the back aperture of the objective lens for a wide field type illumination. A Ti:Sapphire laser can be used for 2PA. It is focused into the sample by the objective lens after passing through an acousto-optic modulator for power control and a 2D galvo scanner. The emitted fluorescence is separated from the excitation and activation light using dichroic mirrors and then split into two beam paths of different lengths using a non-polarizing beam splitter cube. The two paths are then imaged onto separate regions of an EM-CCD camera after passing through a band pass filter.

On the microscope table the beam is coupled out of the fiber using a 10x objective lens (, Newport), expanded using two lenses (AC254-035-A and AC254-250-A, Thorlabs) and focused into the back aperture of the oil-immersion objective lens (UPLSAPO 100XO, Olympus) with another achromatic lens (AC254-500-A,

Thorlabs) to achieve a wide field type illumination in the sample. The objective is mounted on a piezo actuator (Pifoc P-726.1CD, Physik Instrumente L.P.) for axial scanning. A rectangular aperture of about 4.2 mm x 8.3 mm size, located in a conjugated plane to the image plane, creates a well-defined illumination field of about 15 μm x 30 μm in the sample.

Fluorescence is collected in epi mode and separated from the excitation and activation lasers using a dichroic mirror and long pass filter (Di01-R561 and LP02-568RU, Semrock, for the PAFPs mEos2, PAmCherry1, PAmKate and Dendra2 or z488rdc, Chroma, for PA-GFP) in the microscope stand's filter cube and a short pass filter (FF01-680/SP) before the tube lens. After passing through the tube lens and a pair of lenses (AC254-150-A and AC254-300-A, Thorlabs) for an additional 2x magnification it is split equally into two separate beam paths using a non-polarizing beam splitter cube (BS016, Thorlabs) and the two separate paths are then imaged onto different regions of the chip of an EM-CCD camera (iXon DU897DCS-BV, Andor Technology) for the Biplane scheme after passing through an additional band pass filter (FF01-609/57, Semrock, for mEos2, Dendra2, PAmCherry1 and PAmKate or FF01-534/42, Semrock, for PA-GFP). The length difference of the two paths is approximately 13 mm which results in a plane separation of about (650 ± 50) nm (Figure 9c).

Figure 9a shows x-z sections through 3D image stacks of 100 nm fluorescent beads (F-8801, Invitrogen) emitting at 605 nm and excited using the 568 nm laser, recorded at different positions in the FOV (Figure 9b). The size and shape remains the same throughout the FOV. The FWHM of the PSF is (578 ± 8) nm axially and (271 ± 3) nm laterally (Figure 9d, e). A measure for the achievable localization precision is shown in Figure 9f. Here the position of one bead is plotted as determined for each frame of a 10,000 frame series.

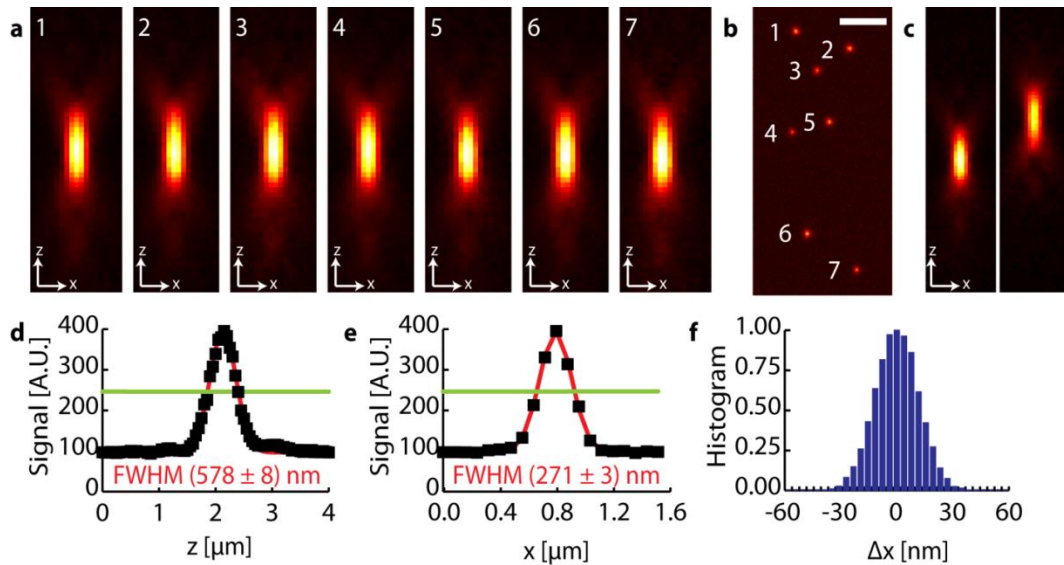


Figure 9. Setup characterization. (a) x-z views of PSFs at different positions in the FOV (b); (c) PSFs of the same bead recorded in the two planes of the Biplane scheme; (d,e) axial (d) and lateral (e) intensity distribution through the center of a PSF; values for the FWHM are averages from the 7 PSFs; (f) normalized histogram of the determined positions of a bead for every frame of a 10,000 frame series; pixel size for (a) and (c) is 80 nm in x- and 50 nm in z-direction; scale bar in (b) is 5 μm;

For 2PA, I incorporated a Ti:Sapphire laser emitting in the near infrared (NIR) into the setup. In order to be able to modulate its power the NIR beam is first passed through an acousto-optic modulator (MT110-B50A1.5-IR-Hk, AA Opto-Electronic). It is then relayed through a two-axes galvo scanner (VMPLUS 500, General Scanning), expanded using two lenses in a 10x-telescope arrangement (AC254-050-B and AC254-500-B, Thorlabs) and coupled into the microscope stand between the tube lens and the dichroic mirror for the visible beam path using a dichroic short-pass mirror (FF670-SDi01, Semrock). The objective then focuses the beam into the sample. The galvo mirrors are located in a plane conjugated to the back aperture of the objective to warrant space invariant focus quality over the FOV.

Figure 10a shows the z-profile of the two-photon excitation created by the scanned Ti:Sapphire laser focus. It was generated from images of fluorescent beads (FF8801, Invitrogen) and demonstrates the quality of the focus with an axial FWHM of (750 ± 70) nm and thus the achievable level of confinement of the activation in a biological sample. This agrees well with typically achievable results using similar optical components (Niesner, Andresen, Neumann, Spiecker, & Gunzer, 2007; Rubart, 2004; Vaziri et al., 2008; York et al., 2011).

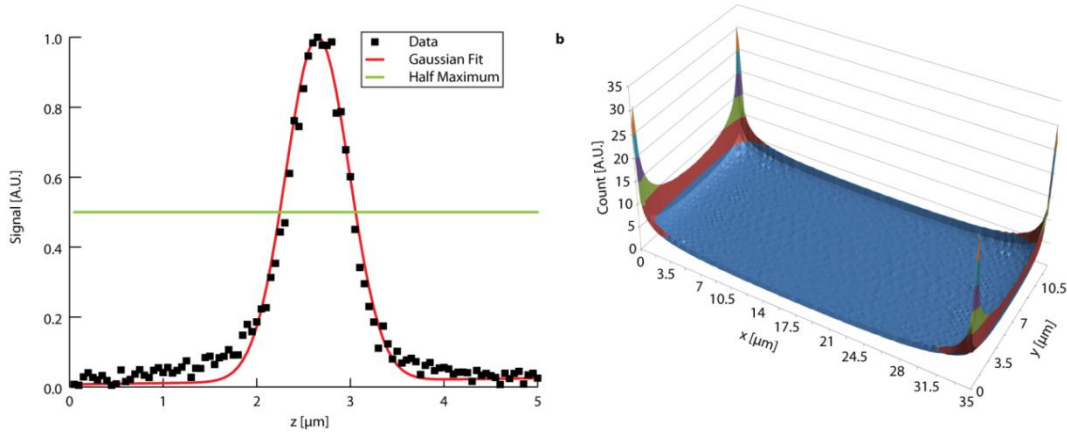


Figure 10. Two-photon setup parameters. (a) z-profile of the system using the Ti:Sapphire laser; (b) time averaged intensity distribution of the scan pattern; the areas of higher intensity along the edges of the scan pattern are blanked by the smaller FOV leaving a homogeneous distribution;

The 2D galvo scanner is set to scan an area of about $35 \mu\text{m} \times 17.5 \mu\text{m}$ using a frequency of 543 Hz on the x-axis and 530 Hz on the y-axis resulting in a Lissajous pattern for the scanned beam path. To achieve a more homogeneous illumination, the scanner runs through three iterations of the Lissajous pattern which are each shifted by about 246 nm along the y-axis against the previous pattern before repeating this cycle. The illumination intensity distribution for the scanned area of the resulting scan pattern is shown in Figure 10b. The illumination dose is about 31 times higher in the corners of the scanned area compared to the center. However, the smaller $30 \mu\text{m} \times 15 \mu\text{m}$ FOV of the excitation beam cuts away the areas at the edge with higher illumination dose resulting in a homogeneous illumination throughout the FOV. Use of this pattern scanning allows us to cover all areas of the FOV in each frame. The incomplete coverage for each individual frame is not a problem because the activation should be sparse anyway and the gaps will be covered in subsequent frames.

To control the instrument, I developed a LabVIEW program that incorporated the controls for each element. The camera, AOTF and piezo actuator were synchronized based on the fire pulse of the EM-CCD camera that was detected using the counter of a data acquisition unit from National Instruments (USB-6008, National Instruments). The software was set up to accept preprogrammed recording conditions (exposure time, FOV size, cycles, z-steps per cycle, frames per z-step, laser power changes, scanning speed and scanned area). Parameters could also be changed manually at any time during the experiment.

3.2 sCMOS setup

The second setup (see Figure 11) uses the same battery of lasers and also uses an AOTF (AOTFnC-400.650, AA Opto-Electronic) to select the laser lines and control the laser power. The beam is then focused onto a rotating diffusor (NT47-989, Edmund Optics) using an achromatic lens (AC254-100-A, Thorlabs) and coupled into a multimode fiber using another lens (AC254-030-A, Thorlabs). The rotation for the diffusor is generated by a computer fan motor and produces a homogeneous intensity distribution at the fiber output when averaged over short time periods.

It uses a Zeiss inverted microscope stand (Axio Observer D1, Zeiss) with a 63x water immersion objective (C-Apochromat 63x/1.2 W Corr, Zeiss). Additionally to the lasers that are coupled onto the optical table with the multimode fiber the setup can be combined with a fiber laser emitting at 642 nm (642 nm Visible Fiber Laser, 500 mW, MPB Communications) using a dichroic mirror (FF505-SDi01, Semrock) on a magnetic mount (KB3X3, Thorlabs). The combined laser beams are then focused into the back aperture of the objective lens using an achromatic lens (AC254-500-A, Thorlabs) to achieve a wide field type illumination.

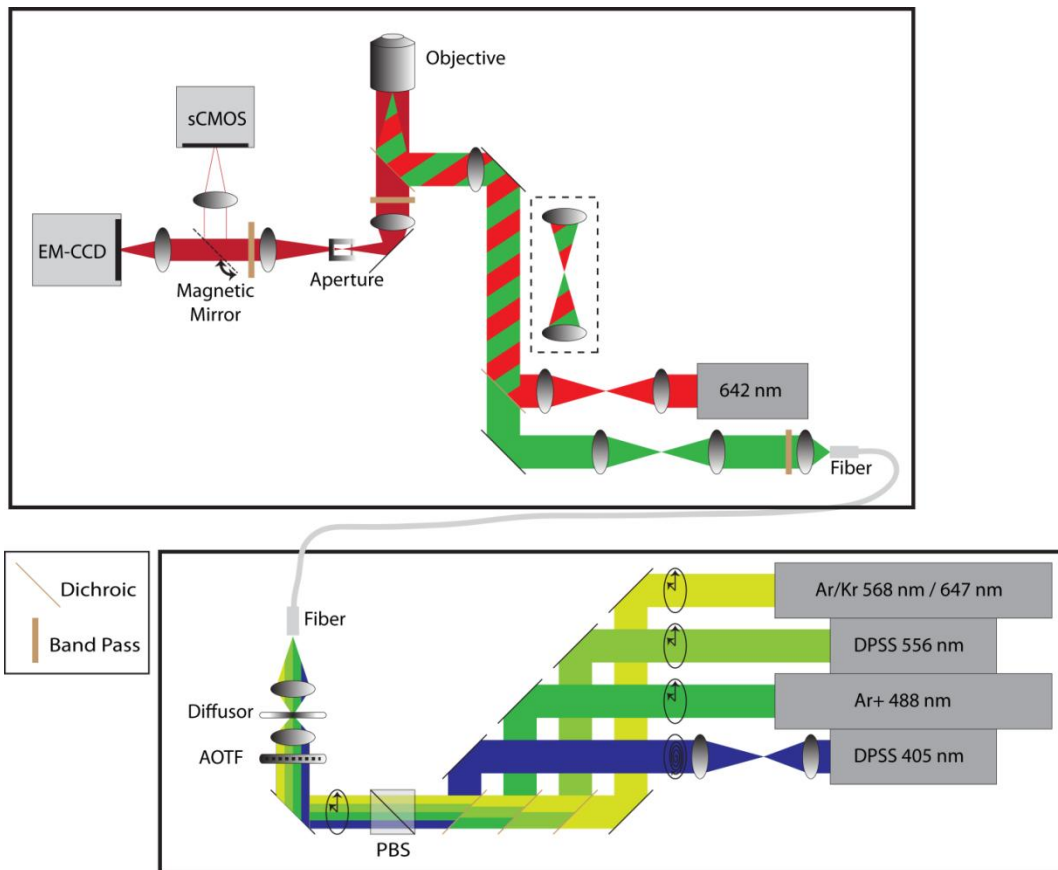


Figure 11. sCMOS setup. The same battery of lasers that was used for the 2PA setup is also used for the sCMOS setup. The laser beam is transmitted through the polarizing beam splitter cube and passed through a half wave plate to orient the polarization according to the input requirements of the AOTF. On the optical table a fiber laser emitting at 642 nm is then combined with the excitation laser beams and focused into the back aperture of the objective for a wide field type illumination. An optional 2x telescope can be flipped into the excitation beam to change the size of the illuminated spot in the sample. The emitted fluorescence is separated from the excitation light using a dichroic mirror and then focused onto either an EM-CCD camera after passing through a pair of lenses for an additional 2.5x magnification or onto a sCMOS camera after an additional 0.6x magnification. The different magnifications are used to match the resulting pixel sizes of the cameras.

The fluorescence is collected in epi mode and separated from the excitation light using a dichroic mirror (Di01-R405/488/561/635, Semrock) and two band pass filter ((FF01-446/523/600/677 and BLP01-635R-25, Semrock). It is then either imaged onto an EM-CCD camera (iXon DU897DCS-BV, Andor Technology) after passing through a pair of lenses (AC254-100-A and AC254-250-A, Thorlabs) for an additional 2.5x-magnification for a pixel size corresponding to 102 nm in the sample or, using a mirror on a magnetic mount (KB3X3, Thorlabs), it is imaged onto a sCMOS camera (Orca Flash 4.0, Hamamatsu) after passing through a pair of lenses (AC254-100-A and AC254-060-A, Thorlabs) for an additional 0.6x-magnification for a pixel size corresponding to 103 nm.

The microscope was controlled using a custom LabVIEW program to control the AOTF and the EM-CCD camera and the software HCimage (Hamamatsu) to control the sCMOS camera.

4 Two-photon activation of photo-activatable fluorescent proteins

To fully take advantage of 2PA, the spectroscopic properties of the available probes have to be known and understood. It is, for example, crucial to know at which wavelengths PAFPs can be activated best to perform imaging experiments most efficiently. This chapter describes my investigations of this question for a number of commonly used PAFPs.

These results are currently being compiled into a manuscript for publication.

4.1 Biological background

4.1.1 Cloning

I obtained bacteria expressing the PAFPs in the cytoplasm from my collaborator. To improve the expression efficiency for mEos2 I first extracted the plasmid and subcloned it into a new, high efficiency vector (pET). The mEos2:pET vector was then used to transform competent cells (Max Efficiency DH5 α , Invitrogen). Positive clones were selected and cultured for further experiments. The exact protocol and plasmid sequences can be found in the appendix.

4.1.2 Sample preparation

I used *E. coli* bacteria expressing PAFP in the cytoplasm. This provides a biological environment for the investigated probe so that obtained results can be more readily applied to super-resolution imaging. Bacteria were grown over night at 37 degree Celsius in LB medium supplemented with 100 $\mu\text{g/ml}$ ampicillin and 0.004% arabinose. They were then washed twice in phosphate-buffered saline (PBS), fixed for 30 minutes in 4% paraformaldehyde at room temperature, and washed again three times in PBS. For imaging, 10-20 μl of the bacteria-PBS stock were added onto a poly-L-lysine coated coverslip (No. 1.5 thickness), mounted on a microscope slide and sealed using two-component silicon glue (twinsil 22, Picodent).

4.2 Recording protocol

Two different illumination schemes were used during experiments. In the first one, the sample is continuously activated by scanning the observation volume (15 x 30 x 3 μm^3) with a focused laser beam from the mode-locked Ti:Sapphire laser and excited by widefield illumination with a continuous-wave laser. The second scheme alternates between the excitation laser illumination and the activation

laser illumination, starting with the excitation period. The duration of the activation and excitation periods are identical and range from 300 ms each up to one second each. The resulting fluorescence signal is imaged in epi fluorescence mode with a 100x, 1.4 NA oil-immersion objective onto an EM-CCD camera. Due to the high sensitivity of this method, only microscopic sample quantities (as little as ~ 5 bacteria) are required per measurement.

4.3 Data analysis

4.3.1 Curve preprocessing

Two regions of equal size are selected on the camera chip. The emitted fluorescence of the sample is imaged into one of the two regions, the FOV (region I, red box in Figure 12), whereas the other region (region II, yellow box in Figure 12) is not illuminated.

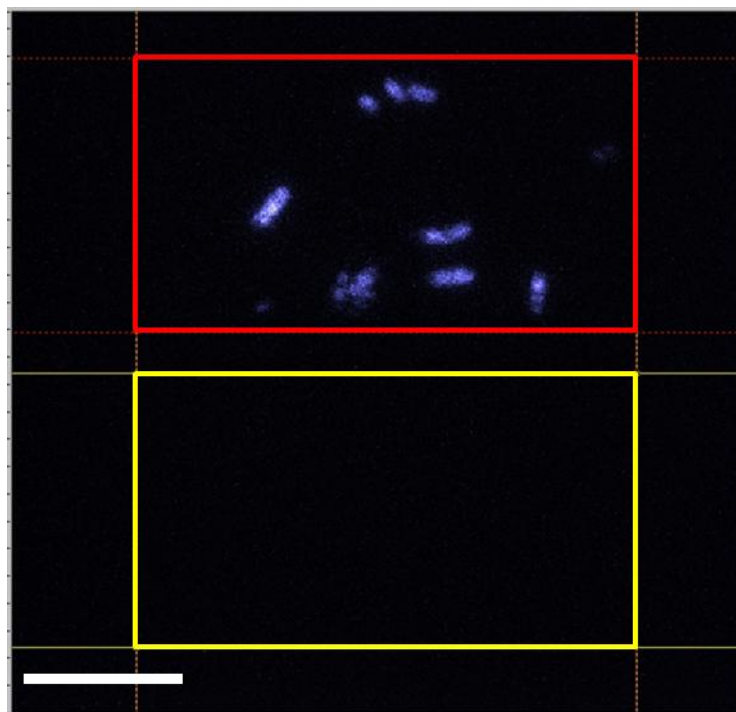


Figure 12. Typical camera frame during acquisition. The fluorescence signal from the sample is imaged in region I (red box) while region II (yellow box) is not directly illuminated and only exhibits background signal. Scale bar: 10 μm .

For each frame the signal in both regions is summed up and the sum of region II is subtracted from the sum of region I to correct for background and camera offset. The resulting data shows a periodic modulation (see inset in Figure 13a) corresponding to the sample moving in and out of focus due to the performed axial

scanning. The periodic increase in signal can also be further affected by two-photon excited fluorescence of the activated species which would increase the signal further when the scanned Ti:Sapphire laser focus is in the same plane as the imaged bacteria. The minima in the signal represent fluorescence caused only by excitation by the 488 nm, 556 nm or 568 nm laser (depending on the experiment). Therefore, for further analysis, only the lower boundary curve (dark line in Figure 13b) is used. To obtain this curve, the data was divided into portions containing 14 frames each, where the first two and last two data points would also be part of the previous and subsequent portion, respectively, and only the minimum of each chunk was selected.

As observed, the signal first increases dramatically due to photo-activation followed by a slow decrease of the signal where photo-bleaching dominates.

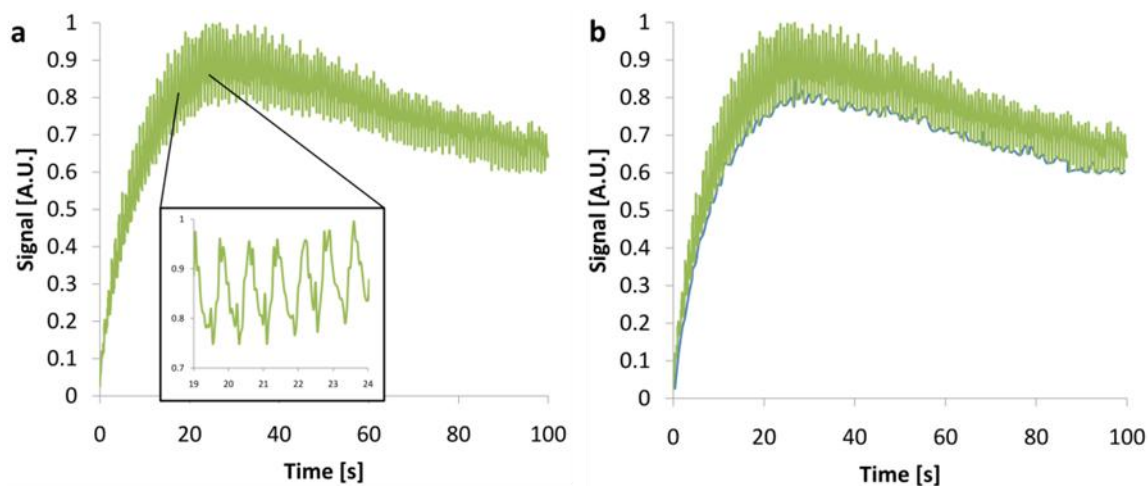


Figure 13. Data pre-processing. (a) Activation curve obtained by integrating the signal over the FOV and subtracting the integrated signal of a non-illuminated region of the same size as the FOV. The periodic modulation (see inset) is due to axial scanning. (b) Activation curve and lower boundary curve (dark line). The lower boundary curve is used for analysis to exclude effects due to two-photon excitation which would exhibit a periodic modulation due to the axial scanning.

4.3.2 Fitting

In order to extract the activation rate from this activation curve, I described the activation process using a three-state model (see Figure 14) in which molecules turn from an initial non-activated state I into a fluorescent state F with an activation rate k_{act} that is only dependent on the activation laser. From there they transfer into a bleached state B described by a bleaching rate k_{bl} .



Figure 14. Three-state model. Molecules are activated out of the dark, inactive state I into the fluorescent state F with the activation rate k_{act} . From there they eventually bleach with the bleaching rate k_{bl} .

This model is represented by the rate equations

$$\frac{dN_I(t)}{dt} = -k_{act} N_I(t) \quad (5)$$

$$\frac{dN_F(t)}{dt} = k_{act} N_I(t) - k_{bl} N_F(t) \quad (6)$$

$$\frac{dN_B(t)}{dt} = k_{bl} N_F(t) \quad (7)$$

where N_I , N_F and N_B represent the number of molecules in the respective states at each time point t . Solving this system of linear differential equations yields the number of fluorescent molecules as a function of time:

$$N_F(t) = A(e^{-k_{act}(t-t_0)} - e^{-k_{bl}(t-t_0)}) + C \quad (8)$$

Here A is an amplitude factor representing the total number of molecules in the observed sample volume, C represents an offset of the recorded signal and to accounts for any pre-activated molecules. Since the observed fluorescence signal is proportional to N_F , we fit the observed data with a curve described by Equation 8. No assumptions about the type of activation have been made, so this allows determining the activation rate independent of the used activation laser, laser power and bleaching rate.

4.4 Activation rates for various photo-activatable fluorescent proteins

Figure 15 shows the determined activation rates k_{act} for the widely used proteins PAmCherry1 (Figure 15a), PAmKate (Figure 15b) and PA-GFP (Figure 15c) as a function of the average activation laser power P_{avg} in the sample for different wavelengths. The also investigated PAFPs Dendra2 and mEos2 did not show sufficient activation using the Ti:Sapphire laser to be quantifiable. Measurements were repeated 3-14 times for different FOVs and samples at each wavelength and P_{avg} . For each wavelength, the data points were fitted with a polynomial function of P_{avg} consisting of a 2nd and 3rd order term representing two-photon and three-photon activation, respectively, and a constant term set to the cross-talk activation value (i.e. activation due to the excitation laser).

Activation rates were observed to decrease with increasing wavelength. The fits show clear two-photon dependence which is replaced by a higher order dependence for higher P_{avg} .

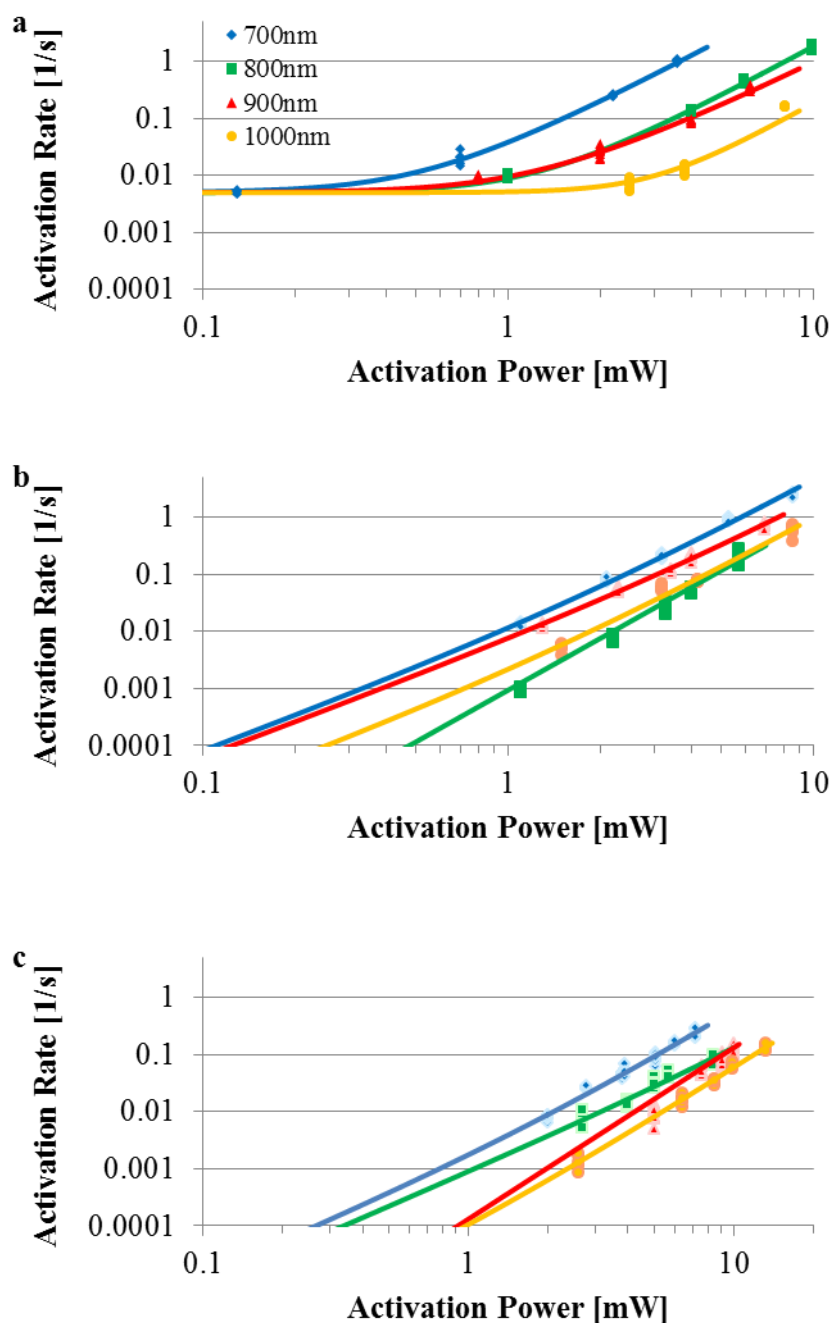


Figure 15. Determined activation rates for PAmCherry1 (a), PAmKate (b) and PA-GFP (c) for different wavelengths (700nm – blue, 800 nm – green, 900 nm – red, 1000 nm – yellow) as a function of activation power (PAmCherry1: 568 nm laser at 17.4 μ W; PAmKate: 556 nm laser at 16.2 μ W; PA-GFP: 488 nm laser at 0.1 μ W).

PAmCherry1 was the only PAFP from the pool of our investigated PAFPs that exhibited measurable activation by the readout laser. A typical recorded activation

curve using only the excitation laser at 556 nm and no activation laser can be seen in Figure 16a (green curve). The recorded signal exhibits a slow continuous increase due to the low activation rate of the 556 nm laser. Additionally shown is an activation curve using a 568 nm laser for excitation instead of the 556 nm laser (blue curve). This small shift in excitation wavelength suppressed any observable cross-talk activation and only reveals a decrease of the signal due to bleaching of the autofluorescence incurred by the mounting. However, when reverting to the original illumination scheme with both the excitation and the activation laser turned on we see a clear dependence of the activation rate on the 568 nm excitation laser power (Figure 16b). Higher 568 nm laser powers yield higher activation rates as is evident in the steeper slopes seen in Figure 16b recorded at 2.0 mW activation laser power at 700 nm and 33 μ W, 66 μ W and 153 μ W of excitation power at 568 nm for the blue, green and red curve respectively.

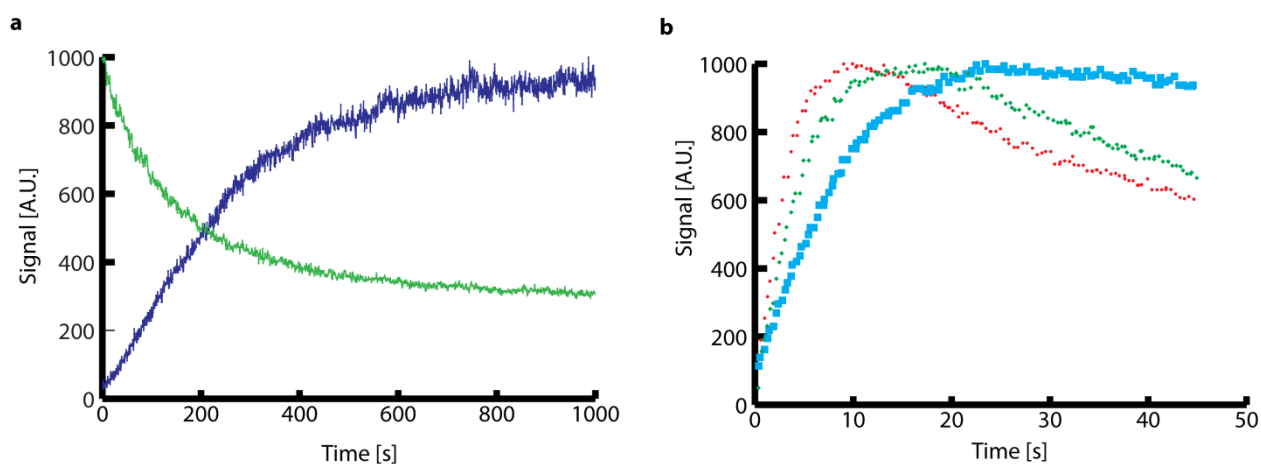


Figure 16. Dependence of the activation curve on the excitation laser. (a) Recorded fluorescence signal for PAmCherry1 illuminated with 556 nm laser light (blue curve) at 16.2 μ W showing a slow increase in signal due to activation by the 556 nm laser, and by 568 nm laser light (green curve) at 271 μ W showing no activation and only a slow bleaching of the autofluorescent background. (b) Activation curves for PAmCherry1 recorded at 2.0 mW of 700 nm laser illumination and 33 μ W, 66 μ W and 153 μ W of 568 nm laser illumination for the blue, green and red curve, respectively. The steepening of the activation slope with increasing 568 nm laser power demonstrates a positive dependence of the activation on the 568 nm laser.

To further probe this phenomenon, I altered the illumination style to a pattern in which I turned on the excitation and activation lasers in an interleaved fashion for identical durations of time.

Figure 17 shows a typical activation curve recorded with this new illumination pattern. The sample was alternately illuminated by the excitation laser at 568 nm (0.6 seconds, 21 μ W) and the Ti:Sapphire laser for activation at 700 nm (0.6 seconds, 2.0 mW). Since PAmCherry1 cannot be excited efficiently via 2PE at 700 nm the signal drops to background level during the activation periods.

As can be seen in the close-up (Figure 17 inset) the signal of the very first excitation period, which starts the experiment, shows no observable activation. This is in agreement with my previous result that the 568 nm laser alone is not sufficient to activate PAmCherry1. The clear jumps in signal that happen during the activation periods (highlighted by the red arrows) are due to activation by the Ti:Sapphire laser. Interestingly however, the signal during the subsequent excitation periods, which are each preceded by a 2PA period, shows an increase in the amplitude during the excitation laser period as highlighted by the blue arrows which cannot be explained using the simple activation model.

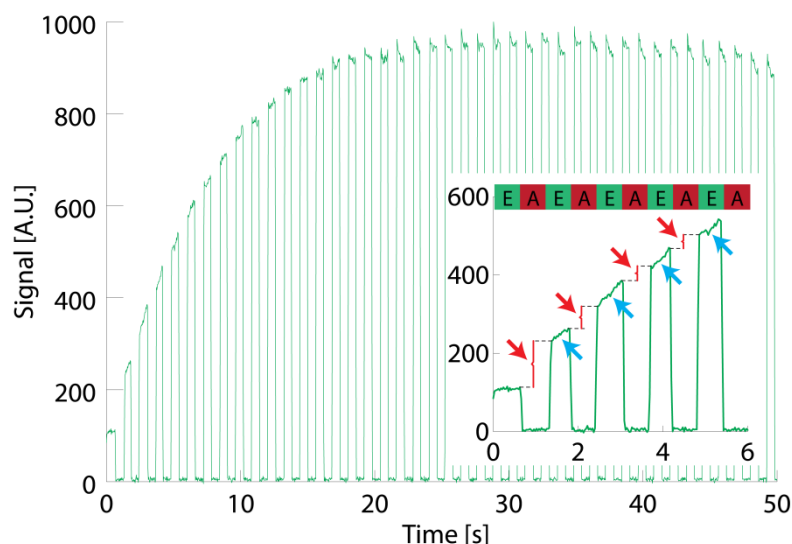


Figure 17. Sequential illumination signal response. Recorded fluorescence signal using a sequential illumination scheme for PAmCherry1. The inset shows a close-up of the first 6 seconds. The sequential illumination pattern is shown with excitation periods in green, marked E, and activation periods in red, marked A. Red arrows highlight abrupt increase of fluorescence signal after an activation period. Blue arrows highlight ongoing activation during excitation periods that were preceded by an activation period.

These deviations from the assumed simple activation model can be explained by expanding the activated, decarboxylated form of PAmCherry1 into at least three sub-states, the cis- and trans-form of the decarboxylated, deprotonated state and the decarboxylated, protonated state as shown in Figure 18, further referred to as state 1, 2 and 3, respectively. The observed results can be explained, if we assume that:

- the 568 nm laser is responsible for transitions from state 1 to state 2, from state 2 to state 1, and from either state 1 or state 2 to state 3;
- the transition rate from state 2 to state 1, $k(2-1)$, is larger than the rate from state 1 to state 2, $k(1-2)$;

-the activation laser (405 nm laser or Ti:Sapphire laser) is responsible for transitions from the inactive state to either state 1 or state 2, and from state 3 to either state 1 or state 2;

If we now look at the dynamics during the interleaved illumination then during an activation period, molecules are pumped from the inactive state and from state 3 into states 1 and 2. This describes the sudden increase in signal after activation periods due to the accumulation of molecules in the fluorescent state 1 (Figure 17 inset, red arrows). During the excitation period, molecules can then be pumped from states 1 or 2 into state 3, from which they cannot escape during the excitation period, and they can be switched back and forth between state 1 and state 2. Since $k(2-1)$ is larger than $k(1-2)$, molecules are primarily transitioning into the fluorescent state 1 which explains the observed activation during the excitation periods (Figure 17 inset, blue arrows).

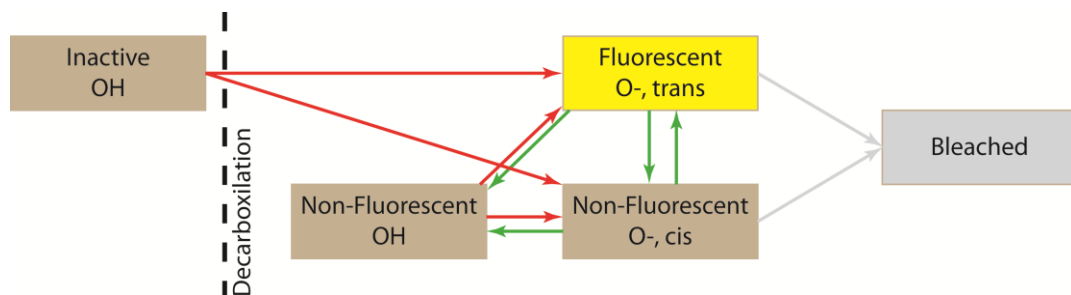


Figure 18. Proposed model of photon-driven transitions during the activation of PAmCherry1. The activation laser (405 nm or Ti:Sapphire laser shown as red arrows) can pump molecules from the carboxylated & protonated state into either the decarboxylated & deprotonated cis or trans state. Additionally, it can pump molecules from the decarboxylated & protonated state into the decarboxylated & deprotonated cis or trans state. The excitation laser (shown as green arrows) can only affect transitions between the cis and the trans state of the decarboxylated & deprotonated forms as well as pump molecules from the decarboxylated & protonated cis or trans state into the decarboxylated & protonated state.

5 Ring Canal imaging

Using single-molecule switching nanoscopy for imaging in thick samples is severely hampered due to the increase in background caused by the conventionally used 405 nm laser for activation. Here I present my results of imaging thick tissue samples using the 2PA setup introduced in chapter 3.

5.1 Biological background

Ring canals are ring-like intercellular connections. In *Drosophila*, they form during oogenesis and are essential for the development of a mature, functional oocyte: one germline cell undergoes four rounds of mitosis to form the oocyte and 15 nurse cells. However, the mitotic cleavage furrows during these cell divisions fail to completely separate the cells and instead halt their development. The addition of an actin cytoskeleton lining along these arrested cleavage furrows at the conclusion of mitosis then transforms them into ring canals and enable the nurse cells to contribute their cytoplasmic contents to the developing oocyte. These 16 interconnected cells form an egg chamber and start growing in size. As a consequence, ring canals can vary in size from several hundred nanometers up to 10 μm depending on the developmental stage of the egg chamber (see Figure 19) (Anderson & Huebner, 1968; KING & MILLS, 1962; Robinson, Cant, & Cooley, 1994).

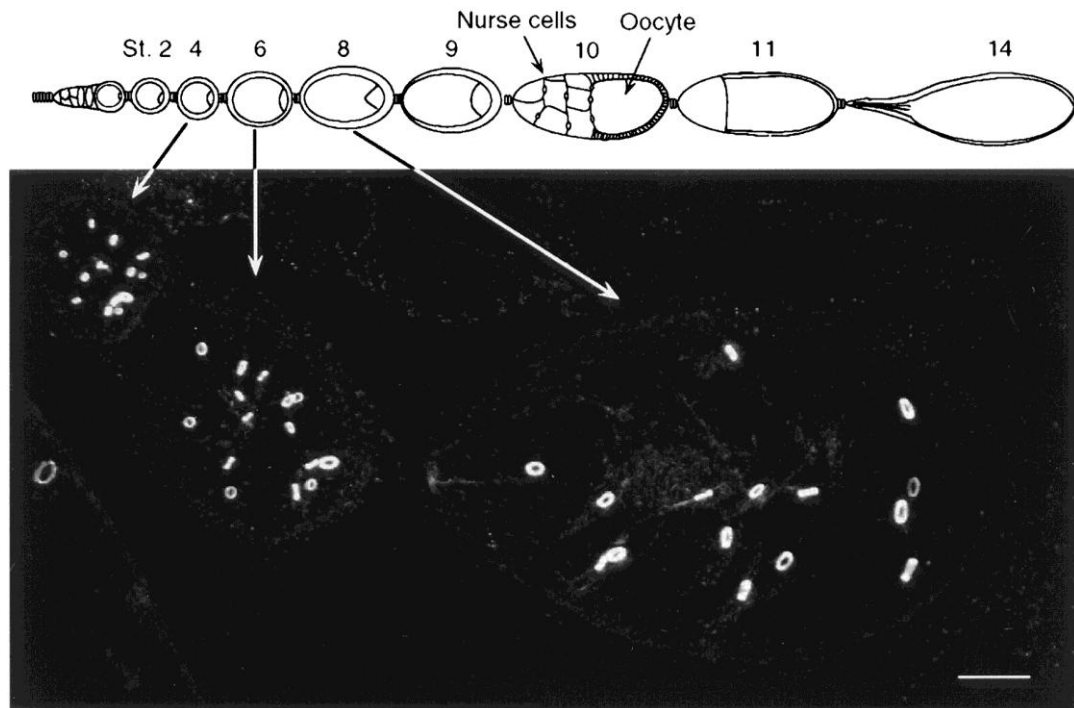


Figure 19. Ring canals labeled with phosphotyrosine via antibodies. Three egg chamber stages are shown to illustrate the growth of ring canals during oogenesis (scale bar is 10 μm). The upper drawing depicts a single ovariole from an ovary that contains a progression of egg chamber stages (Stage 2–14). The stage 10 egg chamber shows the cell types within each egg chamber: nurse cells and oocyte connected by ring canals and surrounded by follicle cells. (*taken from* (Cooley, 1998))

5.2 Comparison of embedding media related influences on the camera background

The localization precision in super-resolution microscopy is strongly affected by background. Especially when trying to image thick samples it is imperative to try and reduce all possible sources of background, starting with the mounting medium. Therefore, I first looked at various types of embedding media about the influence their autofluorescence has on the camera signal under imaging conditions. For each condition I recorded three series of 600 frames each and averaged the signal over the FOV and over the series. The exposure time (50 ms) and laser powers (568nm laser: 23.0 mW, 700 nm laser: 4.9 mW) were chosen to represent conditions during a typical super-resolution experiment. Figure 20 shows the average number of detected photons per pixel. The blue bars represent experiments using only illumination by the 568 nm laser whereas the red bars had both the 568 nm laser and the Ti:Sapphire laser turned on. The error bars show the standard deviation of the mean determined from the three series.

As can be seen, just adding a drop of low auto-fluorescence immersion oil (Olympus) onto the objective creates a background signal of about 17 photons per pixel. Adding a sample consisting of a drop of embedding media sealed between

coverslip and cover slide in general lowers the signal by up to 4 photons. This decrease is mostly caused by the reduced volume of immersion oil in the light path between the objective and the sample. Since glycerol led to the lowest observed background signal it was chosen as the basis for the embedding media for further biological experiments.

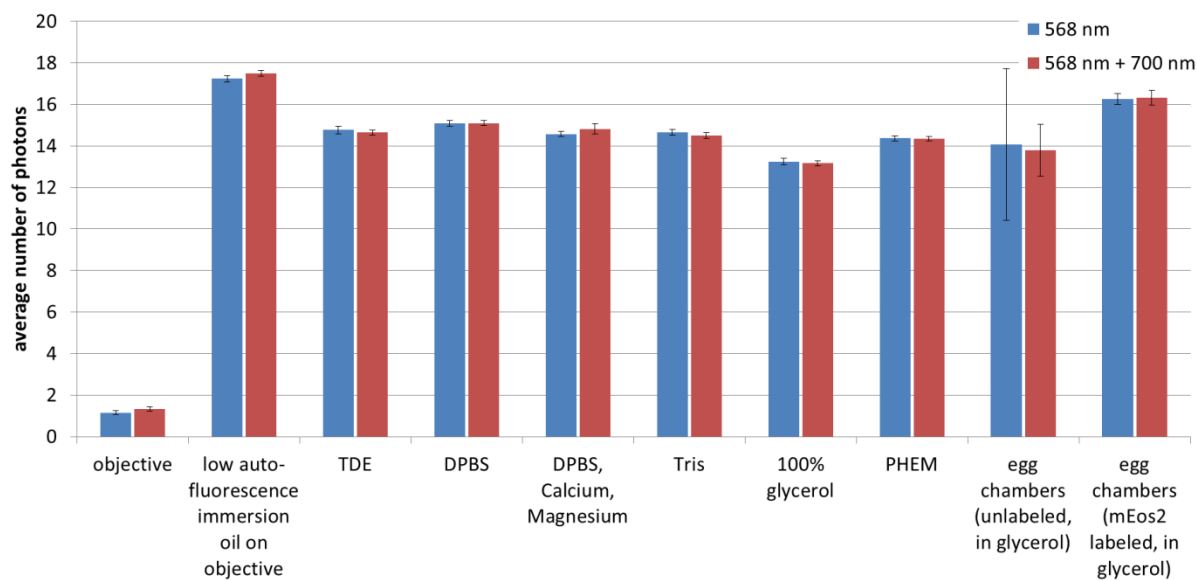


Figure 20. Comparison of autofluorescence of various embedding media. Of the investigated media, glycerol created the lowest background signal. The main contributor was the immersion oil for the oil-immersion objective.

5.3 Recording procedure

Egg chambers were dissected in Schneider's *Drosophila* medium (Invitrogen) supplemented with 0.2 mg/ml insulin. They were then fixed using fresh 4% paraformaldehyde in PBS for 40 minutes. After three 5-minute intervals of washing with PBS the egg chambers were mounted onto a #1.5 coverslip for imaging using a mounting medium consisting of 90% glycerol and 10% Tris buffer (0.2M, pH 8.0).

3D super-resolution imaging was performed with the 2PA setup described in chapter 3.1 using an exposure time of 50 ms per frame, an excitation intensity for the 568 nm laser of 5.1 kW/cm² and activation intensity ranging from 0 to 0.3 W/cm² for the 405 nm laser or an average power ranging from 0 to 4.9 mW for the Ti:Sapphire laser set to 700 nm.

Using the 405 nm laser for activation activates and bleaches probe molecules throughout the whole depth of the sample. To counter this, the volume of interest is recorded in several distinct axial steps with only a few tens to hundreds of

frames per step. This axial scan cycle is then repeated until the majority of the probe molecules have been imaged.

For a typical experiment 12 – 60 cycles were recorded consisting of 11 – 25 steps with 50 – 100 frames per step. The total number of recorded frames was usually between 25,000 and 60,000 frames.

Single molecules are localized from the camera frames and visualized using the commercial super-resolution software SRX (Vutara, Inc.).

5.4 Results

I imaged two different types of ring canal samples. One had actin labeled with PAmCherry1 (actin::PAmCherry1) and was imaged using the Ti:Sapphire laser for activation. The actin forms an extensive, dense cytoskeletal structure around the original arrested cleavage furrow. The other sample had the ring canal protein Pavarotti labeled with mEos2 (pav::mEos2) and was imaged using the 405 nm laser for activation. The Pavarotti, unlike the actin, forms a very compact, thin-walled tube in the ring canals.

Figure 21 shows representative reconstructed super-resolution images of the actin::PAmCherry1 label (a-c) and the pav::mEos2 label (d-g). The diameter of the ring canal for the actin image is about $(2.0 \pm 0.2) \mu\text{m}$ with a wall thickness between 350 – 650 nm. It is reconstructed from about 8,000 localized PAmCherry1 molecules. The actin is not exclusively targeting the ring canal structure but can also be found in the cytoplasm which explains the relatively high occurrence of localized molecules outside of the confines of the ring canal.

The diameter of the pav::mEos2 ring canal is $(2.5 \pm 0.2) \mu\text{m}$ and the reconstructed image is created from 25,000 localized mEos2 molecules. The lower occurrence of molecules outside of the confines of the ring canal compared to the actin-labeled one can be explained by the high specificity of Pavarotti. At the investigated developmental stages it can be found almost exclusively in the ring canals. Figure 21g shows a line profile through the Pavarotti layer in the ring canal along the red line in panel d with a bin size of 10 nm. With a FWHM of $(70 \pm 14) \text{nm}$ it is clearly beyond the resolution capabilities of conventional light microscopy techniques.

Finally, Figure 21h highlights the benefit of using 2PA with these kinds of thick samples. Even with a ring canal diameter of only $(1.4 \pm 0.2) \mu\text{m}$, the background, determined as one of the parameters during localization, is more than two times

higher for the mEos2 labeled sample which is activated with the 405 nm laser compared to the PAmCherry1 labeled sample imaged with 2PA.

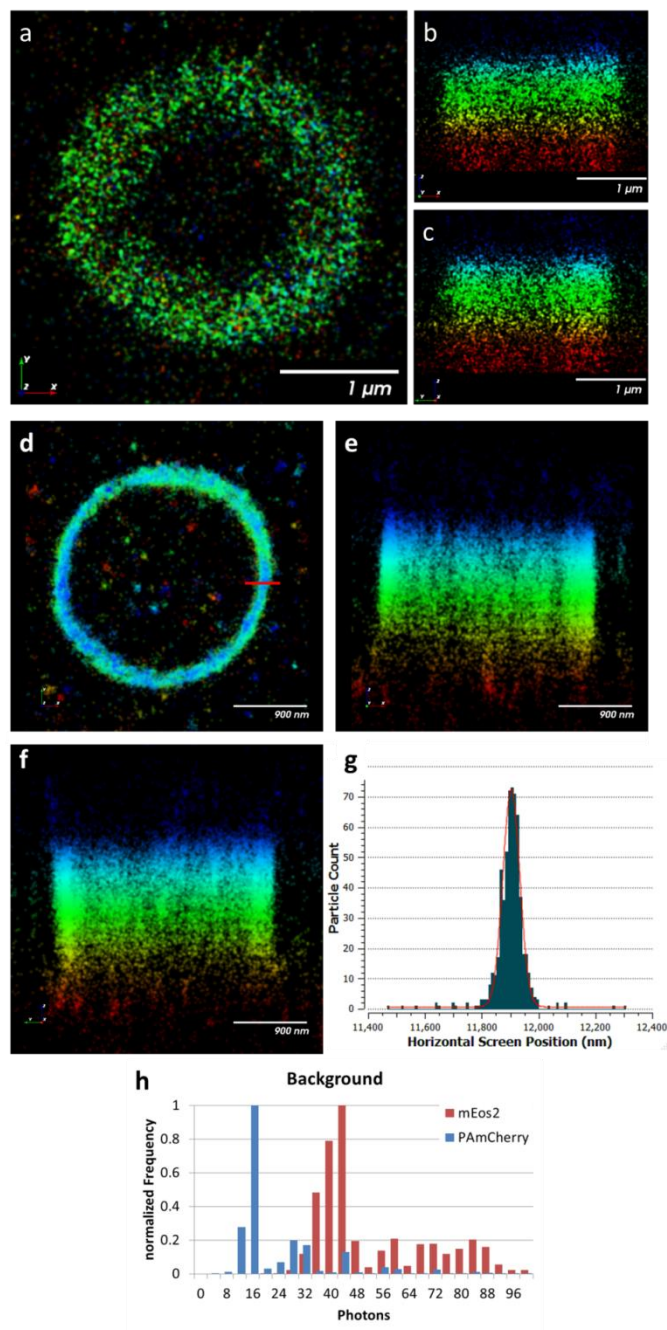


Figure 21. 3D super-resolution images of ring canals in *Drosophila*. (a-c) Super-resolution image of ring canal actin-labeled with PAmCherry1 and activated using the Ti:Sapphire laser at 700 nm; (a) X-Y view; (b) X-Z view; (c) Y-Z view; (d-g) Super-resolution image of ring canal protein Pavarotti labeled with mEos2 and activated using the 405 nm laser; (d) X-Y view; (e) X-Z view; (f) Y-Z view; (g) normalized histogram of localized molecules along the red line in panel (d) reveals a ring canal wall thickness of FWHM (70 ± 14) nm; (h) normalized histograms of detected background photons for two ring canals of similar size labeled with mEos2 and activated at 405 nm (red) and labeled with PAmCherry1 and two-photon activated at 700 nm (blue). In (a-f), the axial position of the localized molecules is color-coded red to blue from 0 to 3.5 μm.

6 sCMOS video-rate imaging

As mentioned in chapter 2, in single molecule switching nanoscopy, tens of thousands of camera frames have to be recorded to reconstruct one super-resolution image at about 25 – 40 nm spatial resolution. A single experiment can take up to an hour acquisition time caused by the slow readout speed of the typically used EM-CCD cameras of ≤ 60 full frames per second.

Here I present the use of a novel sCMOS camera which features much higher readout speeds for fast super-resolution imaging. We were able to demonstrate artifact-free localization despite the pixel-dependent noise behavior of the sCMOS camera by using new sCMOS-specific localization algorithms developed in our lab as mentioned in chapter 2.

These results are part of a manuscript that has been submitted for publication.

6.1 Sample preparation

6.1.1 Cell Culture

COS-7 cells (ATCC) were grown in 35 mm dishes on #1.5 glass coverslips pre-coated with poly-L-lysine (MatTek) and fibronectin. For microtubule imaging, the cells were first washed three times with PBS pre-warmed to 37°C and pre-extracted with 0.2% saponin (Sigma) in Cytoskeleton Buffer (CSB, 10 mM MES pH 6.1 (Sigma), 150 mM NaCl, 5 mM MgCl₂ (Sigma), 5 mM EGTA (Sigma), 5 mM glucose) for 1 min at room temperature. After removing the resulting solution, the cells were fixed with 3% paraformaldehyde (PFA, Electron Microscopy Sciences) and 0.1% glutaraldehyde (Electron Microscopy Sciences) diluted in CBS for 15 min. After three additional 3-min long washing intervals with PBS the cells were permeabilized and blocked with blocking buffer (3% BSA (Sigma) and 0.2% TX-100 in PBS) for 30 minutes while being gently rocked. After removal of the buffer solution the cells were incubated with mouse monoclonal anti- α -tubulin antibody (Sigma, 1:1000 dilution) at room temperature for 1 h and again underwent three 3-min washing intervals using wash buffer (WB; 0.05% TX-100 in PBS). The cells were then incubated with Alexa Fluor 647 goat anti-mouse IgG (Invitrogen) at a concentration of approximately 5 μ g/mL for 1 h before being washed again with WB for three 3-min intervals and post-fixed with 3% PFA and 0.1% glutaraldehyde in CSB for 10 min. The fixed cells were washed for a final round of three times in PBS for 3-min intervals and stored in PBS at 4°C until imaging.

6.1.2 Imaging buffer preparation.

Oxygen scavenging enzymes, 1 kU/mL catalase from bovine liver (Sigma) and 0.135 kU/ml glucose oxidase from *Aspergillus niger* (Sigma), were reconstituted in 20 mM Tris at pH 7.4 (Sigma), 50 mM NaCl (Sigma) and 10 mM 2-mercaptoethanol (2-ME, Sigma). They were separately stored in 50% glycerol at -20°C at concentrations of 500 kU/mL of catalase and 13.5 kU/mL of glucose oxidase. For imaging, the oxygen scavenging enzymes were first diluted with imaging buffer (50 mM Tris, pH 8.0, 50 mM NaCl (Sigma), 10% glucose) and then 20 μ L of glucose oxidase and 4 μ L of catalase stocks were added to 1 mL of 5% (v/v) 2-ME in imaging buffer.

6.2 Imaging experiments

6.2.1 System performance

To compare the performance of the EM-CCD camera to that of the sCMOS camera, we recorded images of the same bead first with the EM-CCD and then with the sCMOS camera. This order was chosen to rule out that the expected better performance of the sCMOS is not caused by a lower number of photons detected per bead for the EM-CCD camera due to bleaching.

Figure 22 a, b shows images that were recorded from the same bead using first the EM-CCD camera (a) and then the sCMOS camera (b). The noise in the sCMOS image is much more obvious because of the lower overall gain, but nevertheless, the localization performance for the sCMOS camera using the sCMOS-specific algorithms is superior to that for the EM-CCD camera. This is shown in the histograms of the localization estimates and the number of detected photons created from 800 EM-CCD and sCMOS images of the same bead in Figure 22 c, d.

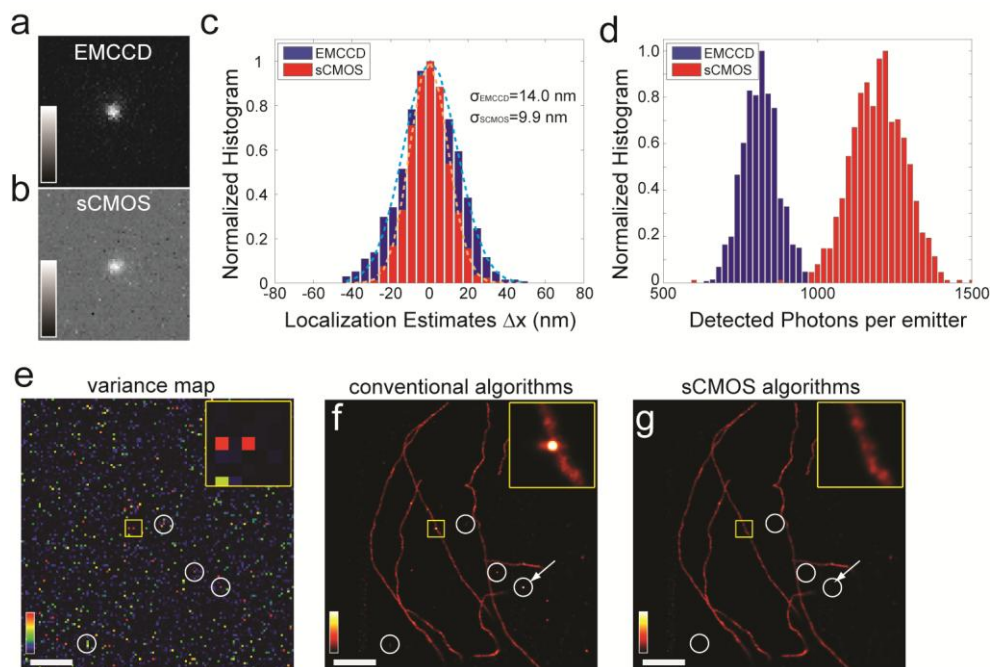


Figure 22. (a, b) Raw EM-CCD (a) and sCMOS (b) images of a 100 nm fluorescent bead. (c, d) Histogram of localization estimates and estimated detected photons per emitter from 800 EM-CCD and sCMOS images of the same bead using conventional and sCMOS-specific localization algorithms, respectively. For EM-CCD images, an effective photon conversion step is performed based on the assumption of Poisson statistics by subtracting the offset and dividing the previously characterized gain from the raw data set such that the pixel count in resulting image follows Poisson distribution as expected from shot-noise. (e) Readout variance map of a 128x128 pixel region on a sCMOS camera. (f, g) Reconstructed super-resolution images of microtubules acquired with a sCMOS camera and analyzed using conventional (f) and sCMOS algorithms (g). (adapted from submitted manuscript)

The effectiveness of the new sCMOS-specific algorithms can best be seen in a side by side comparison with the conventional ones. As mentioned in Chapter 2, the problem for the sCMOS cameras is the pixel-dependent noise. This can be visualized in the form of a variance map of the camera chip. For this we recorded a series of 60,000 dark images and then determined the mean and variance for each pixel individually. Figure 22e shows the variance map of a 128x128 pixel sized region on the camera chip. This same region was then used to image fixed microtubules in COS7 cells that were antibody labeled with Alexa647 at 1600 fps using the 642 nm laser at an intensity of 18.4 kW/cm². The 405 nm laser for activation was manually increased from 0 to 1.8 W/cm². In Figure 22f and g I show the resulting reconstructed images using conventional algorithms (f) and the sCMOS-specific algorithms (g). The highlighted regions show areas of the chip with large differences in the variance of individual pixels. When using the conventional algorithms this leads to artifacts (see inset). The sCMOS-specific algorithms however manage to properly localize the particles.

6.2.2 Reconstructed video-rate imaging of fixed microtubules

Figure 23a and b show the reconstructed super-resolution image (a) and the conventional image in form of a maximum projection of the acquired camera frames (b) of the microtubule network in three cells in a large FOV ($52 \times 52 \mu\text{m}^2$, 512×512 camera pixels). The data was recorded at 400 fps in only 40 seconds, using an intensity of 5.5 kW/cm^2 for the 642 nm laser and a manually increased intensity for the 405 nm laser from 0 to 0.3 W/cm^2 , and resulted in more than 30 million position estimates. The necessary high emitter density per frame was achieved by combining the localization algorithms with multi-emitter fitting analysis. The histogram of the position estimates of an isolated emitter (marked by the small circle in Figure 23a) reveals a localization precision of the super-resolution image of $\sim 32 \text{ nm}$ (Figure 23c). Figure 23d shows a line profile across two adjacent microtubules, located at the position marked by the arrow head in (a), that could clearly be resolved. We then used a smaller FOV ($6.6 \times 6.6 \mu\text{m}^2$, 64×64 pixels) which boosted the frame rate to 3200 fps. The laser intensity for the 642 nm laser was 7.4 kW/cm^2 and for the 405 nm laser it was manually increased from 0 to 1.8 W/cm^2 . Figure 23d-g show the maximum projection of the data set (e) and super-resolution images reconstructed using different fractions of the data (f – h). A reliable super-resolution image could be generated from a 33 ms time window of data (106 recorded camera frames) enabling artifact-free reconstructed video-rate super-resolution imaging.

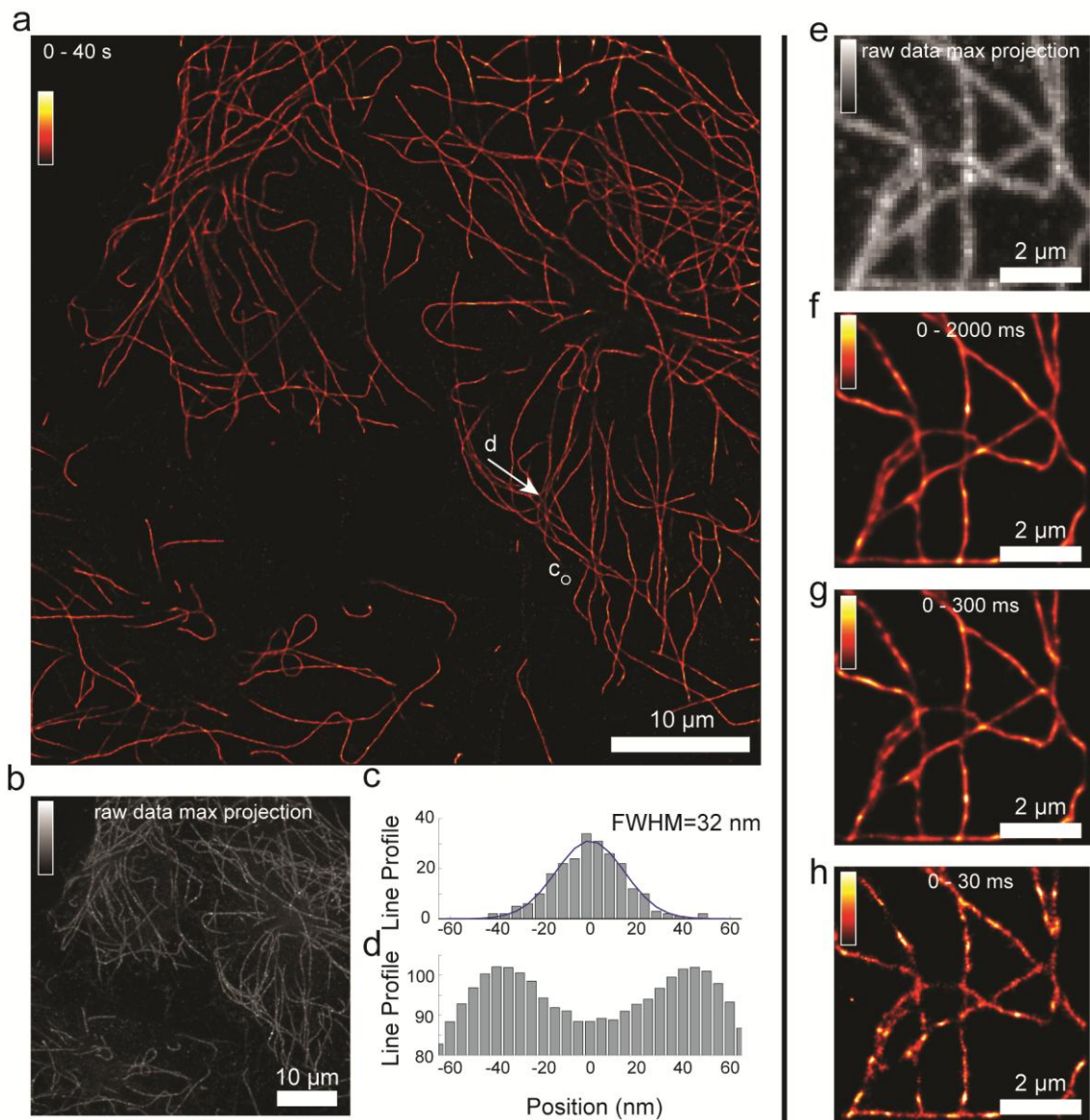


Figure 23. (a) Super-resolution image of microtubule structures in a $52 \times 52 \mu\text{m}^2$ ROI imaged at 400 fps in 40 s. The data set was processed by the new sCMOS-specific multi-emitter fitting algorithm resulting in 30,000,000 position estimates after filtering. (b) Maximum projection of the entire raw data set analyzed in (a) representing the conventional widefield image. (c) Distribution of position estimates from a point-like structure at the position of the white circle in (a). (d) Line profile across two adjacent microtubules located at the arrow head. (e) Maximum projection of a microtubule raw data set imaged in a $6.5 \times 6.5 \mu\text{m}^2$ FOV at 3200 fps over 2 s total. (f-h) Reconstructed super-resolution images obtained from different fractions of the same raw data stack using sCMOS-specific multi-emitter fitting. (adapted from submitted manuscript)

7 Summary and Outlook

In this thesis I have presented a novel Biplane-FPALM microscope with a point-scanned Ti:Sapphire laser for 2PA. The 2PA confines activation events to the focal volume which is scanned across the FOV. The thickness of the thus created optical section has been shown to be $<1 \mu\text{m}$. The new microscope has been used to obtain 2PA rates for the common PAFPs PAmCherry1, PAmKate and PA-GFP. Two further proteins, mEos2 and Dendra2, proved incompatible with 2PA. The developed method to obtain the activation rate requires only microscopic sample volumes and is applicable to any photo-activatable probe. It works by continuously measuring the fraction of the sample in the activated state over time while constantly activating and exciting the sample volume. Further experiments for PAmCherry1 revealed that its activated state consists of at least three different sub-states, only one of which is fluorescent. Once activated, the PAmCherry1 molecules can cycle through those states by absorbing either a 405 nm photon or a 556 nm photon, depending on the direction of the transition, and thus can turn temporarily non-fluorescent. In quantitative measurements, this may lead to false identification of one molecule as several and has to be taken into account during analysis. The microscope was further used to perform 3D super-resolution imaging in thick tissue. Ring canals in thick *Drosophila* egg chambers were labeled with the PAFPs PAmCherry1 or mEos2 and activated using 2PA or one-photon activation, respectively. Super-resolution analysis revealed that the 2PA exhibited a more than two-fold lower background compared to the one-photon activation.

Further development of better probes, that offer higher numbers of photons per molecule before bleaching, and improvements in label density are important milestones from here on. In the future, the characterization of 2PA using the developed method can be expanded to further PAFPs as well as other photo-activatable dyes and can also be applied to characterize one-photon activation. An extensive database of one- and 2PA rates will make it possible to better design experiments. The use of 2PA and a 405 nm laser for activation at the same time when using photo-activatable probes that only react to one of the two activation lasers offers interesting possibilities for multicolor imaging even in the same spectral emission window.

Furthermore, the 2PA can be sped up by parallelizing the scanning of the FOV e.g. by implementing a rotating microlens disc (Bewersdorf, Pick, & Hell, 1998) which splits the beam of the Ti:Sapphire laser into multiple beams, creating multiple foci

in the sample, or by changing to a widefield type temporal focusing of the Ti:Sapphire laser (König, 2000; Zhu, van Howe, Durst, Zipfel, & Xu, 2005). In combination with faster camera technologies like the sCMOS cameras this may allow to image live samples and observe, for example, not only the structure of the ring canals but even protein recruitment during ring canal growth

Additionally, a second super-resolution microscope that can switch between an EM-CCD camera and a sCMOS camera for imaging was developed and characterized. sCMOS-specific algorithms for super-resolution analysis, that have been developed in our group, allow to take advantage of the sCMOS cameras superior speed when compared to the EM-CCD camera without compromising the localization precision. This reduces the overall acquisition time for a super-resolution experiment to down to tens of milliseconds. The combination of the fast sCMOS camera with multi-emitter fitting enabled the first reconstructed video-rate images of microtubules in fixed cells. Reliable, artifact-free super-resolution images could be obtained at 32 nm spatial resolution and 33 ms temporal resolution.

Another way to reduce background, especially when imaging thick samples, is to use sheet illumination for the excitation laser and the 405 nm activation laser (Cella Zanacchi et al., 2011; Greger, Swoger, & Stelzer, 2007; Santi, 2011; Wu et al., 2011). In sheet illumination, the excitation/activation light traverses the sample perpendicular to the detection. Thus, only a thin sheet in the detection focal plane is illuminated and background from molecules outside of the focal plane is suppressed. Due to the perpendicular illumination a more complex optical setup using two objectives and different sample mounting conditions is required. This can be avoided by using only highly inclined light sheets instead of perpendicular ones (Tokunaga, Imamoto, & Sakata-Sogawa, 2008; van 't Hoff, de Sars, & Oheim, 2008). Furthermore, in order to image thicker samples, tissue clearing media like ScaleA/U or FocusClear (Hama et al., 2011; Liu & Chiang, 2003) can be used. They decrease the scattering and autofluorescence in samples and render the tissue transparent while preserving the fluorescent signal.

The two introduced setups demonstrate the great capabilities of current localization-based techniques. 2PA grants exceptional spatial control over the activation volume that can even be useful in different fields such as particle tracking where a small subpopulation could be activated and tracked at a time. The greater speed of sCMOS cameras with the new algorithms and multi-emitter fitting paves the way for live-cell video-rate super-resolution imaging and can also

be combined with the FPALM setup opening up a wealth of biological experiments.

Bibliography

1. Abbe, E. (1873). Beiträge zur Theorie des Mikroskops und der mikroskopischen Wahrnehmung. *Archiv für Mikroskopische Anatomie*, 9(1), 413–418. doi:10.1007/BF02956173
2. Anderson, E., & Huebner, E. (1968). Development of the oocyte and its accessory cells of the polychaete, *Diopatra cuprea* (Bosc). *Journal of Morphology*, 126(2), 163–197. doi:10.1002/jmor.1051260203
3. Baddeley, D., Jayasinghe, I. D., Cremer, C., Cannell, M. B., & Soeller, C. (2009). Light-induced dark states of organic fluochromes enable 30 nm resolution imaging in standard media. *Biophysical journal*, 96(2), L22–4. doi:10.1016/j.bpj.2008.11.002
4. Bates, M., Blosser, T., & Zhuang, X. (2005). Short-Range Spectroscopic Ruler Based on a Single-Molecule Optical Switch. *Physical Review Letters*, 94(10), 1–4. doi:10.1103/PhysRevLett.94.108101
5. Belov, V. N., Bossi, M. L., Fölling, J., Boyarskiy, V. P., & Hell, S. W. (2009). Rhodamine spiroamides for multicolor single-molecule switching fluorescent nanoscopy. *Chemistry (Weinheim an der Bergstrasse, Germany)*, 15(41), 10762–76. doi:10.1002/chem.200901333
6. Betzig, E., Patterson, G. H., Sougrat, R., Lindwasser, O. W., Olenych, S., Bonifacino, J. S., Davidson, M. W., et al. (2006). Imaging intracellular fluorescent proteins at nanometer resolution. *Science (New York, N.Y.)*, 313(5793), 1642–5. doi:10.1126/science.1127344
7. Bewersdorf, J., Pick, R., & Hell, S. W. (1998). Multifocal multiphoton microscopy. *Optics Letters*, 23(9), 655. doi:10.1364/OL.23.000655
8. Cella Zanacchi, F., Lavagnino, Z., Perrone Donnorso, M., Del Bue, A., Furia, L., Faretta, M., & Diaspro, A. (2011). Live-cell 3D super-resolution imaging in thick biological samples. *Nature methods*, 8(12), 1047–9. doi:10.1038/nmeth.1744
9. Cooley, L. (1998). Drosophila ring canal growth requires Src and Tec kinases. *Cell*, 93(6), 913–5. Retrieved from <http://www.ncbi.nlm.nih.gov/pubmed/9635420>
10. Denk, W., Strickler, J. H., & Webb, W. W. (1990). Two-photon laser scanning fluorescence microscopy. *Science (New York, N.Y.)*, 248(4951), 73–6. Retrieved from <http://www.ncbi.nlm.nih.gov/pubmed/2321027>
11. Diaspro, A., Testa, I., Faretta, M., Magrassi, R., Barozzi, S., Parazzoli, D., & Vicidomini, G. (2006). 3D localized photoactivation of pa-GFP in living cells using two-photon interactions. *Conf Proc IEEE Eng Med Biol Soc*, 1, 389–391. doi:10.1109/IEMBS.2006.259967
12. Fölling, J., Bossi, M., Bock, H., Medda, R., Wurm, C. A., Hein, B., Jakobs, S., et al. (2008). Fluorescence nanoscopy by ground-state depletion and single-molecule return. *Nature methods*, 5(11), 943–5. doi:10.1038/nmeth.1257
13. Fölling, J., Polyakova, S., Belov, V., Van Blaaderen, A., Bossi, M. L., & Hell, S. W. (2008). Synthesis and characterization of photoswitchable fluorescent silica nanoparticles. *Small (Weinheim an der Bergstrasse, Germany)*, 4(1), 134–42. doi:10.1002/smll.200700440

14. Gould, T. J., Hess, S. T., & Bewersdorf, J. (2012). Optical nanoscopy: from acquisition to analysis. *Annual review of biomedical engineering*, *14*, 231–54. doi:10.1146/annurev-bioeng-071811-150025
15. Greger, K., Swoger, J., & Stelzer, E. H. K. (2007). Basic building units and properties of a fluorescence single plane illumination microscope. *The Review of scientific instruments*, *78*(2), 023705. Retrieved from <http://www.ncbi.nlm.nih.gov/pubmed/17578115>
16. Gunewardene, M. S., Subach, F. V., Gould, T. J., Penoncello, G. P., Gudheti, M. V., Verkhusha, V. V., & Hess, S. T. (2011). Superresolution Imaging of Multiple Fluorescent Proteins with Highly Overlapping Emission Spectra in Living Cells. *Biophysical Journal*, *101*(6), 1522–1528. doi:10.1016/j.bpj.2011.07.049
17. Gurskaya, N. G., Verkhusha, V. V., Shcheglov, A. S., Staroverov, D. B., Chepurnykh, T. V., Fradkov, A. F., Lukyanov, S., et al. (2006). Engineering of a monomeric green-to-red photoactivatable fluorescent protein induced by blue light. *Nature biotechnology*, *24*(4), 461–5. doi:10.1038/nbt1191
18. Hama, H., Kurokawa, H., Kawano, H., Ando, R., Shimogori, T., Noda, H., Fukami, K., et al. (2011). Scale: a chemical approach for fluorescence imaging and reconstruction of transparent mouse brain. *Nature neuroscience*, *14*(11), 1481–8. doi:10.1038/nn.2928
19. Heilemann, M., Margeat, E., Kasper, R., Sauer, M., & Tinnefeld, P. (2005). Carbocyanine dyes as efficient reversible single-molecule optical switch. *Journal of the American Chemical Society*, *127*(11), 3801–6. doi:10.1021/ja044686x
20. Hell, S W, & Wichmann, J. (1994). Breaking the diffraction resolution limit by stimulated emission: stimulated-emission-depletion fluorescence microscopy. *Optics letters*, *19*(11), 780–2. Retrieved from <http://www.ncbi.nlm.nih.gov/pubmed/19844443>
21. Hell, Stefan W. (2009). Microscopy and its focal switch. *Nature methods*, *6*(1), 24–32. doi:10.1038/nmeth.1291
22. Hermann, J., & Ducuing, J. (1972). Absolute Measurement of Two-Photon Cross Sections. *Physical Review A*, *5*(6), 2557–2568. doi:10.1103/PhysRevA.5.2557
23. Hess, S. T., Girirajan, T. P. K., & Mason, M. D. (2006). Ultra-high resolution imaging by fluorescence photoactivation localization microscopy. *Biophysical journal*, *91*(11), 4258–72. doi:10.1529/biophysj.106.091116
24. Huang, B., Wang, W., Bates, M., & Zhuang, X. (2008). Three-dimensional super-resolution imaging by stochastic optical reconstruction microscopy. *Science (New York, N.Y.)*, *319*(5864), 810–3. doi:10.1126/science.1153529
25. Huang, Z.-L., Zhu, H., Long, F., Ma, H., Qin, L., Liu, Y., Ding, J., et al. (2011). Localization-based super-resolution microscopy with an sCMOS camera. *Optics Express*, *19*(20), 19156. doi:10.1364/OE.19.019156
26. Juette, M. F., Gould, T. J., Lessard, M. D., Mlodzianoski, M. J., Nagpure, B. S., Bennett, B. T., Hess, S. T., et al. (2008). Three-dimensional sub-100 nm resolution fluorescence microscopy of thick samples. *Nature methods*, *5*(6), 527–9. doi:10.1038/nmeth.1211
27. KING, R. C., & MILLS, R. P. (1962). Oogenesis in adult *Drosophila*. XI. Studies of some organelles of the nutrient stream in egg chambers of *D. melanogaster* and *D.*

- willistoni. *Growth*, 26, 235–53. Retrieved from <http://www.ncbi.nlm.nih.gov/pubmed/14032866>
28. König, K. (2000). Multiphoton microscopy in life sciences. *Journal of microscopy*, 200(Pt 2), 83–104. Retrieved from <http://www.ncbi.nlm.nih.gov/pubmed/11106949>
 29. Liu, Y.-C., & Chiang, A.-S. (2003). High-resolution confocal imaging and three-dimensional rendering. *Methods (San Diego, Calif.)*, 30(1), 86–93. Retrieved from <http://www.ncbi.nlm.nih.gov/pubmed/12695106>
 30. McKinney, S. A., Murphy, C. S., Hazelwood, K. L., Davidson, M. W., & Looger, L. L. (2009). A bright and photostable photoconvertible fluorescent protein. *Nature methods*, 6(2), 131–3. doi:10.1038/nmeth.1296
 31. Mlodzianoski, M. J., Juette, M. F., Beane, G. L., & Bewersdorf, J. (2009). Experimental characterization of 3D localization techniques for particle-tracking and super-resolution microscopy. *Optics express*, 17(10), 8264–77. Retrieved from <http://www.ncbi.nlm.nih.gov/pubmed/19434159>
 32. Nakamura, O. (1999). Fundamental of two-photon microscopy. *Microscopy research and technique*, 47(3), 165–71. doi:10.1002/(SICI)1097-0029(19991101)47:3<165::AID-JEMT2>3.0.CO;2-D
 33. Niesner, R., Andresen, V., Neumann, J., Spiecker, H., & Gunzer, M. (2007). The power of single and multibeam two-photon microscopy for high-resolution and high-speed deep tissue and intravital imaging. *Biophysical journal*, 93(7), 2519–29. doi:10.1529/biophysj.106.102459
 34. Patterson, G. H., & Lippincott-Schwartz, J. (2002). A photoactivatable GFP for selective photolabeling of proteins and cells. *Science (New York, N.Y.)*, 297(5588), 1873–7. doi:10.1126/science.1074952
 35. Prabhat, P., Ram, S., Ward, E. S., & Ober, R. J. (2004). Simultaneous imaging of different focal planes in fluorescence microscopy for the study of cellular dynamics in three dimensions. *IEEE transactions on nanobioscience*, 3(4), 237–42. Retrieved from <http://www.pubmedcentral.nih.gov/articlerender.fcgi?artid=2761735&tool=pmcentrez&rendertype=abstract>
 36. Ram, S., Ward, E. S., & Ober, R. J. (2006). Beyond Rayleigh's criterion: a resolution measure with application to single-molecule microscopy. *Proceedings of the National Academy of Sciences of the United States of America*, 103(12), 4457–62. doi:10.1073/pnas.0508047103
 37. Robbins, M. S., Member, S., & Hadwen, B. J. (2003). The Noise Performance of Electron Multiplying Charge-Coupled Devices, 50(5), 1227–1232.
 38. Robinson, D. N., Cant, K., & Cooley, L. (1994). Morphogenesis of Drosophila ovarian ring canals. *Development (Cambridge, England)*, 120(7), 2015–25. Retrieved from <http://www.ncbi.nlm.nih.gov/pubmed/7925006>
 39. Rubart, M. (2004). Two-photon microscopy of cells and tissue. *Circulation research*, 95(12), 1154–66. doi:10.1161/01.RES.0000150593.30324.42
 40. Rust, M. J., Bates, M., & Zhuang, X. (2006). Sub-diffraction-limit imaging by stochastic optical reconstruction microscopy (STORM). *Nature methods*, 3(10), 793–5. doi:10.1038/nmeth929

41. Santi, P. A. (2011). Light sheet fluorescence microscopy: a review. *The journal of histochemistry and cytochemistry : official journal of the Histochemistry Society*, *59*(2), 129–38. doi:10.1369/0022155410394857
42. Saurabh, S., Maji, S., & Bruchez, M. P. (2012). Evaluation of sCMOS cameras for detection and localization of single Cy5 molecules. *Optics express*, *20*(7), 7338–49. Retrieved from <http://www.ncbi.nlm.nih.gov/pubmed/22453414>
43. Schneider, M., Barozzi, S., Testa, I., Faretta, M., & Diaspro, A. (2005). Two-photon activation and excitation properties of PA-GFP in the 720-920-nm region. *Biophysical journal*, *89*(2), 1346–52. doi:10.1529/biophysj.104.054502
44. Stepanenko, O. V., Stepanenko, O. V., Shcherbakova, D. M., Kuznetsova, I. M., Turoverov, K. K., & Verkhusha, V. V. (2011). Modern fluorescent proteins: from chromophore formation to novel intracellular applications. *BioTechniques*, *51*(5), 313–27. doi:10.2144/000113765
45. Subach, F V, Patterson, G. H., Manley, S., Gillette, J. M., Lippincott-Schwartz, J., & Verkhusha, V. V. (2009). Photoactivatable mCherry for high-resolution two-color fluorescence microscopy. *Nat Methods*, *6*(2), 153–159. doi:nmeth.1298 [pii] 10.1038/nmeth.1298
46. Subach, Fedor V, Malashkevich, V. N., Zencheck, W. D., Xiao, H., Filonov, G. S., Almo, S. C., & Verkhusha, V. V. (2009). Photoactivation mechanism of PAmCherry based on crystal structures of the protein in the dark and fluorescent states. *Proceedings of the National Academy of Sciences of the United States of America*, *106*(50), 21097–102. doi:10.1073/pnas.0909204106
47. Testa, I., Garre, M., Parazzoli, D., Barozzi, S., Ponzanelli, I., Mazza, D., Faretta, M., et al. (2008). Photoactivation of pa-GFP in 3D: optical tools for spatial confinement. *Eur Biophys J*, *37*(7), 1219–1227. doi:10.1007/s00249-008-0317-9
48. Testa, I., Parazzoli, D., Barozzi, S., Garrè, M., Faretta, M., & Diaspro, A. (2008). Spatial control of pa-GFP photoactivation in living cells. *Journal of microscopy*, *230*(Pt 1), 48–60. doi:10.1111/j.1365-2818.2008.01951.x
49. Thompson, R. E., Larson, D. R., & Webb, W. W. (2002). Precise nanometer localization analysis for individual fluorescent probes. *Biophysical journal*, *82*(5), 2775–83. doi:10.1016/S0006-3495(02)75618-X
50. Tokunaga, M., Imamoto, N., & Sakata-sogawa, K. (2008). Highly inclined thin illumination enables clear single-molecule imaging in cells. *Nature Methods*, *5*(2), 159–161. doi:10.1038/NMETH.1171
51. Tokunaga, M., Imamoto, N., & Sakata-Sogawa, K. (2008). Highly inclined thin illumination enables clear single-molecule imaging in cells. *Nature methods*, *5*(2), 159–61. doi:10.1038/nmeth1171
52. Toomre, D., & Bewersdorf, J. (2010). A new wave of cellular imaging. *Annual review of cell and developmental biology*, *26*, 285–314. doi:10.1146/annurev-cellbio-100109-104048
53. Van 't Hoff, M., De Sars, V., & Oheim, M. (2008). A programmable light engine for quantitative single molecule TIRF and HILO imaging. *Optics express*, *16*(22), 18495–504. Retrieved from <http://www.ncbi.nlm.nih.gov/pubmed/18958128>

54. Vaziri, A., Tang, J., Shroff, H., & Shank, C. V. (2008). Multilayer three-dimensional super resolution imaging of thick biological samples. *Proc Natl Acad Sci U S A*, *105*(51), 20221–20226. doi:0810636105 [pii] 10.1073/pnas.0810636105
55. Vogelsang, J., Cordes, T., Forthmann, C., Steinhauer, C., & Tinnefeld, P. (2009). Controlling the fluorescence of ordinary oxazine dyes for single-molecule switching and superresolution microscopy. *Proceedings of the National Academy of Sciences of the United States of America*, *106*(20), 8107–12. doi:10.1073/pnas.0811875106
56. Wiedenmann, J., Oswald, F., & Nienhaus, G. U. (2009). Fluorescent proteins for live cell imaging: opportunities, limitations, and challenges. *IUBMB life*, *61*(11), 1029–42. doi:10.1002/iub.256
57. Wu, Y., Ghitani, A., Christensen, R., Santella, A., Du, Z., Rondeau, G., Bao, Z., et al. (2011). Inverted selective plane illumination microscopy (iSPIM) enables coupled cell identity lineaging and neurodevelopmental imaging in *Caenorhabditis elegans*. *October*. doi:10.1073/pnas.1108494108/-/DCSupplemental.www.pnas.org/cgi/doi/10.1073/pnas.1108494108
58. York, A. G., Ghitani, A., Vaziri, A., Davidson, M. W., & Shroff, H. (2011). Confined activation and subdiffractive localization enables whole-cell PALM with genetically expressed probes. *Nature methods*, *8*(4), 327–33. doi:10.1038/nmeth.1571
59. Zhu, G., Van Howe, J., Durst, M., Zipfel, W., & Xu, C. (2005). Simultaneous spatial and temporal focusing of femtosecond pulses. *Optics Express*, *13*(6), 2153. doi:10.1364/OPEX.13.002153
60. Zipfel, W. R., Williams, R. M., & Webb, W. W. (2003). Nonlinear magic: multiphoton microscopy in the biosciences. *Nature biotechnology*, *21*(11), 1369–77. doi:10.1038/nbt899

8 Appendix

8.1 Cloning protocol

Step 1 – grow bacteria

- Pick single colony from plate on pipette tip
- Add to 3ml of growth medium
Growth medium: LB medium with antibiotics (and inducer), e.g. LB with 100µg/ml Ampicillin and 0.004% Arabinose
- Grow overnight (12-16h) @37C while shaking @200-250rpm
- Spin down @5k rpm for 5min
- Transfer to Eppendorf tube
- Spin down @5k rpm for 5min

Step 2 – plasmid isolation

- Add 250µl P1-buffer (shake before adding) to resuspend pellet (pipette-mix)
- Add 250µl P2-buffer; **NO** pipette-mixing! Shake gently until homogeneously blue
- Wait for 5min
- @-10sec add 350 µl N3-buffer; **NO** pipette-mixing! Shake gently until colorless
- Spin down @13k for 12min, 4C
- Take off the supernatant **without** touching the pellet and add it to kit-tube
- Spin down @13k for 30sec, 4C or room temp
- Dump liquid
- Add 750 µl PE-buffer
- Wait 5min
- Spin down @13k for 30sec, 4C or room temp
- Dump liquid
- Spin down again @13k for 2min, 4C or room temp
- Move insert to new Eppendorf tube
- Add 55 µl EB-buffer onto the center of the filter **without** touching it
- Wait for 10-30min
- Spin down @13k for 2min 4C or room temp

Step 3 – PCR

- Dilute primers with H₂O: add 10 µl H₂O per ng of primer to get a 10x-primer solution
- Add 90 µl of H₂O and 10 µl of 10x-primer to make 1x-primer solution
- Add
 - 38 µl H₂O
 - 5 µl Pfu-10x-buffer
 - 1 µl plasmid
 - 1 µl dNTP
 - 2 µl primer 1
 - 2 µl primer 2
 - 1 µl Pfu-polymerase
- Put in PCR machine and select correct program

→ Prepare gel so that it can solidify!

Step 4 – Gel purification

- Prepare gel (density dependent on plasmid size):
 - For 1% -gel: add 1g of pure Agarose powder to 50 ml of TAE-buffer and microwave 1-2min until all the powder is dissolved (use a little over 50ml because buffer will evaporate during microwaving);
 - Let solution cool down a bit until touch-warm/hot (10-15min);
 - Add 1µl of dye (SynGold) (1-5µl);
 - Pour into rinsed and dried gel holder and put well creator in place;
 - Let stand until solidified (1h+)
- Run gel
 - Place gel into voltage chamber with TAE-buffer
 - Load PCR-product into one well and ladder into another well
 - Run @110V for 30min (don't let run past >½ of gel)
 - Remove gel from chamber and put on UV-reader – take a picture
 - Cut out band on UV-reader and put in Eppendorf tube
- Extract from gel using kit
 - Add 850µl of QG-buffer and shake
 - Put @55C for 5-10min until gel is melted; shake every 2min
 - Add 650µl of gel-buffer to kit-tube

- Spin down @14k for 30sec, room temp
- Dump liquid
- Add rest of gel-buffer to tube
- Spin down @14k for 30sec, room temp
- Dump liquid
- Spin down again @14k for 1min, room temp
- Move insert to new Eppendorf tube
- Add 30 µl of EB-buffer onto center of filter **without** touching it (for 1-2 µg of DNA add 20 µl EB-buffer, for 3 µg add 30 µl)
- Wait for 1min
- Spin down @8.2k for 1min, room temp

Step 5 – Digestion

- Mix insert (should be around 28 µl) **ON ICE** with
 - 5 µl buffer-X (buffer-X corresponding to the two restriction sites used for the primers)
 - 14 µl H₂O
 - 1.5 µl site-1 enzyme
 - 1.5 µl site-2 enzyme
 - Mix vector (pET sumo) **ON ICE** with
 - (per 1 µg of DNA add 1 unit (1 µl) of enzyme and add 1h @37C)
 - 3 µl = 3 µg vector
 - 5 µl buffer-X (see above)
 - 39 µl H₂O
 - 1.5 µl site-1 enzyme
 - 1.5 µl site-2 enzyme
 - Put @37C (water bath) for 3.5-4h
- Prepare gel!

Step 6 – Gel Purification

- (see above)

Step 7 – Ligation

- Mix (total of 20 µl):
 - 12 µl H₂O
 - 1 µl vector

- 4 μ l insert (vector:insert ratio should be >1:3)
 - 2 μ l 10x-Ligase-buffer
 - 1 μ l 1x-Ligase-enzyme
- Mix vector-only control:
 - 16 μ l H₂O
 - 1 μ l vector
 - 2 μ l 10x-Ligase-buffer
 - 1 μ l 1x-Ligase-enzyme
- Leave @25C for ½-1h
- Add 30 μ l H₂O
- Add 20 μ l of competent cells **ON ICE**
- Wait for 25min **ON ICE**
- Put in water bath @42C for 30sec
- Put on ICE immediately for 2min
- Add 250 μ l of SOC media, room temp
- Shaking-incubate @37C for ½-1h
- Add onto LB-plate and spread
- Let dry
- Incubate over night

8.2 Plasmid sequence

pBAD/HisB-PAmCherry1:

AAGAAACCAATTGTCCATATTGCATCAGACATTGCCGTCACCTGCGTCTTTTA
CTGGCTCTTCTCGCTAACCAAACCGGTAACCCCGCTTATTAAGCATTTCTG
TAACAAAGCGGGACCAAAGCCATGACAAAAACGCGTAACAAAAGTGTCTA
TAATCACGGCAGAAAAGTCCACATTGATTATTTGCACGGCGTCACACTTTGC
TATGCCATAGCATTTTTATCCATAAGATTAGCGGATCCTACCTGACGCTTTT
TATCGCAACTCTCTACTGTTTCTCCATAACCGTTTTTTGGGCTAACAGGAGG
AATTAACCATGGGGGTTCTCATCATCATCATCATGGTATGGCTAGCAT
GACTGGTGGACAGCAAATGGGTGCGGATCTGTACGACGATGACGATAAGG
ATCCGAGCTCGAGATCTATGGTGAGCAAGGGCGAGGAGGATAACATGGCC
ATCATTAAAGGAGTTCATGCGCTTCAAGGTGCACATGGAGGGGTCCGTGAAC
GGCCACGTGTTTCGAGATCGAGGGCGAGGGCGAGGGCCGCCCTACGAGGG
CACCCAGACCGCCAAGCTGAAGGTGACCAAGGGTGGCCCCCTGCCCTTAC
CTGGGACATCCTGTCCCCTCAATTCATGTACGGCTCCAATGCCTACGTGAAG
CACCCCGCCGACATCCCCGACTACTTTAAGCTGTCCTTCCCCGAGGGCTTCA
AGTGGGAGCGCGTGATGAAATTCGAGGACGGCGGCGTGGTGACCGTGACCC
AGGACTCCTCCCTGCAGGACGGTGAGTTCATCTACAAGGTGAAGCTGCGCG
GCACCAACTTCCCCTCCGACGGCCCCGTAATGCAGAAGAAGACCATGGGCT
GGGAGGCCCTCTCCGAGCGGATGTACCCCGAGGACGGCGCCCTGAAGGGCG
AGGTCAAGCCGAGAGTGAAGCTGAAGGACGGCGGCCACTACGACGCTGAG
GTCAAGACCACCTACAAGGCCAAGAAGCCCGTGCAGCTGCCCGGCGCCTAC
AACGTCAACCGCAAGTTGGACATCACCTCACACAACGAGGACTACACCATC
GTGGAACAGTACGAACGTGCCGAGGGCCGCCACTCCACCGGCGGCATGGAC
GAGCTGTACAAGTAAGAATTCGAAGCTTGGCTGTTTTGGCGGATGAGAGAA
GATTTTCAGCCTGATACAGATTAATCAGAACGCAGAAGCGGTCTGATAAA
ACAGAATTTGCCTGGCGGCAGTAGCGCGGTGGTCCCACCTGACCCCATGCC
GAACTCAGAAGTGAAACGCCGTAGCGCCGATGGTAGTGTGGGGTCTCCCCA
TGCGAGAGTAGGGAAGTCCAGGCATCAAATAAAACGAAAGGCTCAGTCG
AAAGACTGGGCCTTTCGTTTTATCTGTTGTTTGTTCGGTGAACGCTCTCCTGA
GTAGGACAAATCCGCCGGGAGCGGATTTGAACGTTGCGAAGCAACGGCCCCG
GAGGGTGGCGGGCAGGACGCCCGCCATAAACTGCCAGGCATCAAATTAAG
CAGAAGGCCATCCTGACGGATGGCCTTTTTGCGTTTCTACAAACTCTTTTGT
TTATTTTTCTAAATACATTCAAATATGTATCCGCTCATGAGACAATAACCCT
GATAAATGCTTCAATAATATTGAAAAAGGAAGAGTATGAGTATTCAACATT
TCCGTGTCGCCCTTATTCCTTTTTTGGCGCATTTTGCCTTCTGTTTTTGCTC
ACCCAGAAACGCTGGTGAAAGTAAAAGATGCTGAAGATCAGTTGGGTGCA

CGAGTGGGTTACATCGAACTGGATCTCAACAGCGGTAAGATCCTTGAGAGT
TTTCGCCCCGAAGAACGTTTTTCCAATGATGAGCACTTTTAAAGTTCTGCTAT
GTGGCGCGGTATTATCCCGTGTTGACGCCGGCAAGAGCAACTCGGTCGCC
GCATACACTATTCTCAGAATGACTTGGTTGAGTACTCACCAGTCACAGAAA
AGCATCTTACGGATGGCATGACAGTAAGAGAATTATGCAGTGCTGCCATAA
CCATGAGTGATAACACTGCGGCCAACTTACTTCTGACAACGATCGGAGGAC
CGAAGGAGCTAACCGCTTTTTTGCACAACATGGGGGATCATGTAACCTGCC
TTGATCGTTGGGAACCGGAGCTGAATGAAGCCATACCAAACGACGAGCGTG
ACACCACGATGCCTGTAGCAATGGCAACAACGTTGCGCAAACCTATTAACCTG
GCGAACTACTTACTCTAGCTTCCCGGCAACAATTAATAGACTGGATGGAGG
CGGATAAAGTTGCAGGACCACTTCTGCGCTCGGCCCTTCCGGCTGGCTGGTT
TATTGCTGATAAATCTGGAGCCGGTGAGCGTGGGTCTCGCGGTATCATTGC
AGCACTGGGGCCAGATGGTAAGCCCTCCCGTATCGTAGTTATCTACACGAC
GGGAGTCAGGCAACTATGGATGAACGAAATAGACAGATCGCTGAGATAG
GTGCCTCACTGATTAAGCATTGGTAACTGTCAGACCAAGTTTACTCATATAT
ACTTTAGATTGATTTAAAACCTCATTTTTTAATTTAAAAGGATCTAGGTGAAG
ATCCTTTTTGATAATCTCATGACCAAATCCCTTAACGTGAGTTTTCGTTCC
ACTGAGCGTCAGACCCCGTAGAAAAGATCAAAGGATCTTCTTGAGATCCTT
TTTTTCTGCGCGTAATCTGCTGCTTGCAAACAAAAAAACCACCGCTACCAGC
GGTGGTTTTGTTTGCCGGATCAAGAGCTACCAACTCTTTTTCCGAAGGTAAC
GGCTTCAGCAGAGCGCAGATACCAAATACTGTCCTTCTAGTGTAGCCGTAG
TTAGGCCACCACTTCAAGAACTCTGTAGCACCGCCTACATACCTCGCTCTGC
TAATCCTGTTACCAGTGGCTGCTGCCAGTGGCGATAAGTCGTGTCTTACCGG
GTTGGACTCAAGACGATAGTTACCGGATAAGGCGCAGCGGTCTGGGCTGAAC
GGGGGGTTCTGTGCACACAGCCCAGCTTGGAGCGAACGACCTACACCGAACT
GAGATACCTACAGCGTGAGCTATGAGAAAGCGCCACGCTTCCCGAAGGGAG
AAAGGCGGACAGGTATCCGGTAAGCGGCAGGGTCGGAACAGGAGAGCGCA
CGAGGGAGCTTCCAGGGGGAAACGCCTGGTATCTTTATAGTCCTGTCTGGGT
TTCGCCACCTCTGACTTGAGCGTCGATTTTTGTGATGCTCGTCAGGGGGGCG
GAGCCTATGGAAAAACGCCAGCAACGCGGCCTTTTTACGGTTCCTGGCCTTT
TGCTGGCCTTTTTGCTCACATGTTCTTTCCTGCGTTATCCCCTGATTCTGTGGA
TAACCGTATTACCGCCTTTGAGTGAGCTGATACCGCTCGCCGCAGCCGAAC
GACCGAGCGCAGCGAGTCAGTGAGCGAGGAAGCGGAAGAGCGCCTGATGC
GGTATTTTTCTCCTTACGCATCTGTGCGGTATTTACACCCGCATATGGTGAC
TCTCAGTACAATCTGCTCTGATGCCGCATAGTTAAGCCAGTATACACTCCGC
TATCGCTACGTGACTGGGTTCATGGCTGCGCCCCGACACCCGCCAACACCCG
CTGACGCGCCCTGACGGGCTTGTCTGCTCCCGGCATCCGCTTACAGACAAGC
TGTGACCGTCTCCGGGAGCTGCATGTGTCAGAGGTTTTACCGTTCATCACCG

AAACGCGGAGGCAGCAGATCAATTCGCGCGCGAAGGCGAAGCGGCATGC
ATAATGTGCCTGTCAAATGGACGAAGCAGGGATTCTGCAAACCCTATGCTA
CTCCGTCAAGCCGTCAATTGTCTGATTCTGTTACCAATTATGACAACCTTGACG
GCTACATCATTCACTTTTTTCTTCACAACCGGCACGGAACCTCGCTCGGGCTGG
CCCCGGTGCATTTTTTAAATACCCGCGAGAAATAGAGTTGATCGTCAAAC
CAACATTGCGACCGACGGTGGCGATAGGCATCCGGGTGGTGCTCAAAGCA
GCTTCGCCTGGCTGATACGTTGGTCTCGCGCCAGCTTAAGACGCTAATCCC
TAACTGCTGGCGAAAAGATGTGACAGACGCGACGGCGACAAGCAAACAT
GCTGTGCGACGCTGGCGATATCAAATTTGCTGTCTGCCAGGTGATCGCTGA
TGTAAGTACAAGCCTCGCGTACCCGATTATCCATCGGTGGATGGAGCGACT
CGTTAATCGCTTCCATGCGCCGAGTAACAATTGCTCAAGCAGATTTATCGC
CAGCAGCTCCGAATAGCGCCCTTCCCCTTGCCCGGCGTTAATGATTTGCCCA
AACAGGTCGCTGAAATGCGGCTGGTGGCTTCATCCGGGCGAAAGAACCCC
GTATTGGCAAATATTGACGGCCAGTTAAGCCATTCATGCCAGTAGGCGCGC
GGACGAAAGTAAACCCACTGGTGATAACCATTGCGGAGCCTCCGGATGACGA
CCGTAGTGATGAATCTCTCTGGCGGGAACAGCAAATATCACCCGGTTCGG
CAAACAAATTCTCGTCCCTGATTTTTTACCACCCCTGACCGCGAATGGTGA
GATTGAGAATATAACCTTTCATTCCCAGCGGTTCGGTCGATAAAAAAATCGA
GATAACCGTTGGCCTCAATCGGCGTTAAACCCGCCACCAGATGGGCATTAA
ACGAGTATCCCGGCAGCAGGGGATCATTTTTCGCGCTTCAGCCATACTTTTCAT
ACTCCCGCCATTCAGAG

pBAD/HisB-PAmKate:

AAGAAACCAATTGTCCATATTGCATCAGACATTGCCGTCACTGCGTCTTTTA
CTGGCTCTTCTCGCTAACCAAACCGGTAACCCCGCTTATTAAGCATTCTG
TAACAAAGCGGGACCAAAGCCATGACAAAAACGCGTAACAAAAGTGTCTA
TAATCACGGCAGAAAAGTCCACATTGATTATTTGCACGGCGTCACACTTTGC
TATGCCATAGCATTTTTATCCATAAGATTAGCGGATCCTACCTGACGCTTTT
TATCGCAACTCTCTACTGTTTCTCCATAACCCGTTTTTTGGGCTAACAGGAGG
AATTAACCATGGGGGGTTCTCATCATCATCATCATGGTATGGCTAGCAT
GACTGGTGGACAGCAAATGGGTTCGGGATCTGTACGACGATGACGATAAGG
ATCCGAGCTCGAGATCTATGGTGTCTAAGGGCGAAGAGCTGATTAAGGAGA
ACATGCACATGAAGCTGTACATGGAGGGCACCGTGAACAACCACCACTTCA
AGTGCACATCCGAGGGCGAAGGCAAGCCCTACGAGGGCACCCAGACCATG
AGAATCAAGGTGGTCGAGGGCGGCCCTCTCCCCTTCGCTTCGACATCCTGG
CTACCAGCTTCATGTACGGCAGCAAGACCTTCATCAACCACACCCAGGGCA

TCCCCGACTTCTGGAAGCAGTCCTTCCCTGAGGGCTTCACATGGGAGAGAG
TCACCACATACGAAGACGGGGGCGTGCTGACCGCTACCCAGGACACCAGCC
TCCAGGACGGCTGCCTCATCTACAACGTCAAGATCAGAGGGGTGAACTTCC
CATCCAACGGCCCTGTGATGCAGAAGAAAACACTCGGCTGGGAGGCCAACA
CCGAGATGCTGTACCCCGCTGACGGCGGCCTGGAAGGCAGAGGGGACATG
GCCCTGAAGCTCGTGGGCGGGGGCCACCTGATCTGCAACTTGAAGACCACA
TACAGATCCAAGAAACCCGCTAAGAACCTCAAGATGCCCGGCGTCTACTAT
GTGGACCGCAGACTGGAAAGAATCAAGGAGGCCGACAAAGAGACCTACGT
CGAGCAGCACGAGGTGGCTGTGGCCAGATACTGCGACCTCCCTAGCAA
GGGGCACAAGCTTAATTAAGAATTCGAAGCTTGGCTGTTTTGGCGGATGAG
AGAAGATTTTCAGCCTGATACAGATTAATCAGAACGCAGAAGCGGTCTGA
TAAACAGAATTTGCCTGGCGGCAGTAGCGCGGTGGTCCCACCTGACCCCA
TGCCGAACCTCAGAAGTGAAACGCCGTAGCGCCGATGGTAGTGTGGGGTCTC
CCCATGCGAGAGTAGGGAACCTGCCAGGCATCAAATAAAACGAAAGGCTCA
GTCGAAAGACTGGGCCTTTCGTTTTATCTGTTGTTTGTCTGGTGAACGCTCTC
CTGAGTAGGACAAATCCGCCGGGAGCGGATTTGAACGTTGCGAAGCAACG
GCCCCGAGGGTGGCGGGCAGGACGCCCGCCATAAACTGCCAGGCATCAA
TTAAGCAGAAGGCCATCCTGACGGATGGCCTTTTTGCGTTTCTACAAACTCT
TTTGTATTTTTTCTAAATACATTCAAATATGTATCCGCTCATGAGACAATA
ACCCTGATAAATGCTTCAATAATATTGAAAAAGGAAGAGTATGAGTATTCA
ACATTTCCGTGTCGCCCTTATTCCTTTTTTGCGGCATTTCCTTCTGTTTT
TGCTCACCCAGAAACGCTGGTGAAAGTAAAAGATGCTGAAGATCAGTTGGG
TGCACGAGTGGGTTACATCGAACTGGATCTCAACAGCGGTAAGATCCTTGA
GAGTTTTCGCCCCGAAGAACGTTTTCCAATGATGAGCACTTTTAAAGTTCTG
CTATGTGGCGCGGTATTATCCCGTGTGACGCCGGGCAAGAGCAACTCGGT
CGCCGCATACACTATTCTCAGAATGACTTGGTTGAGTACTACCAGTCACAG
AAAAGCATCTTACGGATGGCATGACAGTAAGAGAATTATGCAGTGCTGCCA
TAACCATGAGTGATAACACTGCGGCCAACTTACTTCTGACAACGATCGGAG
GACCGAAGGAGCTAACCGCTTTTTTGCACAACATGGGGGATCATGTAACCTC
GCCTTGATCGTTGGGAACCGGAGCTGAATGAAGCCATACCAAACGACGAGC
GTGACACCACGATGCCTGTAGCAATGGCAACAACGTTGCGCAAACCTATTAA
CTGGCGAACTACTTACTCTAGCTTCCCGGCAACAATTAATAGACTGGATGG
AGGCGGATAAAGTTGCAGGACCACTTCTGCGCTCGGCCCTCCGGCTGGCT
GGTTTTATTGCTGATAAATCTGGAGCCGGTGAGCGTGGGTCTCGCGGTATCAT
TGCAGCACTGGGGCCAGATGGTAAGCCCTCCCGTATCGTAGTTATCTACAC
GACGGGGAGTCAGGCAACTATGGATGAACGAAATAGACAGATCGCTGAGA
TAGGTGCCTCACTGATTAAGCATTGGTAACTGTCAGACCAAGTTTACTCATA
TATACTTTAGATTGATTTAAACTTCATTTTTAATTTAAAGGATCTAGGTG

AAGATCCTTTTTGATAATCTCATGACCAAATCCCTTAACGTGAGTTTTTCGT
TCCACTGAGCGTCAGACCCCGTAGAAAAGATCAAAGGATCTTCTTGAGATC
CTTTTTTCTGCGCGTAATCTGCTGCTTGCAAACAAAAAACACCGCTACC
AGCGGTGTTTTGTTTGCCGGATCAAGAGCTACCAACTCTTTTTCCGAAGGTA
ACTGGCTTCAGCAGAGCGCAGATACCAAATACTGTCCTTCTAGTGTAGCCG
TAGTTAGGCCACCACTTCAAGAACTCTGTAGCACCGCCTACATACCTCGCTC
TGCTAATCCTGTTACCAAGTGGCTGCTGCCAGTGGCGATAAGTCGTGTCTTAC
CGGGTTGGACTIONAAGACGATAGTTACCGGATAAAGGCGCAGCGGTGCGGGCTG
AACGGGGGGTTCGTGCACACAGCCCAGCTTGGAGCGAACGACCTACACCGA
ACTGAGATACCTACAGCGTGAGCTATGAGAAAGCGCCACGCTTCCCGAAGG
GAGAAAGGCGGACAGGTATCCGGTAAGCGGCAGGGTCGGAACAGGAGAGC
GCACGAGGGAGCTTCCAGGGGGAAACGCCTGGTATCTTTATAGTCTGTGCG
GGTTTCGCCACCTCTGACTTGAGCGTCGATTTTTGTGATGCTCGTCAGGGGG
GCGGAGCCTATGGAAAACGCCAGCAACGCGGCCTTTTTACGGTTCCTGGC
CTTTTGCTGGCCTTTTGCTCACATGTTCTTCTCCTGCGTTATCCCCTGATTCTG
TGGATAACCGTATTACCGCCTTTGAGTGAGCTGATACCGCTCGCCGCAGCCG
AACGACCGAGCGCAGCGAGTCAGTGAGCGAGGAAGCGGAAGAGCGCCTGA
TGCGGTATTTTCTCCTTACGCATCTGTGCGGTATTTACACCCGCATATGGTG
CACTCTCAGTACAATCTGCTCTGATGCCGCATAGTTAAGCCAGTATACACTC
CGCTATCGCTACGTGACTGGGTGATGGCTGCGCCCCGACACCCGCCAACAC
CCGCTGACGCGCCCTGACGGGCTTGTCTGCTCCCGGCATCCGCTTACAGACA
AGCTGTGACCGTCTCCGGGAGCTGCATGTGTGTCAGAGGTTTTACCGTTCATCA
CCGAAACGCGCGAGGCAGCAGATCAATTCGCGCGCGAAGGCGAAGCGGCA
TGCATAATGTGCTGTCAAATGGACGAAGCAGGGATTCTGCAAACCCTATG
CTACTCCGTCAAGCCGTCAATTGTCTGATTCGTTACCAATTATGACAACTTG
ACGGCTACATCATTTCACTTTTTCTTACAAACCGGCACGGAACCTCGCTCGGGC
TGGCCCCGGTGCATTTTTTAAATACCCGCGAGAAATAGAGTTGATCGTCAA
AACCAACATTGCGACCGACGGTGGCGATAGGCATCCGGGTGGTGCTCAAAA
GCAGCTTCGCCTGGCTGATACGTTGGTCCTCGCGCCAGCTTAAGACGCTAAT
CCCTAACTGCTGGCGGAAAAGATGTGACAGACGCGACGGCGACAAGCAA
CATGCTGTGCGACGCTGGCGATATCAAATTGCTGTCTGCCAGGTGATCGCT
GATGTACTGACAAGCCTCGCGTACCCGATTATCCATCGGTGGATGGAGCGA
CTCGTTAATCGCTTCCATGCGCCGAGTAACAATTGCTCAAGCAGATTTATC
GCCAGCAGCTCCGAATAGCGCCCTTCCCCTTGCCCGGCGTTAATGATTTGCC
CAAACAGGTCGCTGAAATGCGGCTGGTGCGCTTCATCCGGGCGAAAGAACC
CCGTATTGGCAAATATTGACGGCCAGTTAAGCCATTCATGCCAGTAGGGCG
GCGGACGAAAGTAAACCCACTGGTGATACCATTGCGGAGCCTCCGGATGAC
GACCGTAGTGATGAATCTCTCCTGGCGGGAACAGCAAAATATCACCCGGTC

GGCAAACAAATTCTCGTCCCTGATTTTTTCACCACCCCCTGACCGCGAATGGT
GAGATTGAGAATATAACCTTTCATTCCCAGCGGTCCGGTCGATAAAAAAATC
GAGATAACCGTTGGCCTCAATCGGCGTTAAACCCGCCACCAGATGGGCATT
AAACGAGTATCCCGGCAGCAGGGGATCATTTTGCGCTTCAGCCATACTTTTC
ATACTCCCGCCATTCAGAG

pBAD/HisB-mEos2:

AAGAAACCAATTGTCCATATTGCATCAGACATTGCCGTCACTGCGTCTTTTA
CTGGCTCTTCTCGCTAACCAAACCGGTAACCCCGCTTATTAAGCATTCTG
TAACAAAGCGGGACCAAAGCCATGACAAAAACGCGTAACAAAAGTGTCTA
TAATCACGGCAGAAAAGTCCACATTGATTATTTGCACGGCGTCACACTTTGC
TATGCCATAGCATTTTTATCCATAAGATTAGCGGATCCTACCTGACGCTTTT
TATCGCAACTCTCTACTGTTTCTCCATAACCCGTTTTTTGGGCTAACAGGAGG
AATTAACCATGGGGGGTTCTCATCATCATCATCATGGTATGGCTAGCAT
GACTGGTGGACAGCAAATGGGTCGGGATCTGTACGACGATGACGATAAGG
ATCCGAGCTCGAGATCTATGAGTGCGATTAAGCCAGACATGAAGATCAAAC
TCCGTATGGAAGGCAACGTAACGGGCACCACTTTGTGATCGACGGAGATG
GTACAGGCAAGCCTTTTGAGGGAAAACAGAGTATGGATCTTGAAGTCAAAG
AGGGCGGACCTCTGCCTTTTGCCTTTGATATCCTGACCACTGCATTCCATTA
CGGCAACAGGGTATTCGCCAAATATCCAGACAACATAACAAGACTATTTTAA
GCAGTCGTTTCCTAAGGGGTATTCGTGGGAACGAAGCTTGACTTTCGAAGA
CGGGGGCATTTCATTGCCAGAAACGACATAACAATGGAAGGGGACACTTT
CTATAATAAAGTTCGATTTTATGGTACCAACTTTCCCGCCAATGGTCCAGTT
ATGCAGAAGAAGACGCTGAAATGGGAGCCCTCCACTGAGAAAATGTATGT
GCGTGATGGAGTGCTGACGGGTGATATTCATATGGCTTTGTTGCTTGAAGG
AAATGCCATTACCGATGTGACTTCAGAACTACTTACAAAGCTAAGGAGAA
GGGTGTCAAGTTACCAGGCTACCCTTTGTGGACCACTGCATTGAGATTTTA
AGCCATGACAAAGATTACAACAAGGTTAAGCTGTATGAGCATGCTGTTGCT
CATTCTGGATTGCCTGACAATGCCAGACGATAAGAATTTCGAAGCTTGGCTG
TTTTGGCGGATGAGAGAAGATTTTCAGCCTGATACAGATTAATCAGAACG
CAGAAGCGGTCTGATAAAACAGAATTTGCCTGGCGGCAGTAGCGCGGTGGT
CCCACCTGACCCCATGCCGAACTCAGAAGTGAAACGCCGTAGCGCCGATGG
TAGTGTGGGGTCTCCCATGCGAGAGTAGGGAAGTCCAGGCATCAAATAA
AACGAAAGGCTCAGTCGAAAGACTGGGCCTTTTCGTTTTATCTGTTGTTTGT
GGTGAACGCTCTCCTGAGTAGGACAAATCCGCCGGGAGCGGATTTGAACGT
TGCGAAGCAACGGCCCCGGAGGGTGGCGGGCAGGACGCCCGCCATAAACTG

CCAGGCATCAAATTAAGCAGAAGGCCATCCTGACGGATGGCCTTTTTGCGT
TTCTACAAACTCTTTTGTATTATTTTTCTAAATACATTCAAATATGTATCCGCT
CATGAGACAATAACCCTGATAAATGCTTCAATAATATTGAAAAAGGAAGAG
TATGAGTATTCAACATTTCCGTGTCGCCCTTATTCCCTTTTTTGGCGCATTTT
GCCTTCCTGTTTTTGTCTACCCAGAAACGCTGGTGAAAGTAAAAGATGCTG
AAGATCAGTTGGGTGCACGAGTGGGTACATCGAACTGGATCTCAACAGCG
GTAAGATCCTTGAGAGTTTTCGCCCCGAAGAACGTTTTCCAATGATGAGCA
CTTTTAAAGTTCTGCTATGTGGCGCGGTATTATCCCGTGTTGACGCCGGCA
AGAGCAACTCGGTCCGCATACACTATTCTCAGAATGACTTGGTTGAGTA
CTCACCAGTCACAGAAAAGCATCTTACGGATGGCATGACAGTAAGAGAATT
ATGCAGTGCTGCCATAACCATGAGTGATAAACTGCGGCCAACTTACTTCT
GACAACGATCGGAGGACCGAAGGAGCTAACCGCTTTTTTGCACAACATGGG
GGATCATGTAACCTCGCCTTGATCGTTGGGAACCGGAGCTGAATGAAGCCAT
ACCAAACGACGAGCGTGACACCACGATGCCTGTAGCAATGGCAACAACGTT
GCGCAAACCTATTAACCTGGCGAACTACTTACTCTAGCTTCCCGGCAACAATTA
ATAGACTGGATGGAGGCGGATAAAGTTGCAGGACCCTTCTGCGCTCGGCC
CTTCCGGCTGGCTGGTTTATTGCTGATAAATCTGGAGCCGGTGAGCGTGGGT
CTCGCGGTATCATTGCAGCACTGGGGCCAGATGGTAAGCCCTCCCGTATCGT
AGTTATCTACACGACGGGGAGTCAGGCAACTATGGATGAACGAAATAGAC
AGATCGCTGAGATAGGTGCCTCACTGATTAAGCATTGGTAACTGTCAGACC
AAGTTTACTCATATATACTTTAGATTGATTTAAAACCTTCATTTTTAATTTAA
AAGGATCTAGGTGAAGATCCTTTTTGATAATCTCATGACCAAATCCCTTAA
CGTGAGTTTTCGTTCCACTGAGCGTCAGACCCCGTAGAAAAGATCAAAGGA
TCTTCTTGAGATCCTTTTTTTCTGCGCGTAATCTGCTGCTTGCAAACAAAAA
AACCACCGCTACCAGCGGTGGTTTGTGGCCGGATCAAGAGCTACCAACTCT
TTTTCCGAAGGTAACCTGGCTTCAGCAGAGCGCAGATACCAAATACTGTCTT
CTAGTGTAGCCGTAGTTAGGCCACCACTTCAAGAACTCTGTAGCACCGCCTA
CATACCTCGCTCTGCTAATCCTGTTACCAGTGGCTGCTGCCAGTGGCGATAA
GTCGTGTCTTACCGGGTTGGACTCAAGACGATAGTTACCGGATAAAGGCGCA
GCGGTCCGGGCTGAACGGGGGGTTCGTGCACACAGCCCAGCTTGGAGCGAAC
GACCTACACCGAACTGAGATACCTACAGCGTGAGCTATGAGAAAGCGCCAC
GCTTCCCGAAGGGAGAAAGGCGGACAGGTATCCGGTAAGCGGCAGGGTCG
GAACAGGAGAGCGCACGAGGGAGCTTCCAGGGGGAAACGCCTGGTATCTT
TATAGTCTGTGCGGTTTCGCCACCTCTGACTTGAGCGTCGATTTTTGTGAT
GCTCGTCAGGGGGGCGGAGCCTATGGAAAAACGCCAGCAACGCGGCCTTTT
TACGGTTCCTGGCCTTTTGTGGCCTTTTGTCTACATGTTCTTTCTGCGTTA
TCCCCTGATTCTGTGGATAACCGTATTACCGCCTTTGAGTGAGCTGATACCG
CTCGCCGCAGCCGAACGACCGAGCGCAGCGAGTCAGTGAGCGAGGAAGCG

GAAGAGCGCCTGATGCGGTATTTTCTCCTTACGCATCTGTGCGGTATTTAC
ACCGCATATGGTGCACCTCTCAGTACAATCTGCTCTGATGCCGCATAGTTAAG
CCAGTATACACTCCGCTATCGCTACGTGACTGGGTTCATGGCTGCGCCCGAC
ACCCGCCAACCCCGCTGACGCGCCCTGACGGGCTTGTCTGCTCCCGGCATC
CGCTTACAGACAAGCTGTGACCGTCTCCGGGAGCTGCATGTGTCAGAGGTT
TTCACCGTCATCACCGAAACGCGCGAGGCAGCAGATCAATTCGCGCGCGAA
GGCGAAGCGGCATGCATAATGTGCCTGTCAAATGGACGAAGCAGGGATTCT
GCAAACCCCTATGCTACTCCGTCAAGCCGTCAATTGTCTGATTCGTTACCAAT
TATGACAACCTTGACGGCTACATCATTCACTTTTTCTTCACAACCCGGCACGGA
ACTCGCTCGGGCTGGCCCCGGTGCATTTTTTAAATACCCGCGAGAAATAGA
GTTGATCGTCAAACCAACATTGCGACCGACGGTGGCGATAGGCATCCGGG
TGGTGCTCAAAGCAGCTTCGCCTGGCTGATACGTTGGTCTCGCGCCAGCT
TAAGACGCTAATCCCTAACTGCTGGCGGAAAAGATGTGACAGACGCGACGG
CGACAAGCAAACATGCTGTGCGACGCTGGCGATATCAAATGCTGTCTGC
CAGGTGATCGCTGATGTACTGACAAGCCTCGCGTACCCGATTATCCATCGGT
GGATGGAGCGACTCGTTAATCGCTTCCATGCGCCGCAGTAACAATTGCTCA
AGCAGATTTATCGCCAGCAGCTCCGAATAGCGCCCTTCCCCTTGCCCGGCGT
TAATGATTTGCCCAAACAGGTCGCTGAAATGCGGCTGGTGCCTTCATCCG
GGCGAAAGAACCCCGTATTGGCAAATATTGACGGCCAGTTAAGCCATTCAT
GCCAGTAGGCGCGCGGACGAAAGTAAACCCACTGGTGATAACCATTGCGGAG
CCTCCGGATGACGACCGTAGTGATGAATCTCTCCTGGCGGGAACAGCAAAA
TATCACCCGGTTCGGCAAACAAATTCTCGTCCCTGATTTTTTACCACCCCTG
ACCGCGAATGGTGAGATTGAGAATATAACCTTTCATTCCCAGCGGTTCGGTC
GATAAAAAAATCGAGATAACCGTTGGCCTCAATCGGCGTTAAACCCGCCAC
CAGATGGGCATTAAACGAGTATCCCGGCAGCAGGGGATCATTTTTGCGCTTC
AGCCATACTTTTCATACTCCCGCCATTCAGAG

pET-mEos2:

CAAGGAGATGGCGCCCAACAGTCCCCCGGCCACGGGGCCTGCCACCATAACC
CACGCCGAAACAAGCGCTCATGAGCCCGAAGTGGCGAGCCCGATCTTCCCC
ATCGGTGATGTGCGCGATATAGGCGCCAGCAACCGCACCTGTGGCGCCGGT
GATGCCGGCCACGATGCGTCCGGCGTAGAGGATCGAGATCTCGATCCCGCG
AAATTAATACGACTCACTATAGGGGAATTGTGAGCGGATAACAATTCCCCT
CTAGAAATAATTTTGTTTAACTTTAAGAAGGAGATATACATATGGGCAGCA
GCCATCATCATCATCACGGCAGCGGCCTGGTGCCGCGCGGCAGCGCTA
GCATGTCGGACTCAGAAGTCAATCAAGAAGCTAAGCCAGAGGTCAAGCCA

GAAGTCAAGCCTGAGACTCACATCAATTTAAAGGTGTCCGATGGATCTTCA
GAGATCTTCTTCAAGATCAAAAAGACCACTCCTTTAAGAAGGCTGATGGAA
GCGTTCGCTAAAAGACAGGGTAAGGAAATGGACTCCTTAAGATTCTTGTAC
GACGGTATTAGAATTCATGAGTGGGATTAAGCCAGACATGAAGATCAAAC
CCGTATGGAAGGCAACGTAAACGGGCACCACTTTGTGATCGACGGAGATGG
TACAGGCAAGCCTTTTGAGGGAAAACAGAGTATGGATCTTGAAGTCAAAGA
GGGCGGACCTCTGCCTTTTGCCTTTGATATCCTGACCACTGCATTCCATTAC
GGCAACAGGGTATTTCGCCAAATATCCAGACAACATAACAAGACTATTTTAAG
CAGTCGTTTCCTAAGGGGTATTTCGTGGGAACGAAGCTTGACTTTCGAAGAC
GGGGGCATTTGCATTGCCAGAAACGACATAACAATGGAAGGGGACACTTTC
TATAATAAAGTTCGATTTTATGGTACCAACTTTCCCGCCAATGGTCCAGTTA
TGCAGAAGAAGACGCTGAAATGGGAGCCCTCCACTGAGAAAATGTATGTGC
GTGATGGAGTGCTGACGGGTGATATTCATATGGCTTTGTTGCTTGAAGGAA
ATGCCATTACCGATGTGACTTCAGAACTACTTACAAAGCTAAGGAGAAGG
GTGTCAAGTTACCAGGCTACCACTTTGTGGACCACTGCATTGAGATTTTAAG
CCATGACAAAGATTACAACAAGGTTAAGCTGTATGAGCATGCTGTTGCTCA
TTCTGGATTGCCTGACAATGCCAGACGATAAAAGCTGATCAGACCCCTGAA
GATTTGGACATGGAGGATAACGATATTATTGAGGCTCACAGAGAACAGATT
GGTGGTAGACAAGCTTAGGTATTTATTCGGCGCAAAGTGCGTCCGGGTGATG
CTGCCAACTTAGTCGAGCACCACCACCACCACCACTGAGATCCGGCTGCTA
ACAAAGCCCGAAAGGAAGCTGAGTTGGCTGCTGCCACCGCTGAGCAATAAC
TAGCATAACCCCTTGGGGCCTCTAAACGGGTCTTGAGGGGTTTTTTTGTGAA
AGGAGGAACTATATCCGGATTGGCGAATGGGACGCGCCCTGTAGCGGCGCA
TTAAGCGCGGCGGGTGTGGTGGTTACGCGCAGCGTGACCGCTACACTTGCC
AGCGCCCTAGCGCCCGCTCCTTTTCGCTTTCTTCCCTTCCTTTCTCGCCACGTT
CGCCGGCTTTCCCGTCAAGCTCTAAATCGGGGGCTCCCTTTAGGGTTCCGA
TTTAGTGCTTTACGGCACCTCGACCCCAAAAACTTGATTAGGGTGATGGTT
CACGTAGTGGGCCATCGCCCTGATAGACGTTTTTTTCGCCCTTTGACGTTGGA
GTCCACGTTCTTTAATAGTGGACTCTTGTTCCAAACCTGGAACAACACTCAAC
CCTATCTCGGTCTATTCTTTTATTTATAAGGGATTTTGCCGATTTTCGGCCTA
TTGGTTAAAAAATGAGCTGATTTAACAAAAATTTAACGCGAATTTTAACAA
AATATTAACGCTTACAATTTAGGTGGCACTTTTCGGGGAAATGTGCGCGGA
ACCCCTATTTGTTTATTTTTCTAAATACATTCAAATATGTATCCGCTCATGAA
TTAATCTTAGAAAACTCATCGAGCATCAAATGAAACTGCAATTTATTCAT
ATCAGGATTATCAATACCATATTTTTGAAAAAGCCGTTTCTGTAATGAAGG
AGAAAACTCACCGAGGCAGTTCATAGGATGGCAAGATCCTGGTATCGGTC
TGCGATTCCGACTCGTCCAACATCAATACAACCTATTAATTTCCCTCGTCA
AAAATAAGGTTATCAAGTGAGAAATCACCATGAGTGACGACTGAATCCGGT

GAGAATGGCAAAAGTTTATGCATTTCTTTCCAGACTTGTTCAACAGGCCAGC
CATTACGCTCGTCATCAAAATCACTCGCATCAACCAAACCGTTATTCATTCCG
TGATTGCGCCTGAGCGAGACGAAATACGCGATCGCTGTTAAAAGGACAATT
ACAAACAGGAATCGAATGCAACCGGCGCAGGAACACTGCCAGCGCATCAA
CAATATTTTCACCTGAATCAGGATATTCTTCTAATACCTGGAATGCTGTTTT
CCCGGGGATCGCAGTGGTGAGTAACCATGCATCATCAGGAGTACGGATAAA
ATGCTTGATGGTCGGAAGAGGCATAAATTCGGTCAGCCAGTTTAGTCTGAC
CATCTCATCTGTAACATCATTGGCAACGCTACCTTTGCCATGTTTCAGAAAC
AACTCTGGCGCATCGGGCTTCCCATAACAATCGATAGATTGTTCGCACCTGATT
GCCCAGACATTATCGCGAGCCATTTATACCCATATAAATCAGCATCCATGTT
GGAATTTAATCGCGGCCTAGAGCAAGACGTTTCCCGTTGAATATGGCTCAT
AACACCCCTTGTATTACTGTTTATGTAAGCAGACAGTTTTATTGTTTCATGAC
CAAATCCCTTAACGTGAGTTTTCGTTCCACTGAGCGTCAGACCCCGTAGAA
AAGATCAAAGGATCTTCTTGAGATCCTTTTTTTCTGCGCGTAATCTGCTGCT
TGCAAACAAAAAACCACCGCTACCAGCGGTGGTTTTGTTTGCCGGATCAAG
AGCTACCAACTCTTTTTCCGAAGGTAACTGGCTTCAGCAGAGCGCAGATAC
CAAATACTGTCCTTCTAGTGTAGCCGTAGTTAGGCCACCACCTCAAGAACTC
TGTAGCACCGCCTACATACCTCGCTCTGCTAATCCTGTTACCAGTGGCTGCT
GCCAGTGGCGATAAGTCGTGTCTTACCGGGTTGGACTCAAGACGATAGTTA
CCGGATAAGGCGCAGCGGTCTGGGCTGAACGGGGGGTTTCGTGCACACAGCCC
AGCTTGGAGCGAACGACCTACACCGAACTGAGATACCTACAGCGTGAGCTA
TGAGAAAGCGCCACGCTTCCCAGAGGGAGAAAGGCGGACAGGTATCCGGT
AAGCGGCAGGGTTCGGAACAGGAGAGCGCACGAGGGAGCTTCCAGGGGGAA
ACGCCTGGTATCTTTATAGTCCTGTCTGGGTTTTCGCCACCTCTGACTTGAGCG
TCGATTTTTGTGATGCTCGTCAGGGGGGCGGAGCCTATGGAAAAACGCCAG
CAACGCGGCCTTTTTACGGTTCCTGGCCTTTTTGCTGGCCTTTTTGCTCACATGT
TCTTTCCTGCGTTATCCCCTGATTCTGTGGATAACCGTATTACCGCCTTTGAG
TGAGCTGATACCGCTCGCCGCAGCCGAACGACCGAGCGCAGCGAGTCAGTG
AGCGAGGAAGCGGAAGAGCGCCTGATGCGGTATTTTCTCCTTACGCATCTG
TGCGGTATTTACACCGCAATGGTGCCTCTCAGTACAATCTGCTCTGATGC
CGCATAGTTAAGCCAGTATACTCCGCTATCGCTACGTGACTGGGTCATGG
CTGCGCCCCGACACCCGCCAACACCCGCTGACGCGCCCTGACGGGCTTGTCT
GCTCCCGGCATCCGCTTACAGACAAGCTGTGACCGTCTCCGGGAGCTGCAT
GTGTCAGAGGTTTTACCGTCATACCGAAACGCGCGAGGCAGCTGCGGTA
AAGCTCATCAGCGTGGTCGTGAAGCGATTCACAGATGTCTGCCTGTTTCATCC
GCGTCCAGCTCGTTGAGTTTTCTCCAGAAGCGTTAATGTCTGGCTTCTGATAA
AGCGGGCCATGTTAAGGGCGGTTTTTTCTGTTTGGTCACTGATGCCTCCGT
GTAAGGGGGATTTCTGTTTCATGGGGGTAATGATACCGATGAAACGAGAGAG

GATGCTCACGATACGGGTTACTGATGATGAACATGCCCGGTTACTGGAACG
TTGTGAGGGTAAACAACCTGGCGGTATGGATGCGGCGGGACCAGAGAAAAA
TCACTCAGGGTCAATGCCAGCGCTTCGTTAATACAGATGTAGGTGTTCCACA
GGGTAGCCAGCAGCATCCTGCGATGCAGATCCGGAACATAATGGTGCAGGG
CGCTGACTTCCGCGTTTCCAGACTTTACGAAACACGGAAACCGAAGACCAT
TCATGTTGTTGCTCAGGTCCGAGACGTTTTTGCAGCAGCAGTCCGTTACGTT
CGCTCGCGTATCGGTGATTCATTCTGCTAACCAGTAAGGCAACCCCGCCAGC
CTAGCCGGGTCCCAACGACAGGAGCAGATCATGCGCACCCGTGGGGCCG
CCATGCCGGCGATAATGGCCTGCTTCTCGCCGAAACGTTTGGTGGCGGGAC
CAGTGACGAAGGCTTGAGCGAGGGCGTGCAAGATTCCGAATACCGCAAGC
GACAGGCCGATCATCGTCGCGCTCCAGCGAAAGCGGTCCTCGCCGAAAATG
ACCCAGAGCGCTGCCGGCACCTGTCCTACGAGTTGCATGATAAAGAAGACA
GTCATAAGTGCGGCGACGATAGTCATGCCCCGCGCCCACCGGAAGGAGCTG
ACTGGGTTGAAGGCTCTCAAGGGCATCGGTGAGATCCCGGTGCCTAATGA
GTGAGCTAACTTACATTAATTGCGTTGCGCTCACTGCCCGCTTCCAGTCGG
GAAACCTGTCGTGCCAGCTGCATTAATGAATCGGCCAACGCGCGGGGAGAG
GCGGTTTGGTATTGGGCGCCAGGGTGGTTTTTCTTTTACCAGTGAGACGG
GCAACAGCTGATTGCCCTTACC GCCTGGCCCTGAGAGAGTTGCAGCAAGC
GGTCCACGCTGGTTTGGCCAGCAGGCGAAAATCCTGTTTGATGGTGGTTA
ACGGCGGGATATAACATGAGCTGTCTTCGGTATCGTCGTATCCC ACTACCGA
GATATCCGCACCAACGCGCAGCCCGACTCGGTAATGGCGCGCATTGCGCC
CAGCGCCATCTGATCGTTGGCAACCAGCATCGCAGTGGGAACGATGCCCTC
ATTCAGCATTGTCATGGTTTGTGAAAACCGGACATGGCACTCCAGTCGCCT
TCCCGTTCCGCTATCGGCTGAATTTGATTGCGAGTGAGATATTTATGCCAGC
CAGCCAGACGCAGACGCGCCGAGACAGAACTTAATGGGCCC GCTAACAGC
GCGATTTGCTGGTGACCCAATGCGACCAGATGCTCCACGCCAGTCGCGTA
CCGTCTTCATGGGAGAAAATAATACTGTTGATGGGTGTCTGGTCAGAGACA
TCAAGAAATAACGCCGGAACATTAGTGCAGGCAGCTTCCACAGCAATGGCA
TCCTGGTCATCCAGCGGATAGTTAATGATCAGCCACTGACGCGTTGCGCG
AGAAGATTGTGCACCGCCGCTTTACAGGCTTCGACGCCGCTTCGTTCTACCA
TCGACACCACCAGCTGGCACCCAGTTGATCGGCGCGAGATTTAATCGCCG
CGACAATTTGCGACGGCGCGTGCAGGGCCAGACTGGAGGTGGCAACGCCA
ATCAGCAACGACTGTTTGGCCGCCAGTTGTTGTGCCACGCGGTTGGGAATGT
AATTCAGCTCCGCCATCGCCGCTTCCACTTTTTCCCGCGTTTTTCGCAGAAAC
GTGGCTGGCCTGGTTCACCACGCGGGAAACGGTCTGATAAGAGACACCGGC
ATACTCTGCGACATCGTATAACGTTACTGGTTTCACATTCACCACCCTGAAT
TGACTCTCTTCCGGGCGCTATCATGCCATAACCGCGAAAGTTTTGCGCCATT
CGATGGTGTCCGGGATCTCGACGCTCTCCCTTATGCGACTCCTGCATTAGGA

AGCAGCCCAGTAGTAGGTTGAGGCCGTTGAGCACCGCCGCCGCAAGGAATG
GTGCATG

pBAD/HisB-Dendra2:

AAGAAACCAATTGTCCATATTGCATCAGACATTGCCGTCACTGCGTCTTTTA
CTGGCTCTTCTCGCTAACCAAACCGGTAACCCCGCTTATTAAGCATTCTG
TAACAAAGCGGGACCAAAGCCATGACAAAAACGCGTAACAAAAGTGTCTA
TAATCACGGCAGAAAAGTCCACATTGATTATTTGCACGGCGTCACACTTTGC
TATGCCATAGCATTTTTATCCATAAGATTAGCGGATCCTACCTGACGCTTTT
TATCGCAACTCTCTACTGTTTCTCCATACCCGTTTTTTGGGCTAACAGGAGG
AATTAACCATGGGGGTTCTCATCATCATCATCATGGTATGGCTAGCAT
GACTGGTGGACAGCAAATGGGTCGGGATCTGTACGACGATGACGATAAGG
ATCCGAGCTCGAGATCTATGAACACCCCGGAATTAACCTGATCAAGGAGG
ACATGCGCGTGAAGGTGCACATGGAGGGCAACGTGAACGGCCACGCCTTCG
TGATCGAGGGCGAGGGCAAGGGCAAGCCCTACGAGGGCACCCAGACCCGCC
AACCTGACCGTGAAGGAGGGCGCCCCCTGCCCTTCAGCTACGACATCCTG
ACCACCGCCGTGCACTACGGCAACCGGGTGTTCACCAAGTACCCCGAGGAC
ATCCCGACTACTTCAAGCAGAGCTTCCCCGAGGGCTACAGCTGGGAGCGC
ACCATGACCTTCGAGGACAAGGGCATCTGCACCATCCGCAGCGACATCAGC
CTGGAGGGCGACTGCTTCTTCCAGAACGTGCGCTTCAAGGGCACCAACTTC
CCCCCAACGGCCCCGTGATGCAGAAGAAGACCCTGAAGTGGGAGCCCAGC
ACCGAGAAGCTGCACGTGCGCGACGGCCTGCTGGTGGGCAACATCAACATG
GCCCTGCTGCTGGAGGGCGGCGGCCACTACCTGTGCGACTTCAAGACCACC
TACAAGGCCAAGAAGGTGGTGCAGCTGCCCCGACGCCACTTCGTGGACCAC
CGCATCGAGATCCTGGGCAACGACAGCGACTACAACAAGGTGAAGCTGTAC
GAGCACGCCGTGGCCCCGTACAGCCCCCTGCCAGCCAGGTGTGGTAAGAA
TTCGAAGCTTGGCTGTTTTGGCGGATGAGAGAAGATTTTCAGCCTGATACA
GATTAATCAGAACGCAGAAGCGGTCTGATAAACAGAATTTGCCTGGCGG
CAGTAGCGCGGTGGTCCCACCTGACCCCATGCCGAACTCAGAAGTGAAACG
CCGTAGCGCCGATGGTAGTGTGGGGTCTCCCCATGCGAGAGTAGGGAACTG
CCAGGCATCAAATAAAACGAAAGGCTCAGTCGAAAGACTGGGCCTTTTCGTT
TTATCTGTTGTTTGTTCGGTGAACGCTCTCCTGAGTAGGACAAATCCGCCGGG
AGCGGATTTGAACGTTGCGAAGCAACGGCCCCGAGGGTGGCGGGCAGGAC
GCCCCGCATAAACTGCCAGGCATCAAATTAAGCAGAAGGCCATCCTGACGG
ATGGCCTTTTTGCGTTTCTACAAACTCTTTTGTTTATTTTTCTAAATACATTC
AAATATGTATCCGCTCATGAGACAATAACCCTGATAAATGCTTCAATAATA

TTGAAAAAGGAAGAGTATGAGTATTCAACATTTCCGTGTCCGCTTATTCCC
TTTTTTGCGGCATTTTGCCTTCCTGTTTTTGCTCACCCAGAAACGCTGGTGAA
AGTAAAAGATGCTGAAGATCAGTTGGGTGCACGAGTGGGTACATCGAACT
GGATCTCAACAGCGGTAAGATCCTTGAGAGTTTTTCGCCCCGAAGAACGTTT
TCCAATGATGAGCACTTTTAAAGTTCTGCTATGTGGCGGGTATTATCCCGT
GTTGACGCCGGGCAAGAGCAACTCGGTGCGCCGATACACTATTCTCAGAAT
GACTTGGTTGAGTACTCACCAGTCACAGAAAAGCATCTTACGGATGGCATG
ACAGTAAGAGAATTATGCAGTGCTGCCATAACCATGAGTGATAACACTGCG
GCCAACTTACTTCTGACAACGATCGGAGGACCGAAGGAGCTAACCGCTTTT
TTGCACAACATGGGGGATCATGTAACCTCGCCTTGATCGTTGGGAACCGGAG
CTGAATGAAGCCATACCAAACGACGAGCGTGACACCACGATGCCTGTAGCA
ATGGCAACAACGTTGCGCAAATACTAATACTGGCGAACTACTTACTCTAGCTT
CCCGGCAACAATTAATAGACTGGATGGAGGCGGATAAAGTTGCAGGACCA
CTTCTGCGCTCGGCCCTCCGGCTGGCTGGTTTATTGCTGATAAATCTGGAG
CCGGTGAGCGTGGGTCTCGCGGTATCATTGCAGCACTGGGGCCAGATGGTA
AGCCCTCCCGTATCGTAGTTATCTACACGACGGGGAGTCAGGCAACTATGG
ATGAACGAAATAGACAGATCGCTGAGATAGGTGCCTCACTGATTAAGCATT
GGTAACTGTCAGACCAAGTTTACTCATATATACTTTAGATTGATTTAAACT
TCATTTTTAATTTAAAAGGATCTAGGTGAAGATCCTTTTTTGATAATCTCATG
ACCAAATCCCTTAACGTGAGTTTTCGTTCCACTGAGCGTCAGACCCCGTAG
AAAAGATCAAAGGATCTTCTTGAGATCCTTTTTTTCTGCGCGTAATCTGCTG
CTTGCAAACAAAAAACACCGCTACCAGCGGTGGTTTGTGGCCGGATCA
AGAGCTACCAACTCTTTTTCCGAAGGTAACCTGGCTTCAGCAGAGCGCAGAT
ACCAAATACTGTCCTTCTAGTGTAGCCGTAGTTAGGCCACCACTTCAAGAAC
TCTGTAGCACCGCCTACATACTCGCTCTGCTAATCCTGTTACCAGTGGCTG
CTGCCAGTGGCGATAAGTCGTGTCTTACCGGGTTGGACTCAAGACGATAGT
TACCGGATAAGGCGCAGCGGTGCGGCTGAACGGGGGGTTCGTGCACACAGC
CCAGCTTGAGCGAACGACCTACACCGAACTGAGATACCTACAGCGTGAGC
TATGAGAAAGCGCCACGCTTCCCGAAGGGAGAAAGGCGGACAGGTATCCG
GTAAGCGGCAGGGTCGGAACAGGAGAGCGCACGAGGGAGCTTCCAGGGGG
AAACGCCTGGTATCTTTATAGTCCTGTCGGGTTTTCGCCACCTCTGACTTGAG
CGTCGATTTTTGTGATGCTCGTCAGGGGGGCGGAGCCTATGGAAAACGCC
AGCAACGCGGCCTTTTTACGGTTCTGGCCTTTTGCTGGCCTTTTGCTCACAT
GTTCTTTCTGCGTTATCCCCTGATTCTGTGGATAACCGTATTACCGCCTTTG
AGTGAGCTGATACCGCTCGCCGCAGCCGAACGACCGAGCGCAGCGAGTCAG
TGAGCGAGGAAGCGGAAGAGCGCCTGATGCGGTATTTCTCCTTACGCATC
TGTGCGGTATTTACACCGCATATGGTGCCTCTCAGTACAATCTGCTCTGA
TGCCGCATAGTTAAGCCAGTATACACTCCGCTATCGCTACGTGACTGGGTCA

TGGCTGCGCCCCGACACCCGCCAACACCCGCTGACGCGCCCTGACGGGCTT
GTCTGCTCCCGGCATCCGCTTACAGACAAGCTGTGACCGTCTCCGGGAGCTG
CATGTGTCAGAGGTTTTACCGTCATCACCGAAACGCGCGAGGCAGCAGAT
CAATTCGCGCGCGAAGGCCAAGCGGCATGCATAATGTGCCTGTCAAATGGA
CGAAGCAGGGATTCTGCAAACCCTATGCTACTCCGTCAAGCCGTCAATTGTC
TGATTCGTTACCAATTATGACAACCTTGACGGCTACATCATTCACTTTTTCTTC
ACAACCGGCACGGAACCTCGCTCGGGCTGGCCCCGGTGCATTTTTTAAATAC
CCGCGAGAAATAGAGTTGATCGTCAAACCAACATTGCGACCGACGGTGGC
GATAGGCATCCGGGTGGTGCTCAAAGCAGCTTCGCCTGGCTGATACGTTG
GTCCCTCGCGCCAGCTTAAGACGCTAATCCCTAACTGCTGGCGGAAAAGATG
TGACAGACGCGACGGCGACAAGCAAACATGCTGTGCGACGCTGGCGATATC
AAAATTGCTGTCTGCCAGGTGATCGCTGATGTACTGACAAGCCTCGCGTACC
CGATTATCCATCGGTGGATGGAGCGACTCGTTAATCGCTTCCATGCGCCGCA
GTAACAATTGCTCAAGCAGATTTATCGCCAGCAGCTCCGAATAGCGCCCTTC
CCCTTGCCCGGCGTTAATGATTTGCCCAAACAGGTGCTGAAATGCGGCTG
GTGCGCTTCATCCGGGCGAAAGAACCCCGTATTGGCAAATATTGACGGCCA
GTTAAGCCATTCATGCCAGTAGGCGCGCGGACGAAAGTAAACCCACTGGTG
ATACCATTGCGGAGCCTCCGGATGACGACCGTAGTGATGAATCTCTCCTGGC
GGGAACAGCAAATATCACCCGGTCGGCAAACAAATTCTCGTCCCTGATTT
TTCACCACCCCCTGACCGCGAATGGTGAGATTGAGAATATAACCTTTCATTC
CCAGCGGTGCGTCGATAAAAAAATCGAGATAACCGTTGGCCTCAATCGGCG
TTAAACCCGCCACCAGATGGGCATTAACGAGTATCCCGGCAGCAGGGGAT
CATTTTGCGCTTCAGCCATACTTTTCATACTCCCGCCATTCAGAG

pBAD/HisB-PA-GFP:

AAGAAACCAATTGTCCATATTGCATCAGACATTGCCGTCCTGCGTCTTTTA
CTGGCTCTTCTCGCTAACCAAACCGGTAACCCCGCTTATTTAAAGCATTCTG
TAACAAAGCGGGACCAAAGCCATGACAAAAACGCGTAACAAAAGTGTCTA
TAATCACGGCAGAAAAGTCCACATTGATTATTTGCACGGCGTCACACTTTGC
TATGCCATAGCATTTTTATCCATAAGATTAGCGGATCCTACCTGACGCTTTT
TATCGCAACTCTCTACTGTTTCTCCATAACCCGTTTTTTGGGCTAACAGGAGG
AATTAACCATGGGGGGTTCTCATCATCATCATCATGGTATGGCTAGCAT
GACTGGTGGACAGCAAATGGGTCGGGATCTGTACGACGATGACGATAAGG
ATCCGAGCTCGAGATCTATGTCCATGGTGAGCAAGGGCGAGGAGCTGTTCA
CCGGGGTGGTGGCCATCCTGGTCGAGCTGGACGGCGACGTAAACGGCCACA
AGTTCAGCGTGTCCGGCGAGGGCGAGGGCGATGCCACCTACGGCAAGCTGA

CCCTGAAGTTCATCTGCACCACCGGCAAGCTGCCCGTGCCCTGGCCCACCCT
CGTGACCACCTTCAGCTACGGCGTGCAAGTGCCTTCAGCCGCTACCCCGACCAC
ATGAAGCAGCAGACTTCTTCAAGTCCGCCATGCCCGAAGGCTACGTCCAG
GAGCGCACCATCTTCTTCAAGGACGACGGCAACTACAAGACCCGCGCCGAG
GTGAAGTTCGAGGGCGACACCCTGGTGAACCGCATCGAGCTGAAGGGCATC
GACTTCAAGGAGGACGGCAACATCCTGGGGCACAAGCTGGAGTACAACACTAC
AACAGCCACAACGTCTATATCATGGCCGACAAGCAGAAGAACGGCATCAA
GGCCAACCTTCAAGATCCGCCACAACATCGAGGACGGCAGCGTGCAGCTCGC
CGACCACTACCAGCAGAACACCCCATCGGGCAGCGCCCCGTGCTGCTGCC
CGACAACCACTACCTGAGCCACCAGTCCAAGCTGAGCAAAGACCCCAACGA
GAAGCGCGATCACATGGTCTGCTGGAGTTCGTGACCGCCGCCCCGGGATCA
CTCTCGGCATGGACGAGCTGTACAAGTAAGAATTCGAAGCTTGGCTGTTTT
GGCGGATGAGAGAAGATTTTCAGCCTGATACAGATTAAATCAGAACGCAGA
AGCGGTCTGATAAAACAGAATTTGCCTGGCGGCAGTAGCGCGGTGGTCCCA
CCTGACCCCATGCCGAACCTCAGAAGTGAAACGCCGTAGCGCCGATGGTAGT
GTGGGGTCTCCCCATGCGAGAGTAGGGAACCTGCCAGGCATCAAATAAAACG
AAAGGCTCAGTCGAAAGACTGGGCCTTTTCGTTTTATCTGTTGTTTGTTCGGTG
AACGCTCTCCTGAGTAGGACAAATCCGCCGGGAGCGGATTTGAACGTTGCG
AAGCAACGGCCCCGAGGGTGGCGGGCAGGACGCCCGCCATAAACTGCCAG
GCATCAAATTAAGCAGAAGGCCATCCTGACGGATGGCCTTTTTTGCCTTTCTA
CAAACCTTTTTGTTTTATTTTTCTAAATACATTCAAATATGTATCCGCTCATGA
GACAATAACCCTGATAAATGCTTCAATAATATTGAAAAAGGAAGAGTATGA
GTATTCAACATTTCCGTGTCGCCCTTATTCCCTTTTTTGCGGCATTTTGCCTT
CCTGTTTTTGTCTACCCAGAAACGCTGGTGAAAGTAAAAGATGCTGAAGAT
CAGTTGGGTGCACGAGTGGGTTACATCGAACTGGATCTCAACAGCGGTAAG
ATCCTTGAGAGTTTTTCGCCCCGAAGAACGTTTTTCCAATGATGAGCACTTTTA
AAGTTCTGCTATGTGGCGCGGTATTATCCCGTGTTGACGCCGGGCAAGAGC
AACTCGGTGCGGCATACACTATTCTCAGAATGACTTGGTTGAGTACTCACC
AGTCACAGAAAAGCATCTTACGGATGGCATGACAGTAAGAGAATTATGCAG
TGCTGCCATAACCATGAGTGATAAACTGCGGCCAACTTACTTCTGACAAC
GATCGGAGGACCGAAGGAGCTAACCGCTTTTTTGCACAACATGGGGGATCA
TGTAACCTCGCCTTGATCGTTGGGAACCGGAGCTGAATGAAGCCATACCAA
CGACGAGCGTGACACCACGATGCCTGTAGCAATGGCAACAACGTTGCGCAA
ACTATTAACCTGGCGAACTACTTACTCTAGCTTCCCGGCAACAATTAATAGAC
TGGATGGAGGCGGATAAAGTTGCAGGACCACTTCTGCGCTCGGCCCTTCCG
GCTGGCTGGTTTATTGCTGATAAATCTGGAGCCGGTGAGCGTGGGTCTCGC
GGTATCATTGCAGCACTGGGGCCAGATGGTAAGCCCTCCCGTATCGTAGTT
ATCTACACGACGGGGAGTCAGGCAACTATGGATGAACGAAATAGACAGAT

CGCTGAGATAGGTGCCTCACTGATTAAGCATTGGTAACTGTCAGACCAAGT
TACTCATATATACTTTAGATTGATTTAAAACCTTCATTTTTAATTTAAAAGG
ATCTAGGTGAAGATCCTTTTTGATAATCTCATGACCAAATCCCTTAACGTG
AGTTTTCGTTCCACTGAGCGTCAGACCCCGTAGAAAAGATCAAAGGATCTT
CTTGAGATCCTTTTTTTCTGCGCGTAATCTGCTGCTTGCAAACAAAAAAC
ACCGCTACCAGCGGTGGTTTTGTTTGCCGGATCAAGAGCTACCAACTCTTTTT
CCGAAGGTAACCTGGCTTCAGCAGAGCGCAGATACCAAATACTGTCCTTCTA
GTGTAGCCGTAGTTAGGCCACCACTTCAAGAACTCTGTAGCACCGCCTACAT
ACCTCGCTCTGCTAATCCTGTTACCAGTGGCTGCTGCCAGTGGCGATAAGTC
GTGTCTTACCGGGTTGACTCAAGACGATAGTTACCGGATAAAGGCGCAGCG
GTCGGGCTGAACGGGGGGTTCGTGCACACAGCCCAGCTTGGAGCGAACGAC
CTACACCGAACTGAGATACCTACAGCGTGAGCTATGAGAAAGCGCCACGCT
TCCCGAAGGGAGAAAGGCGGACAGGTATCCGGTAAGCGGCAGGGTCGGAA
CAGGAGAGCGCACGAGGGAGCTTCCAGGGGGAAACGCCTGGTATCTTTATA
GTCCTGTCGGGTTTCGCCACCTCTGACTTGAGCGTCGATTTTTGTGATGCTC
GTCAGGGGGGCGGAGCCTATGGAAAACGCCAGCAACGCGGCCTTTTTACG
GTTCTTGGCCTTTTTGCTGGCCTTTTTGCTCACATGTTCTTCTGCGTTATCCC
CTGATTCTGTGGATAACCGTATTACCGCCTTTGAGTGAGCTGATACCGCTCG
CCGCAGCCGAACGACCGAGCGCAGCGAGTCAGTGAGCGAGGAAGCGGAAG
AGCGCCTGATGCGGTATTTTCTCCTTACGCATCTGTGCGGTATTTACACCG
CATATGGTGCCTCTCAGTACAATCTGCTCTGATGCCGCATAGTTAAGCCAG
TATACACTCCGCTATCGCTACGTGACTGGGTCATGGCTGCGCCCCGACACCC
GCCAACACCCGCTGACGCGCCCTGACGGGCTTGTCTGCTCCCGGCATCCGCT
TACAGACAAGCTGTGACCGTCTCCGGGAGCTGCATGTGTCAGAGGTTTTCA
CCGTCATCACCGAAACGCGCGAGGCAGCAGATCAATTCGCGCGCGAAGGCG
AAGCGGCATGCATAATGTGCCTGTCAAATGGACGAAGCAGGGATTCTGCAA
ACCCTATGCTACTCCGTCAAGCCGTCAATTGTCTGATTCGTTACCAATTATG
ACAACTTGACGGCTACATCATTCACTTTTTCTTACAACCGGCACGGAATC
GCTCGGGCTGGCCCCGGTGCATTTTTTAAATACCCGCGAGAAATAGAGTTG
ATCGTCAAACCAACATTGCGACCGACGGTGGCGATAGGCATCCGGGTGGT
GCTCAAAGCAGCTTCGCCTGGCTGATACGTTGGTCCTCGCGCCAGCTTAAG
ACGCTAATCCCTAACTGCTGGCGGAAAAGATGTGACAGACGCGACGGCGAC
AAGCAAACATGCTGTGCGACGCTGGCGATATCAAATGCTGTCTGCCAGG
TGATCGCTGATGTAAGTACAAGCCTCGCGTACCCGATTATCCATCGGTGGAT
GGAGCGACTCGTTAATCGCTTCCATGCGCCGAGTAACAATTGCTCAAGCA
GATTTATCGCCAGCAGCTCCGAATAGCGCCCTTCCCCTTGCCCGGCGTTAAT
GATTTGCCCAAACAGGTGCTGAAATGCGGCTGGTGGCTTCATCCGGGCG
AAAGAACCCCGTATTGGCAAATATTGACGGCCAGTTAAGCCATTCATGCCA

GTAGGCGCGCGGACGAAAGTAAACCCACTGGTGATACCATTGCGGAGCCTC
CGGATGACGACCGTAGTGATGAATCTCTCCTGGCGGGAACAGCAAAATATC
ACCCGGTCGGCAAACAAATTCTCGTCCCTGATTTTTACACCACCCCTGACCG
CGAATGGTGAGATTGAGAATATAACCTTTCATTCCCAGCGGTTCGGTCGATA
AAAAAATCGAGATAACCGTTGGCCTCAATCGGCGTTAAACCCGCCACCAGA
TGGGCATTAAACGAGTATCCCGGCAGCAGGGGATCATTTTGCCTTCAGCC
ATACTTTTCATACTCCCGCCATTCAGAG

Acknowledgements

It would not have been possible to write this doctoral thesis without the help and support of the kind people around me, to only some of whom it is possible to give particular mention here.

I wish to thank Prof. Joachim Spatz, who was so generous to agree to supervise my work and referee my thesis. His support and willingness to help have been invaluable to me.

This thesis would not have been possible without the help, support and patience of my supervisor, Prof. Jörg Bewersdorf. He has been a great mentor over the years and patiently provided the vision, encouragement and advice necessary for me to proceed through the doctoral program and complete my dissertation.

All the members in the Bewersdorf Lab also deserve my sincerest thanks, their friendship and assistance has meant more to me than I could ever express. I could not have completed my work without the invaluable friendly assistance of Ed Allgeyer, Travis Gould, Fang Huang, Manuel Jütte, Emil Kromann, Yu Lin, Jane Long, Mike Mlodzianoski, Jordan Myers and George Sirinakis.

Special thanks to Prof. Matthias Bartelmann and Prof. Ulrich Uwer for kindly agreeing to be part of my defense committee.

My heartfelt gratitude goes out to Prof. Vladislav Verkhusha, Prof. Lynn Cooley, Andrew Hudson, Peter McLean and Fedor Subach for the great collaborations on the biological projects. Their insights and advice have been instrumental in shaping this thesis.

Advice and support given by Intaek Lee and Neeraj Tiwari on everything related to biology has been a tremendous help.

I wish to acknowledge the help provided by Marsha Maresca in the Department of Cell Biology at Yale University and Yvette Harbers in the Department of Physics at Heidelberg University for all their help with the administrative formalities.

I wish to thank my parents, brother and sister, Brigitte and Gerhard Hartwich, Julius Hartwich and Andrea-Janina Lutz, for their unconditional support and love which was my driving force. I owe them everything and wish I could show them just how much I love and appreciate them.

And finally, my wife, Yang Yang-Hartwich, whose love and encouragement allowed me to finish this journey. She already has my heart so I will just give her a heartfelt "Thanks".

Statement of Authorship

This thesis is my own work. I have only used the sources indicated and have not made unauthorized use of services of a third party. Where the work of others has been quoted or reproduced, the source is always given. I have not presented this thesis or parts thereof to a university as part of an examination or degree.

New Haven, December 1, 2012

Tobias M. P. Hartwich

Erklärung der Urheberrechtschaft

Bei der vorliegenden Dissertation handelt es sich um meine eigenständig erbrachte Leistung. Ich habe nur die angegebenen Quellen und Hilfsmittel benutzt und mich keiner unzulässigen Hilfe Dritter bedient. Insbesondere habe ich wörtlich oder sinngemäß aus anderen Texten übernommene Inhalte als solche kenntlich gemacht. Die Arbeit oder Teile davon habe ich bislang nicht an einer Hochschule des In- oder Auslands als Bestandteil einer Prüfungs- oder Qualifikationsleistung vorgelegt.

New Haven, den 1. Dezember 2012

Tobias Hartwich